Investigating the effects of extracellular biomolecules on Aβ1-42 oligomer uptake and trafficking by microglia cells

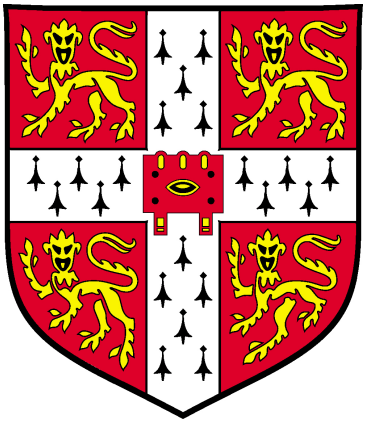

Nina Denise KLOSS

Hughes Hall

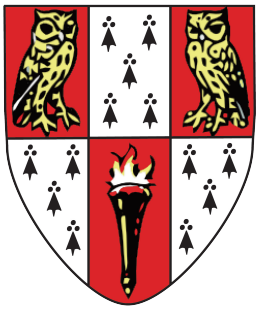

This dissertation is submitted for the Degree of Doctor of Philosophy

University of Cambridge

April 9, 2020

ABSTRACT

Title: Investigating the effects of extracellular biomolecules on Aβ1-42 oligomer uptake and trafficking by microglia cells

Author: Nina Denise Kloss

Arguably, the most prominent of the protein-misfolding disorders is Alzheimer's disease (AD), a debilitating neurodegenerative disorder pathologically characterised by the deposition of tau fibrillary tangles and Aβ1-42 amyloid plaques in the brain.

To date, the cause of AD is unknown and rising patient numbers pile pressure on the search for a cure. The protein assembly pathway converting soluble Aβ1-42 to mature fibrils is complex and the heterogeneity of aggregate morphology significantly contributes to the difficulty of studying how the pathogenic aggregates confer cellular dysfunction. Previous studies have pointed towards soluble oligomers (SO) as opposed to mature amyloid fibrils as the predominant toxic species. This thesis explores the internalisation of SO by a microglia cell line (EOC 13.31) and provides new insights into the modulation of this process by naturally occuring extracellular biomolecules, namely the chaperone clusterin (Clu) and the antimicrobial enzyme lysozyme, an important component of the innate immune system. Microglia cells are the primary immune cells of the brain and as such, considered to be the first line of defense against intruders. In more recent years, chronic neuroinflammation has been suggested as a central mechanism, even a driver, of AD, which has led to a surge of investigations into underlying cellular processes that govern SO interactions with microglia.

The oligomer formation of synthetic Aβ1-42 is characterised using different biophysical and biochemical techniques in Chapter 3. Initial studies of the interaction of these SO with EOC 13.31 cells in the presence of Clu suggest that unlike observations in neuroblastoma cells, where Clu prevented SO interactions, the mechanism in microglia cells is more complex.

The preliminary internalisation experiments of Chapter 3 have prompted a more detailed investigation into the effect of Clu on SO interaction with EOC 13.31. Chapter 4 uses confocal microscopy

to probe how Clu alters uptake and trafficking of fluorescently-labelled Aβ1-42 oligomers by EOC 13.31 cells, including studying morphological changes in the microglia. Furthermore, exploratory studies of pro-inflammatory cytokine release using ELISA and qPCR in response to SO and Clu are discussed.

Chapter 5 explores the effect of lysozyme on SO interactions with EOC 13.31 cells, and compares this with Clu. The employed biophysical as well as advanced imaging techniques suggest a protective role for both biomolecules, which appears to be receptor-independent.

The results in this thesis have demonstrated how different biomolecules can alter SO internalisation by microglia cells. These insights can contribute to understanding the molecular mechanisms by which amyloid species are processed in a cellular environment and facilitate the development of effective therapies for AD.

To my parents

Hiltrud and Andre Kloss

... and to my brother

Dennis Kloss

"The important thing is not to stop questioning. Curiosity has its own reason for existing."

Albert Einstein

ACKNOWLEDGEMENTS

Setting out for a PhD felt like navigating uncharted waters; while I was very excited about the whole ocean of ideas and opportunities to be explored, the unknown nature of this task seemed rather daunting. In hindsight, however, my concerns were unfounded as I was joined by the best crew I could have possibly imagined for this journey.

I would like to thank the people involved in the completion of my PhD and express my deepest gratitude to my research supervisors, the late Professor Sir Chris Dobson and Dr. Janet Kumita. Your guidance, support, and feedback throughout the past years have led this research to fruitful results, while I was given the freedom and resources to further explore my scientific interests, though not always fruitfully. Chris has been a wonderful teacher in all aspects of research and beyond. He has inspired me to embrace the unexpected, to remain curious, and to aim to thrive in what I set out to do with passion, compassion, and humour. Strikingly, Chris's most burning question in our meetings was not concerning my results but whether I was happy, which I gladly affirmed every single time. This, in large part, was due to Janet's unprecedented mentoring on the day-to-day basis. Janet was repeatedly subjected to random musings, half-baked practice talks, and a whole lot of proofreading. She has been extremely helpful in resolving any sort of equipment trouble either by digging up something from the Bronze Age or by means of strategic sourcing. Her support goes well beyond her role, making it possible to navigate even the stormiest of times. Most of all, I would like to thank Janet for her constant support, encouragement, and believing in me when I doubted myself, which has ultimately enabled me to follow my dreams...once the world has resurfaced from its lockdown that is.

I would moreover like to thank Professor Michele Vendruscolo for stepping in as my supervisior over the last months of my PhD program, and I would like to further extend my thanks to Dr. Marie Bongiovanni, Dr. Maya Hanspal, Dr. Patrick Flagmeier and the staff at the Cambridge Advanced Imaging Centre, who have all been extremely supportive in my experimental pursuits, especially those that involved novel imaging techniques.

Special thanks go to my family for supporting me in my decisions and for providing a refuge to hide from the consequences of those decisions whenever needed.

Lastly, I would like to thank my friends, near and far, for their continuous loving words of encouragement and their continuous loving interruptions, respectively. Special thanks go to Dr. Zein Azhari for introducing me to Aromi's Pistachio Lattes, as well as for helping me with anything LaTeX-related and beyond.

DECLARATION

This thesis is the result of my own work and includes nothing which is the outcome of work done in collaboration except as declared in the preface and specified in the text.

It is not substantially the same as any work that has already been submitted before for any degree or other qualification except as declared in the preface and specified in the text.

It does not exceed the prescribed word limit for the Department of Chemistry Degree Committee.

Nina Denise Kloss

February 14, 2021

Contents

List of Figures

List of Tables

LIST OF ACRONYMS

Aβ	Amyloid beta
AD	Alzheimer's disease
ADDL	Aβ-derived diffusible ligands
AF	Alexa Fluor
ALP	Autophagy-lysosome pathway
APOE	Apolipoprotein E
APP	Amyloid precursor protein
BCA	Bicinchoninic acid
BMG	Buffered minimal glycerol
BMM	Buffered minimal methanol
BSA	Bovine serum albumin
Clu	Clusterin
CNS	Central nervous system
CO_2	Carbon dioxide
CSF	Cerebrospinal fluid
CTCF	Corrected total cell fluorescence
dH_2O	Deionised water
DMEM	Dulbecco's Modified Eagle Medium
DMSO	Dimethyl sulfoxide

DPBS	Dulbecco's Phosphate Buffered Saline
ELISA	Enzyme-linked immunosorbent assay
EMEM	Eagle's Minimum Essential Medium
EOAD	Early onset Alzheimer's disease
ER	Endoplasmic reticulum
fAD	Familial Alzheimer's disease
FBS	Fetal bovine serum
GdnHCl	Guanidine hydrochloride
GWAS	Genome-wide association study
HBSS	Hank's Balanced Salt Solution
HFIP	1,1,1,3,3,3,-Hexafluoro-2-propanol
HMW	High molecular weight
IDP	Intrinsically disordered peptide
IL	Interleukin
LAMP-1	Lysosomal-associated membrane protein 1
LB	Loading buffer
LDL	Low-density lipoprotein
LOAD	Late onset Alzheimer's disease
LPS	Lipopolysaccharide
LRP1	Lipoprotein receptor-related protein 1
LRPAP	Low density lipoprotein receptor-related protein-associated protein 1, also named RAP
LSPB	Low-salt phosphate buffer
LTP	Long-term potentiation

Lys	Lysozyme
MAb	Monoclonal antibody
MTT	3-4,5-dimethylthiazol-2-yl-2,5-diphenyltetrazolium bromide
MW	Molecular weight
NaCl	Sodium chloride
Na_2HPO_4	Disodium phosphate
NFT	Neurofibrillary tangle
NGS	Next generation sequencing
NH_4OH	Ammonium hydroxide
NO	Nitric oxide
PAMPs	Pathogen-associated molecular patterns
PBS	Phosphate buffered saline
PEG	Polyethylene glycol
PFA	Paraformaldehyde
POPC	1-palmitoyl-2-oleoyl-sn-glycero-3-phosphocholine
PRR	Pattern recognition receptor
PSEN	Presenelin
PTM	Post-translational modification
PVDF	Polyvinylidene difluoride
ROS	Reactive oxygen species
RT	Room temperature
SD	Standard deviation
SDS PAGE	Sodium dodecyl sulphate polyacrylamide gel electrophoresis
SNP	Single nucleotide polymorphism

SO	Soluble oligomer
TAMRA	5-Carboxytetramethylrhodamine
TEM	Transmission electron microscopy
TFA	Trifluoracetic acid
TIRFM	Total internal reflection microscopy
TLR	Toll-like receptor
TNFα	Tumor necrosis factor alpha
TREM2	Triggering receptor expressed on myeloid cells 2
UPS	Ubiquitin-proteasome system
v	Volume
w	Weight
WGA	Wheat germ agglutinin

1

INTRODUCTION

1.1 Amyloid aggregation in disease

Since the 19th century it has been known that the progressive accumulation of insoluble protein deposits can cause devastating diseases. Over the years, more than fourty proteins or peptides, of diverse composition and native function, have been linked with protein-misfolding disorders, including neurodegenerative diseases and also systemic amyloidosis [1].

Alzheimer's disease (AD) is the arguably most prominent of the protein-misfolding diseases, a disease category characterised by β-sheet-rich protein aggregates, termed amyloid fibrils, that are deposited into various tissues, where they become hallmarks of respective disease pathologies. Although there are many studies trying to elucidate the molecular mechanisms by which these proteins misfold to form amyloid fibrils, the process is still not fully understood (see Fig. 1.1). Protein misfolding can occur when the monomeric protein adopts a structure that favours intermolecular interactions which may lead to the formation of "off pathway" oligomers, amorphous aggregates or amyloid fibril formation. The protein assembly pathway leading to mature fibrils is complex and the heterogeneity of aggregate morphology significantly contributes to the difficulty of studying how the pathogenic aggregates confer cellular dysfunction.

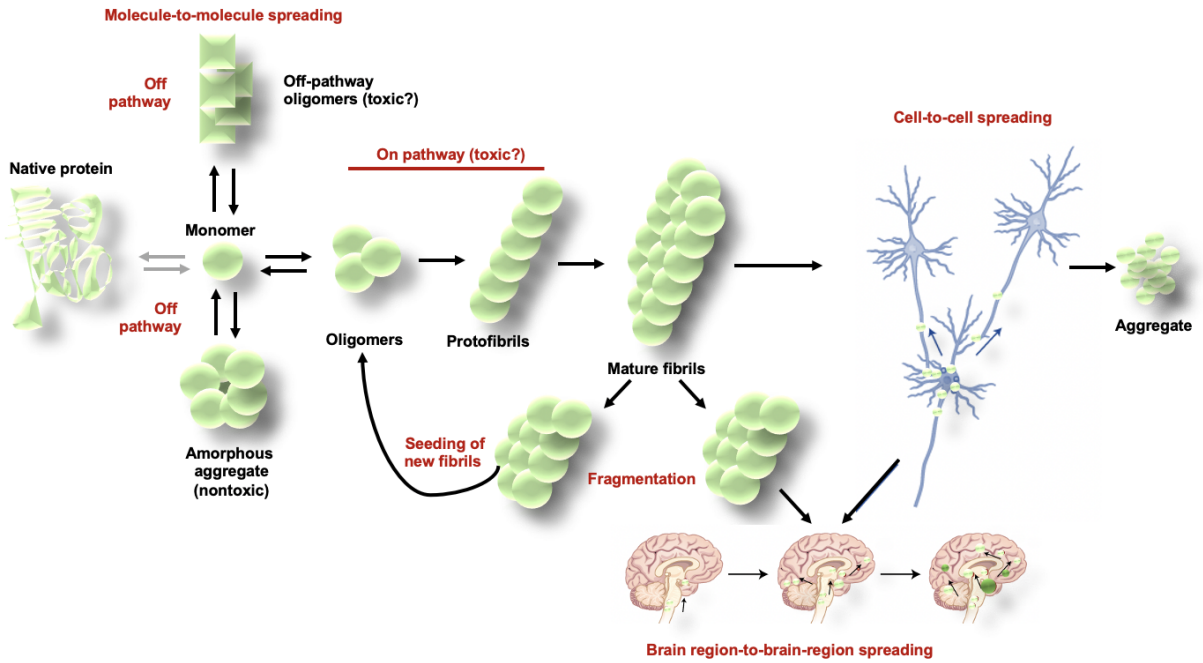

Figure 1.1: Proposed mechanism for amyloid formation and spreading: The first step along the aggregation pathway involves oligomers, which form fibrils and eventually get deposited throughout the brain. Spreading of protein misfolding can occur on different levels. Schematic adapted from Soto and Pritzkow [2].

Proteins form an essential part of all living organisms. The large biomolecules are crucial for the structure and regulation of the body's cells. The functions performed by proteins are manifold and range from DNA replication, to catalysing metabolic reactions and transporting molecules within and between cells [3]. Proteins distinguish themselves from one another through their unique amino acid sequence, which in return is encoded by the cellular DNA. The amino acid sequence together with the cellular environment dictate the complex folding pathways that proteins undergo to obtain 3-dimensional (3D), functionally active structures [4, 5]. En route to obtaining their respective 3D conformations, different structural levels in protein folding are passed as illustrated in Fig. 1.2. The primary structure of the protein is determined by the amino acid sequence, which directs local confirmations defined as the secondary structure of the protein. These include α-helices, β-sheets and random coils. In order to reach the tertiary, or native structure, the secondary structure is further packed into a globular configuration by which the most aggregation-prone regions, such as hydrophobic patches, are buried within the folded protein [6]. In some cases, a quaternary structure is obtained by assembly of discontinuous polypeptide chains, which is required for the protein to be fully functional [7].

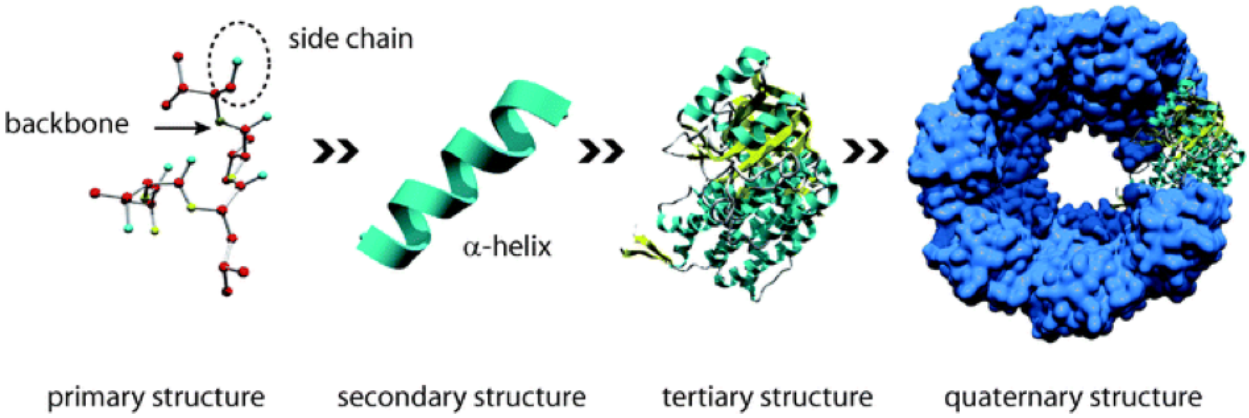

Figure 1.2: Overview of the four levels of protein structure. The sequence of amino acids is termed the primary structure of proteins. Interactions between adjacent amino acids allow for the formation of α-helices and β-sheets, referred to as the secondary structure. The 3D folding of the polypeptide marks its tertiary structure and the interaction of multiple polypeptides can lead to the formation of a quaternary structure. Figure as first shown by Helm and colleagues [6].

Within cells, proteins are synthesised on ribosomes based on the genetic information contained in the nucleotide sequences of the DNA [8]. Proteins that are not able to obtain the functionally active native state are generally identified as misfolded and targeted to a degradation pathway [9,10]. Proper protein folding into 3D structures is crucial for protein function. Cells therefore maintain an efficient quality-control system to prevent the accumulation of misfolded proteins. The mechanisms involved in clearing protein aggregates in the cell include molecular chaperones, the ubiquitin-proteasome system (UPS), and autophagy-lysosome pathways (ALPs) as outlined hereinafter.

1.1.1 Cellular uptake and trafficking of amyloidogenic aggregates

To ensure protein homeostasis, which describes the normal cellular repertoire of functional proteins, cells contain coordinated quality-control systems. These are highly complex interconnections of pathways, some of which promote protein folding and refolding (e.g. heat shock proteins belonging to the HSP40, HSP70, and HSP90 families and endomembrane compartments, such as the endoplasmic reticulum (ER), the Golgi apparatus, and endosomes), while others initiate degradation (e.g. the UPS and membrane-sequestered ALPs) [11,12].

Proteins that are targeted for clearance via UPS or ALP are poly-ubiquitinated, which involves the covalent ligation to at least four small, highly conserved ubiquitin molecules [13]. The majority of damaged proteins, as well as smaller protein aggregates, are generally tagged with a specific ubiquitin chain marking them for proteasomal degradation. The proteasome is a barrel-shaped structure forming a channel in which the proteins are enzymatically degraded to small peptides as they pass through [13,14]. Proteasomes are present in the nucleus and cytosol of all cells. Proteins and cel-

lular organelles that are too large to enter the narrow proteasome may be tagged for degradation via one of the three ALPs, namely the macro-autophagy, micro-autophagy, and chaperone-mediated autophagy-lysosomal pathways [15]. Macro-autophagy involves the engulfment of proteins or protein aggregates within a double-membrane forming the autophagosome that, once matured, fuses with lysosomes [16,17]. Micro-autophagy describes a process by which cytosolic components are directly taken up by lysosomes through invagination of the lysosomal membrane, thereby eliminating the need for an intermediary [18, 19]. In chaperone-mediated autophagy, proteins rely on chaperone proteins for translocation across the lysosomal membrane [20–22]. Lysosomes contain different proteolytic enzymes, such as acid-optimal proteases, like cathepsins, as well as acid hydrolases that degrade the internalised cargo [23].

Increasing evidence suggests that even small perturbations in protein homeostasis can cause extensive cell and tissue damage [24–27]. To date, factors such as harsh environments, oxidative stress, mutations, increased hydrophobicity or β-sheet propensity, low net charge, surface interactions with membranes, and ageing have been associated with an increased likelihood of protein misfolding and aggregation [28–32]. If the level of protein aggregation exceeds the capacity of the degradation pathways, misfolded proteins accumulate and become pathogenic. Under certain circumstances, such as loss-of-function or gain-of-function mutations in the nucleotide sequence, proteins can acquire a high misfolding propensity and escape the protective mechanisms of the cell. These misfolded proteins not only lack their distinctive function, but are also prone to self-association into either highly disordered (amorphous) or ordered (amyloidogenic) aggregates [9, 33]. The different intracellular proteostasis components and their dysregulation by amyloid aggregates are shown in Fig. 1.3 [34].

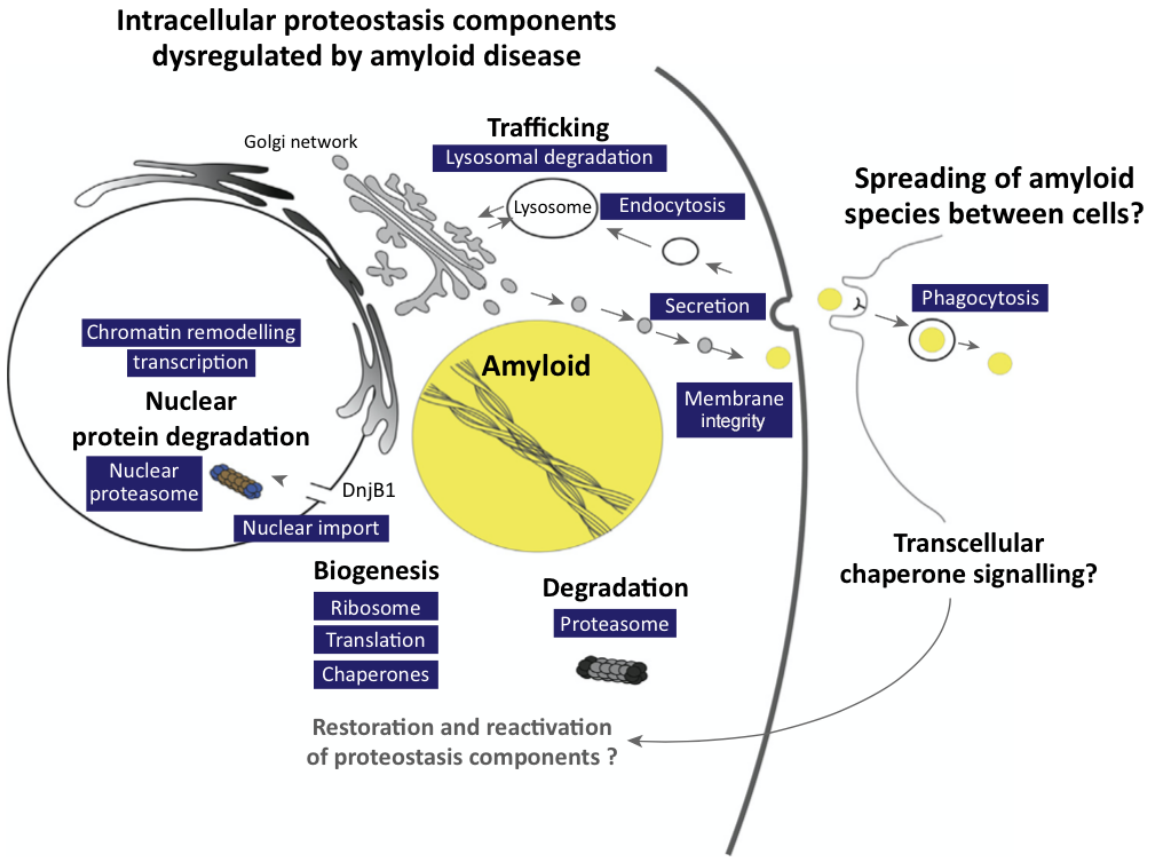

Figure 1.3: Proteostasis components and protective mechanisms dysregulated by amyloid disease. Intracellular components of the proteostasis network are impaired by the presence of amyloid species (shown in yellow) in the cytosol. Figure first shown by Tipping et al. [34].

Remarkably, amyloid fibrils formed by various proteins share common features despite the differences in their respective amino acid sequences and in their native 3D conformations [35–37]. Amyloid fibrils are composed of filaments that are often flat or able to form periodical helicity, which are detectable as characteristic unbranched, linear structures by transmission electron microscopy (TEM) or atomic force microscopy (AFM) [4]. In each protofilament, the protein molecules are arranged so that the polypeptide chain forms β-strands perpendicular to the long axis of the fibril as initially shown via synchrotron X-ray diffraction [1, 35, 38]. Fibrils have a diameter of 2-20 nm and can reach a few microns in length [39].

Using *in vitro* methods such as light scattering, turbidity, as well as fluorescence and absorption spectroscopy of intrinsic fluorophores and extrinsic dyes (e.g. Congo red and Thioflavin T, ThT), the kinetics of amyloid fibril formation have been well established: during an initial lag phase, protein monomers self-associate into soluble oligomeric species that act as a critical nucleus, which elongates as more monomeric protein is added until a plateau phase is reached, at which point the monomeric

proteins are depleted [39–41]. The steps involved in the aggregation process are illustrated in Fig. 1.4. New aggregates can be formed from monomers through primary nucleation, from existing fibrils through fragmentation or from both, monomeric and aggregated species via secondary nucleation, which is a surface-catalysed process [42, 43]. Secondary nucleation becomes the predominant route of oligomer formation once a critical concentration (ca. a few tens of nM) is reached and significantly contributes to the proliferation of toxic species [44].

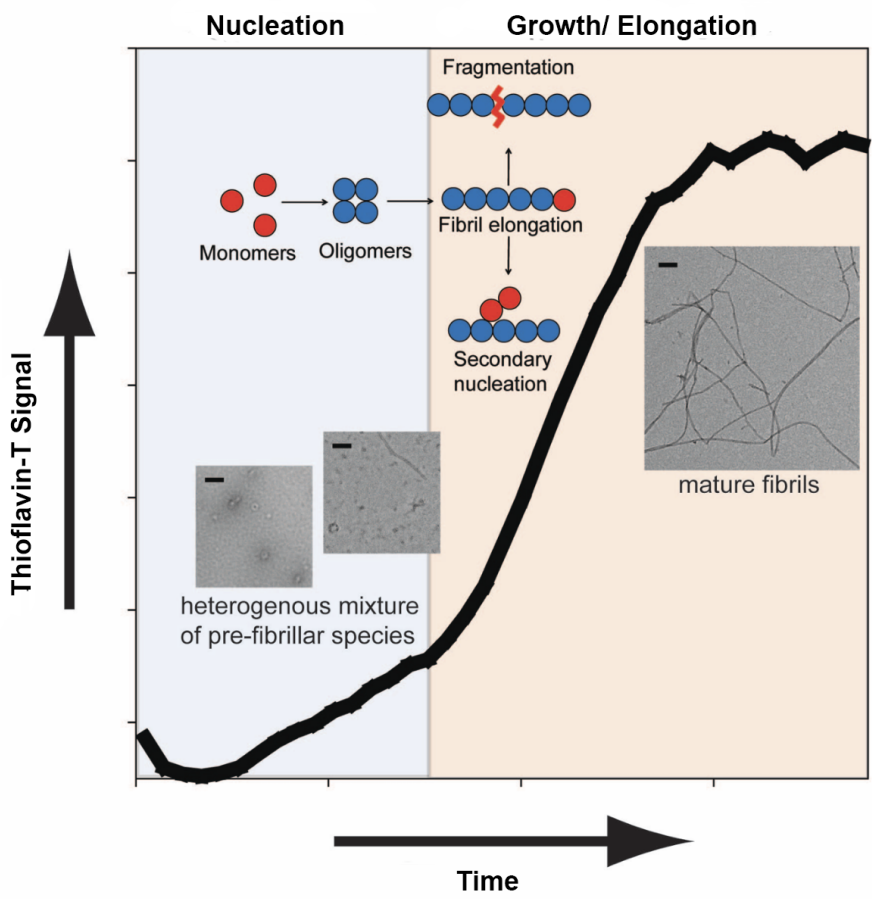

Figure 1.4: Schematic representation of the kinetics of amyloid fibril formation. Monomers of the misfolded proteins initially accumulate and form small, soluble oligomers (SO). Addition of further protein molecules leads to an elongation to larger, soluble protofibrillar species and lastly, to insoluble fibrils. TEM images show typical species of Aβ1-42. The scale bars represent 100 nm. Figure first published by Hook et al. [45].

Given that aggregating proteins can differ greatly in their primary amino acid sequence, the fibril-forming ability has been ascribed to the peptide backbone as opposed to the amino-acid side chains [33,46]. The amino-acid side chains, on the contrary, determine the rate and propensity of protein aggregation under respective conditions and knowledge of the amino-acid sequence serves as a proxy for its aggregation propensity [28, 47, 48].

1.2 Dementia and Alzheimer's disease

AD is one of the most prevalent neurodegenerative diseases and makes up 60-70 % of all dementia cases, an umbrella term used to describe the progressive deterioration of memory, thinking, and the ability to perform tasks. An estimated 44 million people worldwide currently suffer from dementia and while it predominantly affects older people, it is not considered a normal part of ageing [49]. The economic burden associated with the treatment of dementia is predicted to increase by 16 % every year, having amounted to total costs of $948 billion in 2016 [50]. Both, the high unmet medical need as well as the escalating fiscal burden on healthcare systems around the world necessitate a better understanding of causation and progression of the disease in order to develop effective therapies.

1.2.1 Disease pathology

The first medical record of what is now known as Alzheimer's disease dates back to the early 20th century. At a medical congress in Tuebingen in November 1906, Alois Alzheimer, for the first time, described the appearance of plaques and neurofibrillary tangles in the brain of his deceased patient Auguste D. The woman had previously been admitted into his care due to progressive cognitive impairment and hallucinations [51]. The pathological hallmarks and terminology used to describe AD back then are still applicable today. While there have been advances in the understanding of plaque composition and the processes leading to neurofibrillary tangles (NFTs), it was not until the 1980s that the underlying structures making up senile plaques were identified as amyloid fibrils consisting of Aβ peptides [52–54]. Moreover, the underlying structure of tangles was identified as hyperphosphorylated tau [55–57]. However, for some decades and much like a chicken-and-egg problem, the question of how AD develops has split the scientific community into two camps, the so-called *tauists* and the *baptists*.

Tau is a microtubule-associated protein located in neurons where it promotes microtubule polymerisation as well as their stabilisation. The phosphorylation of tau plays a crucial role in intracellular trafficking: it facilitates the removal of tau from microtubules thereby enabling transport, followed by dephosphorylation to return tau to the microtubule. Post-translational modifications (PTMs) of tau can cause hyperphosphorylation. Hyperphosphorylation of tau, in return, leads to a loss of its normal physiological function and is responsible for a gain of toxicity and aggregation culminating in NFTs [58, 59]. While there are several studies linking the tau gene MAPT to various tauopathies, such as Parkinson's disease, supranuclear palsy, and frontotemporal dementia, the evidence linking the tau gene to AD has been a lot hazier and to date, there is no compelling proof of a genetic

association between tau and AD [60–64].

Partly attributable to the lack of genetic evidence for the tau hypothesis, the predominant framework that has governed Alzheimer's research over the last few decades is provided by the amyloid cascade hypothesis, which postulates that Aβ is a causative agent in pathogenesis as opposed to a secondary event [50]. The seed of the idea that Aβ could, in fact, be causative of AD was originally planted by Glenner and Wong in 1984 and later refined [52, 65–68]. Despite extensive research, the contribution of the extracellular Aβ aggregates and the NFTs to disease pathogenesis and progression are still not fully understood and none of the clinical efforts to date have yielded an effective treatment for AD. However, in more recent years, the two camps have come closer together in trying to better understand the intersection of the two pathologies [69–73]. Since the early 2000s, a third line of research has entered the AD field, namely neuroinflammation, which may provide the missing link in the cascade of events that ultimately leads to the symptomatic disease pathology [74–77]. While this work predominantly focuses on Aβ and neuroinflammation, it is acknowledged that understanding tauopathy in AD is equally important, especially as rising patient numbers increase the pressure on finding a cure.

1.2.2 Genetics and risk factors

Data supporting the amyloid cascade hypothesis are derived from human genetics. Four main approaches have largely guided the field of AD genetics: genetic linkage analysis, study of candidate genes, genome-wide association studies (GWASs), and next generation sequencing (NGS) [78–83]. Even though AD is primarily sporadic, also referred to as late onset AD (LOAD, >90 % of cases), familial forms of AD (fAD/early onset [EOAD]), have been linked to mutations in three genes, namely *APP*, *PSEN1*, and *PSEN2*. These are all dominantly inherited, substantially involved in Aβ production, and accelerate the accumulation of Aβ plaques [50]. By identifying AD-linked mutations in both, the precursor of Aβ (*APP*) and the enzymes involved in its generation (*PSEN1* and *PSEN2*), the amyloid hypothesis of AD has significantly informed our current understanding of the underlying disease mechanisms. A brief overview of these genes, the involvement of their gene products in Aβ production, and selected mutations follows.

1.2.2.1 APP processing and Aβ generation

The *APP* gene encodes the transmembrane amyloid precursor protein (APP), whose function is still largely unknown. The genes, *PSEN1* and *PSEN2*, encode the catalytic subunits of the γ-secretase

complex, Presenelin 1 and 2, which are the final endoproteases that cleave APP generating either Aβ1-40 (ca. 80-90 %) or Aβ1-42 peptides (ca. 5-10 %) [82–85]. Aβ1-42 peptides are more hydrophobic, fibrillogenic, and more readily form toxic oligomers than Aβ1-40 peptides [86,87].

Prior to the cleavage of APP by the membrane-bound γ-secretase, APP is first cleaved by β-secretase releasing a large secreted derivative called sAPPβ (see Fig. 1.5 for a schematic overview of APP processing). An APP fragment of 99 amino acids (CTFβ) remains membrane bound, and is subsequently cleaved by γ-secretase yielding Aβ peptides that are between 39-42 amino acids in length. The bulk of APP is, however, processed via another route and does not yield the AD-associated Aβ peptides. Roughly 90 % of APP is initially cleaved by α-secretase generating sAPPα. Subsequent processing of the remaining membrane-bound fragment (CTFα) by γ-secretase results in a short fragment called p3. The activity of β-secretase is therefore believed to be the rate-limiting step in the amyloidogenic pathway as it processes the remaining 10 % of APP that ultimately result in Aβ aggregation [88].

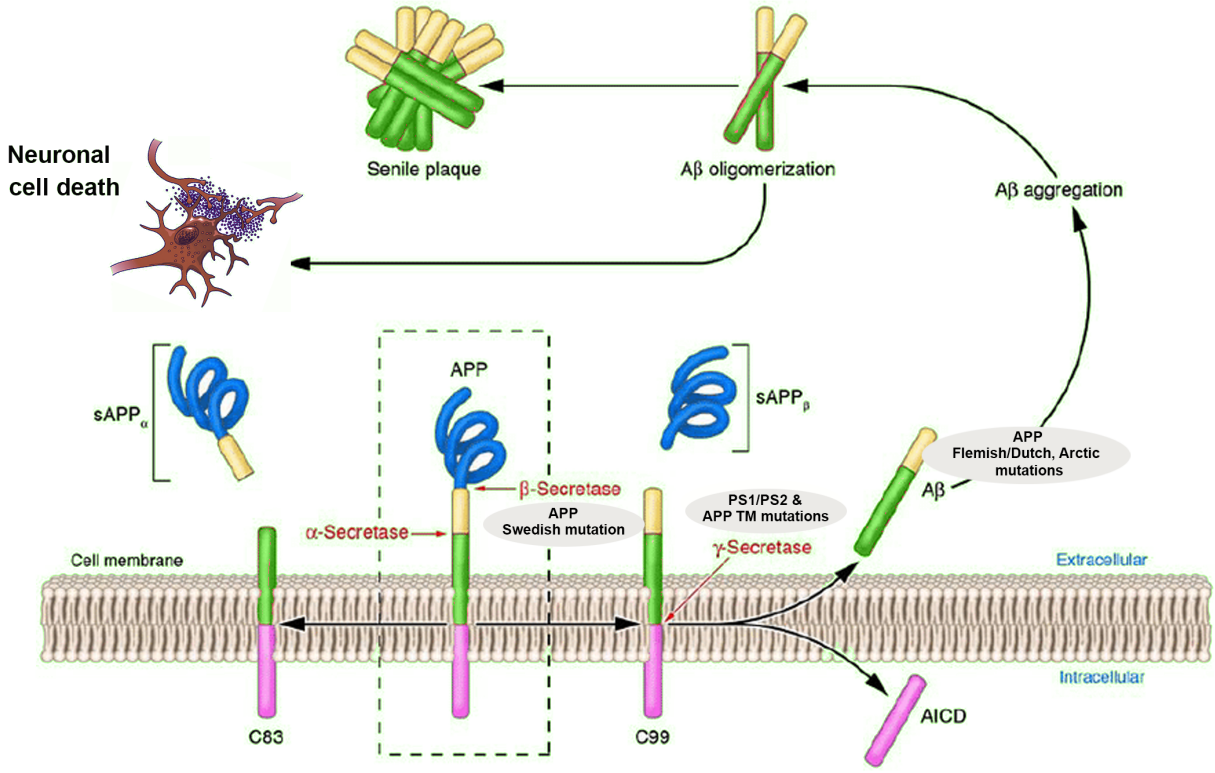

Figure 1.5: APP processing: Formation of Aβ peptides through sequential cleavage of APP by β- and γ-secretases. Schematic adapted from Spies et al. and the NIH [89,90].

1.2.2.2 Genetic mutations linked with EOAD and known risk factors of LOAD

All known mutations causing fAD affect Aβ metabolism and stability: mutations within *APP* result in an increased Aβ load or mutated Aβ peptides (e.g. *Swedish* and *London* mutations) and mutations

of γ-secretase lead to increased Aβ1-42 production relative to Aβ1-40 (see Table 1.1) [91]. While the mutations in *APP* and the presenelins causing fAD account for less than 5 % of all AD cases, they are fully penetrant and have become the focus of several functional and pathway studies with the hope of generating transferable insights into AD progression. Late onset AD, on the contrary, is a lot more common and it is believed that LOAD is affected by highly prevalent genetic variants with low penetrance [92]. Hence, LOAD is genetically far more complex and the possible involvement of multiple genes, as well as environmental factors, adds to the challenge of making meaningful inferences from experimental studies.

Table 1.1: Overview of AD genes associated with autosomal dominant or sporadic inheritance. The AD genes are located on four different chromosomes. Table adapted from Bekris et al. [93].

Gene symbol	**Gene name**	**Chromosome**	**Inheritance**
APP	Amyloid precursor protein	21q21	Autosomal dominant
APOE	Apolipoprotein E	19q13.32	Sporadic
PSEN1	Presenilin 1	14q24.2	Autosomal dominant
PSEN2	Presenilin 2	1q42.13	Autosomal dominant

The mapping of the APP gene to chromosome 21 led to the observation that patients with Down syndrome (trisomy 21) display a tendency to develop amyloid deposits and the neuropathological features of AD in their 40s [94]. Today, over thirty APP missense mutations in over eighty families have been identified with the majority of these located in the region of the Aβ peptide sequence [93].

Interestingly, the only gene that has been consistently associated with sporadic LOAD across multiple genetic studies is *APOE*. *APOE* has three common polymorphisms resulting in three different allelle variations, *APOE*-ε*2*, -ε*3*, and -ε*4*. *APOE*-ε*4* can increase the risk for LOAD 3-fold (1 copy) and 12-fold (2 copies), respectively [95]. The protein APOE is a lipoprotein and acts as a major cholesterol carrier in the brain, where it is mostly produced by astrocites and microglia [95, 96]. The initial discovery of *APOE* as a susceptibility gene for AD arose from genetic linkage studies and was later confirmed by GWAS [79, 80]. With the advent of high-throughput genotyping and the completion of the human genome project in 2003, GWASs have become an important tool in the search for genetic risk factors for complex diseases, including AD. Briefly, a GWAS usually analyses single nucleotide polymorphisms (SNPs) throughout the genome with the goal of identifying disease-associated genetic variants. The fact that the method enables the simultaneous assessment

of thousands of genetic variants, including non-coding regions, without prior hypotheses about biological pathways has made GWAS a particularly powerful approach. To date, all studies, apart from one, have identified *APOE* (encoding apolipoprotein E) as a gene associated with LOAD [97]. Another study conducted on over 16,000 individuals identified the chaperone, clusterin (Clu), to be associated with AD, which reinforced findings of earlier studies that had suggested a link between Clu and the Aβ peptide [81,98]. Overall, it emerged that the roughly 20 AD-associated gene loci that have been identified by GWASs are involved in one or more of the following three areas: I) inflammatory response (e.g. *CLU, TREM2, CD33, CR1*), II) lipid metabolism (*APOE, CLU, SORL1, ABCA7*), and III) endocytosis (*PICALM, SORL1, CD2AP*) [99]. In order to put these findings into context, it is vital to first take a closer look at the aggregation pathway of Aβ and to address the question of how the pathogenic aggregates confer cellular dysfunction.

1.2.3 An overview of the different types of Aβ aggregates

APP can be cleaved and processed in several ways, resulting in Aβ variants that differ in length, cytotoxicity and proportion in the AD brain. Clinical studies have revealed that a variety of toxic aggregates of different Aβ isoforms is variably distributed as depositions in the diseased brains [100]. As mentioned in Section 1.2.2, the most common variant is the 40-residue peptide. Aβ is an intrinsically disordered peptide (IDP) whose function remains largely unknown. IDPs, also referred to as natively unfolded proteins, are dynamic conformational ensembles that do not fold into a homogeneous 3D structure partially due to their sequence-bias towards a low proportion of hydrophobic and aromatic amino acids and a high proportion of charged residues [101]. They, however, still experience conformational fluctuations which may result in folded or partially folded states. Moreover, protein folding can be triggered by external factors such as pH, temperature, peptide concentration, and interactions with other molecules [102]. IDPs play a central role in the regulation of signaling pathways as well as cellular processes including but not limited to transcription, translation, and the cell cycle [103,104].

Both, Aβ1-40 and Aβ1-42 are particularly prone to aggregation. Due to its additional C-terminal amino acids, namely the hydrophobic residues isoleucine and alanine, Aβ1-42 is believed to have a greater propensity for aggregation (see Fig. 1.6). While in the CSF, the relative Aβ1-40-to-Aβ1-42 ratio has been experimentally identified as 9:1, senile plaques are predominantly made up of mature fibrils of Aβ1-42 [105–107]. Hence, the field of AD has long been dominated by the notion that mature Aβ fibrils are the main toxic species. However, a lack of correlation between plaque load and cognitive impairment as well as a discrepancy between location of neuronal injury and Aβ plaques

has put this hypothesis under scrutiny. More recent studies employing Western blot analysis and quantitative ELISA paired with advanced tissue extraction as well as a shift of focus on patients with mild-to-moderate as opposed to late-stage AD are pointing at soluble oligomers (SO), rather than mature amyloid fibrils, as the predominant toxic species [108–111]. In addition to aforementioned studies that correlate Aβ SO concentration with cognitive impairment in AD patients, Walsh et al. demonstrated that Aβ SO can inhibit long-term potentiation (LTP), a sustained increase in the strength of neuronal signals, when injected in the hippocampus of living rats [112]. In light of this more recent paradigm shift and the growing body of evidence linking Aβ SO to AD pathology, this thesis will focus on Aβ1-42 SO and their associated toxicity.

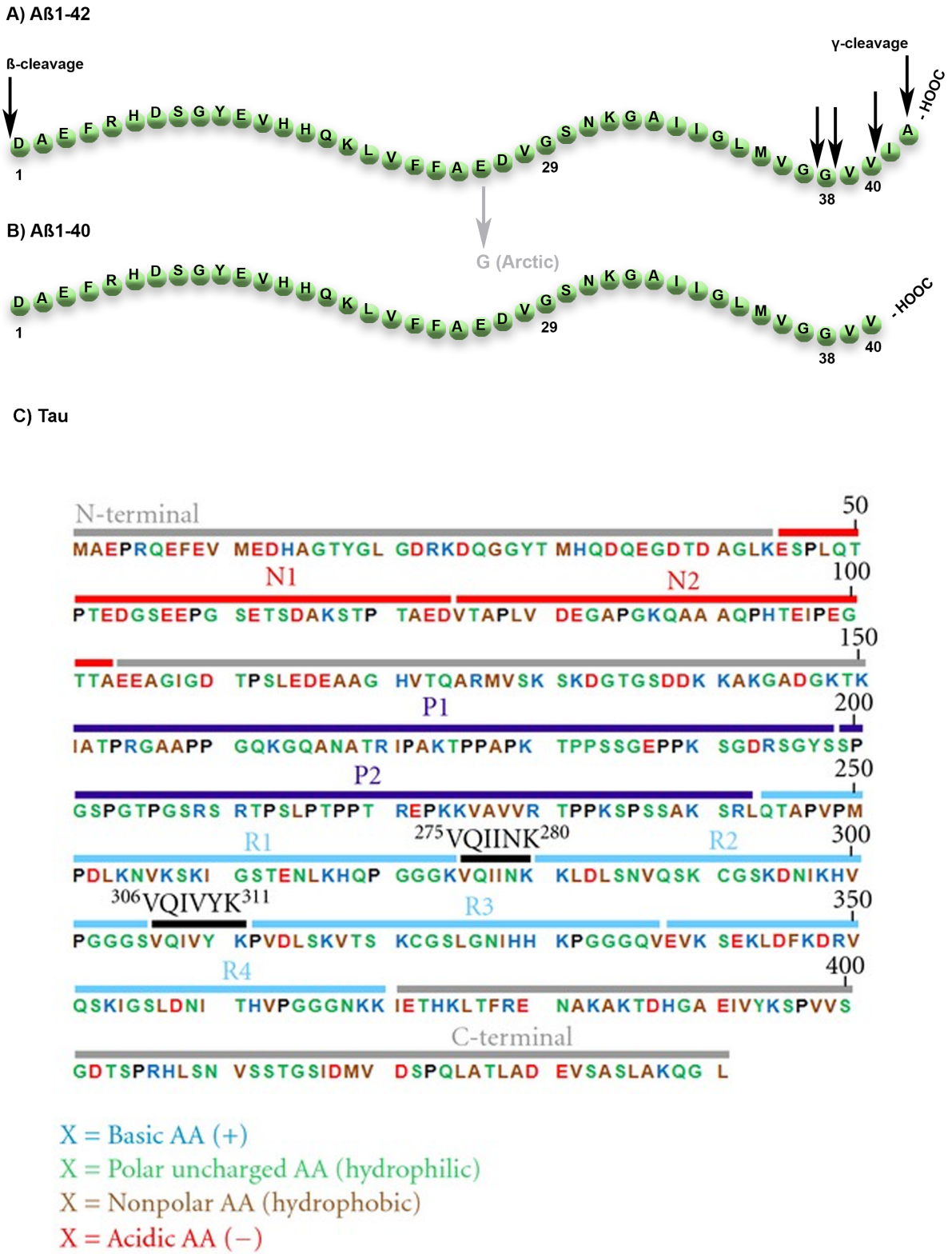

Figure 1.6: Amino acid sequences of Aβ1-42 (A), Aβ1-40 (B), and tau (C). Schematic adapted from Kolarova et al. [113].

1.2.4 Cytotoxicity of soluble Aβ1-42 oligomers (SO)

In vivo, SO have been located extracellularly in the CSF and in interstitial fluid [114–116]. As previously mentioned, there is extensive behavioural, neuropathological, and biochemical evidence indicating that elevated levels of SO are pathogenic [108–112]. However, the fundamental question of how SO confer toxicity has not been answered. The study of the SO structure-toxicity relationship has been extremely difficult due to the transient nature of SO resulting in heterogeneous populations of polymorphic, metastable Aβ SO generated via multiple pathways [102,117]. Moreover, there remains uncertainty regarding the precise identity of the most potent SO structures amongst the multiplicity of SO species (natural and generated *in vitro*) [100,118,119].

Despite these challenges, there are certain patterns emerging from the literature. For instance, SO, irrespective of their origin (AD patient, animal model, or synthetic) can be classified as "toxic" or "non-toxic" on the grounds of their quaternary structure, molecular weight (MW), and antibody reactivity: toxic SO tend to have a higher molecular weight (HMW, > 50 kDA) compared to their non-toxic counterparts, and bind to the anti-amyloid oligomer antibody A11 [119–122]. The conformation-selective polyclonal A11 antibody detects structural epitopes of amyloid-forming proteins independent of primary amino acid sequence. Specifically, the A11 antibody has been suggested to recognise out-of-register anti-parallel β-sheet structures [123]. While the exact link between SO formation and cell death remains elusive, it is postulated that these HMW SO interact with cellular membranes and confer cellular toxicity by inducing membrane disruptions. Several mechanisms through which SO can cause membrane disruption have been described and include pore formation, bilayer destabilisation (due to detergent-like behaviour of SO), membrane destabilisation due to surface aggregation (carpet model), and membrane destabilisation due to the formation of peptide-rich microdomains inside the bilayer by means of peptide fibrilisation [124–126]. It has been moreover observed that, once internalised, SO can self-propagate via prion-like cell-to-cell transmission thereby spreading toxicity [127–129].

When discussing SO characterisation and their involvement in AD pathogenesis, it is important to note that our understanding to-date is derived from both, *in vitro* and *ex vivo* experiments, which each have their advantages and shortcomings. Here, we focus on SO that have been generated *in vitro* with the advantage of precise control of the starting materials, such as peptide and buffer conditions. Moreover, *in vitro*-generated SO have been shown to meet the general criteria for a pathogenic protein species, namely that their stability is sensitive to AD-associated mutations, that they can also be generated from wildtype protein (given AD is largely sporadic), and they can be

associated with a pathogenic mechanism [100]. The aforementioned multiplicity of SO species does not only stem from the use of *in vitro* vs. *ex vivo* SO, but also from the variation in techniques used to isolate or generate SO. However, several studies have demonstrated that antibodies raised against specific types of exogenous SO were able to confirm the presence of the same types of SO in AD patients, which implies that observations made *in vitro* are relevant and facilitate our understanding of SO toxicity in AD patients [130–132].

1.2.4.1 Aβ-derived diffusable ligands

In this thesis, Aβ-derived diffusible ligands (ADDLs) are used for the experimental work, which have been first described in 1998 by Lambert and colleagues [133]. It was shown that incubation of Aβ1-42 peptide in low ionic strength solution at low temperature resulted in the formation of small globular Aβ1-42 oligomers that are nonfibrillar, readily diffusible, and toxic to mature CNS neurons at nanomolar concentrations. ADDLs have further been demonstrated to potently inhibit hippocampal long-term potentiation, which is a paradigm for synaptic plasticity. Using rats and transgenic mouse models of AD, ADDLs have since been linked to synapse loss as well as reversible memory failure [134].

Since their discovery, ADDLs have been well characterised using methods such as AFM, TEM, and SDS-PAGE [135, 136]. Chromy and colleagues showed that Aβ1-42 can self-assemble into small, stable globular assemblies free of fibrils and protofibrils. Using AFM and nondenaturing gel electrophoresis, they were able to verify absence of large molecules, while denaturing electrophoresis revealed that the globular assemblies comprised oligomers ranging from trimers to 24-mers. Moreover, it was shown that oligomers prepared at 4 °C stayed fibril-free for days and that the oligomers were toxic to PC12 cells, as seen by impaired MTT reduction [135]. By using fluorescence and circular dichroism spectroscopies, while taking advantage of the intrinsic fluorescent properties and susceptibility to fluorescence quenching of Tyr^{10}, Aran Terol and colleagues provided further insights into the molecular characteristics of ADDLs. The authors reported that Aβ1-42 oligomers contain a relatively homogeneous population of small aggregates with spherical morphology as observed by AFM and analysis of TEM images further indicated that their approximate diameters were 10-20 nm. The authors concluded that while Aβ1-42 oligomers show the presence of a degree of β-sheet structure, they are distinctly less ordered than fibrils [136]. Evidence of ADDL-resemblance to naturally occurring forms of Aβ1-42 oligomers was provided by Gong and colleagues, who demonstrated that antibodies raised against *in vitro* ADDLs also recognise oligomeric species that are elevated in AD brains [137].

Even though the study of SO-triggered toxicity presents its challenges, our understanding has progressed by collating findings from many studies employing various biochemical, cellular, and imaging techniques. There is growing consensus that one approach of developing effective AD treatment strategies is by means of regulating SO-induced toxicity.

1.3 The role of microglia in AD

Microglia cells are the macrophages of the brain and the first line of defense to pathogenic intruders. Microglia are derived from the embryonic yolk sac and make up the largest population of myeloid cells in the CNS. They migrate to the brain during early development, where they maintain abundance by local self-renewal [138]. In the healthy brain, they are involved in various neural activities, such as synaptogenesis, neurogenesis, and the release of neurotrophic factors [139, 140]. Depending on the brain region, microglia constitute 0.5-16 % of the total cell population in the human brain and 5-15 % in the mouse brain [141, 142]. In response to an insult, microglia assume different functional states that are characterised by morphological changes as well as phagocytic activity and the release of proinflammatory cytokines [143]. The revelation that late-onset AD is associated with a strong activation of the innate immune system has shifted the focus on neuroinflammation as a key contributor to AD pathogenesis [144].

1.3.1 Microglial activation and cytokine release

Microglial phenotypes are very heterogeneous, both, across CNS regions and within a single tissue. Their diverse plasticity is not only illustrated by their morphological changes, but also by the variety of reactive phenotypes in response to changes in their microenvironment with both, neuroprotective and neuroinflammatory properties [145]. The morphological features of microglial cells and their function are tightly coupled, however, no morphological classification standards exist, which make the objective quantification of the pathological status difficult [146, 147].

Despite the difficulty of morphologically distinguishing the fluid transition from "resting" to "activated" state, activated microglia share three prominent features: I) they display an enlarged cell body, II) they retract their branches, appearing round, and III) they accumulate in great numbers (see 1.7) [148]. The term "resting" is commonly used to describe non-activated microglial cells, however, it should be clarified that these cells are still highly motile. Using real-time recordings in the mouse brain, it was shown that "resting" microglial cells undergo continuous cycles of extension and retraction of their smaller processes [149]. This movement enables the constant surveillance of the

brain environment for neuronal damage. Because the cell bodies and larger processes remain static, the subtlety of this movement has been initially overlooked and this misperception has manifested itself in the nomenclature. In this context, when the term "activated" is used hereinafter, we refer to a shift in the cell activity rather than an activation in itself. Due to their heterogeneity, microglia can be induced into several activation phenotypes to detect pathogenic substances and eliminate cell debris, they can also contribute to nerve regeneration and tissue reconstruction and as such, they are an important nexus between immunological and neurological processes in the CNS. Here, we focus on the microglial response to pathogenic intruders, which is also referred to as "classical" or "M1" activation. This is distinctly different to so-called "alternatively" activated microglia (M2), which has been observed in microglia upon encounter with tumor cells [150].

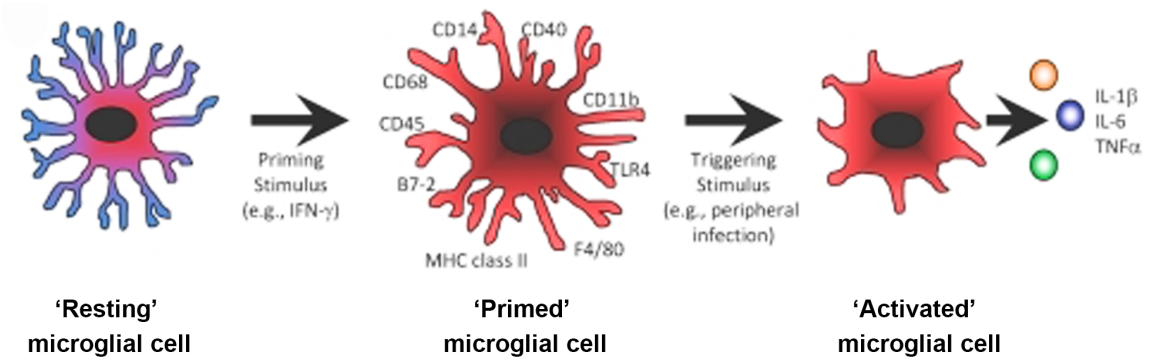

Figure 1.7: Schematic representation of microglial activation (adapted from Dilger et al. [151]). Upon pathophysiological stimuli such as injury or infection, microglia undergo morphological transitions from a ramified state with many branching processes to an amoeboid state with retracted processes and enlarged cell bodies.

Microglial activation in response to a pathogenic stimulus elicits a whole cascade of processes including cytoskeletal remodeling, transcriptional changes, cell proliferation, and migration to the source of the insult, where the cells take part in the phagocytosis of the pathogen and removal of cellular debris [152]. These processes are mitigated by the production of pro-inflammatory mediators, such as cytokines (TNFα, Interleukin (IL-6, and IL-1β), chemokines, reactive oxygen species (ROS), and nitric oxide (NO)) [153]. Different mechanisms have been found to contribute to microglial activation, which include their interaction with neurons and other glial cells, through secreted mediators, the activation and inhibition of transcription factors, and the regulation of surface and nuclear receptors. In AD, the effects of microglial activation are believed to be dichotomous: on the one hand, microglial activation leads to reduced Aβ accumulation by means of increasing its phagocytosis and degradation thereby preventing plaque formation, while on the other hand, their chronic activation and concomitant release of pro-inflammatory cytokines contribute to neuronal damage [154, 155]. Continuous activation of microglia is potentially elicited by protein aggregates, therefore, the inter-

actions observed between Aβ1-42 amyloidogenic aggregate species and microglia are an interesting target for the study of events leading to cellular dysfunction.

1.3.1.1 Receptor-mediated and receptor-independent uptake

Microglia express a diverse set of pattern recognition receptor (PRRs) for pathogen-associated molecular patterns (PAMPs) that include Toll-like receptors (TLRs) and inflammasomes. Several members of the TLR and inflammasome family also recognise endogenously derived molecules that are generated as a consequence of tissue injury or other pathological processes. Recognition by PAMPs or endogenous ligands by PRRs in microglia induces the robust activation of innate immune responses leading to the production of pro-inflammatory mediators and the activation of adaptive immunity [156].

In the context of AD, it has been previously suggested that Aβ SO are internalised by microglial cells via TLR-signalling pathways [157]. Moreover, the low-density lipoprotein receptor related protein-1 (LRP1, also see Chapter 5) has been linked to the uptake and clearance of Aβ, which has been shown to be involved in the internalisation and the degradation of lipoproteins as well as the endocytosis of fibrillar Aβ [158, 159].

1.3.2 Microglial uptake and trafficking of Aβ1-42

The process of internalisation of extracellular material via different routes is collectively referred to as endocytosis. Internalised material follows branching vesicular transport pathways and as previously mentioned, the internalised substrates are sorted and targeted to degradative organelles, such as the acidic late endosomes and lysosomes, where degradation occurs.

There are three main endocytic mechanisms: macropinocytosis, phagocytosis and clathrin-mediated endocytosis (see Fig. 1.8) [160]. Pinocytosis is a non-selective process by which the plasma membrane forms vesicles that engulf extracellular fluid [161]. A large amount of receptor-mediated endocytosis occurs via clathrin-coated pits [162]. Upon receptor-mediated endocytosis, substrates bound to receptors undergo sorting in endosomes and receptors are recycled back to the plasma membrane. Phagocytosis describes the process by which cells engage in the noninflammatory clearance of apoptotic cells and cell debris as part of their scavenging role and it is the predominant endocytic pathway found in microglia cells [163]. Briefly, apoptotic cells release ligands that act as chemoattractants to recruit microglia (so-called "find me" signals, such as ATP and UDP) and this initiates phagocytosis [164, 165]. Once the microglia cell has migrated to the site of perturbance, so-called "eat me"

signals or ligands such as phosphatidylserine, calreticulin and complement components C1q and C3, are recognised by selected microglia surface receptors, which initiate engulfment and phagocytosis [163]. One receptor involved in the recognition of such "eat me" signals is the triggering receptor expressed on myeloid cells 2 (TREM2), which is exclusively expressed by microglial cells. This receptor has interestingly been shown to enhance phagocytosis of Aβ1-42 as well as inhibit Aβ-induced pro-inflammatory responses in microglial cells thereby modifying their function, while CD33 regulates β-amyloid phagocytosis negatively [166]. In the context of AD, it has been moreover suggested that Aβ SO are internalised by microglial cells via TLR-signalling pathways [157]. Despite advances in our understanding of microglial function in the brain, two main questions in the context of AD remain unanswered: can microglia phagocytose Aβ and contribute to effective clearance and can they become progressively dysfunctional thereby contributing to the development of disease onset and progression?

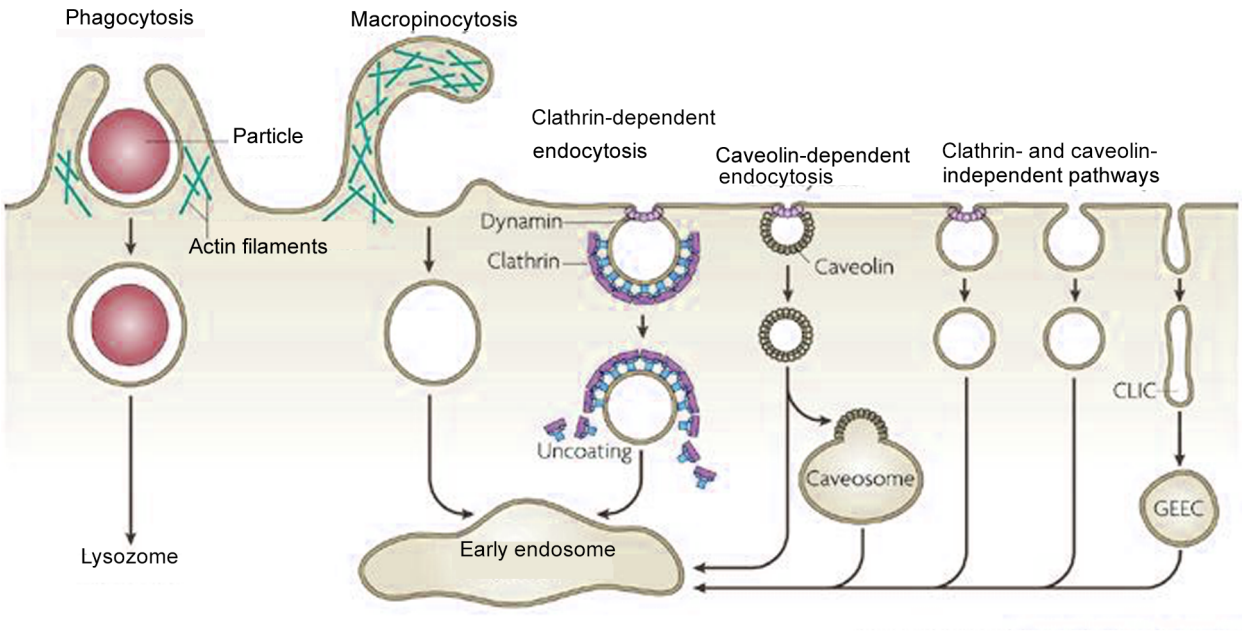

Figure 1.8: Schematic representation of the different pathways of cell entry (adapted from Mayor and Pagano [160]). The three main endocytic mechanisms, macropinocytosis, phagocytosis and clathrin-mediated endocytosis, are illustrated.

1.4 Chaperones and aggregation-modulating biomolecules

In the crowded environment of the cell, many proteins rely on so-called molecular chaperones, special kinds of ubiquitous proteins, which enhance folding efficiency by reducing the likelihood of competing reactions, such as aggregation [9, 33]. Chaperones are present in all types of cells and cellular compartments and while some chaperones interact with nascent polypeptide chains emerging

from the ribosomes, others guide the translocation to different cellular compartments [33,167]. In the context of AD, the chaperone, Clusterin (Clu) has been repeatedly linked to the disease by means of various experimental strategies that range from large-scale GWAS to molecular-level toxicity analyses [81,168,169]. Chaperones are not the only proteins that have disease-modulating properties. As a major player of innate immunity, the "old" antimicrobial enzyme lysozyme (Lys) is experiencing a renaissance in the Alzheimer's community as a growing body of research suggests a beneficial effect of this endogenous protein in AD [170,171]. Lysozyme, like serum amyloid P, can be classified as an aggregation-modulating biomolecule. These are biomolecules that can associate with aggregates but do not have the potent capacity as chaperones to block the kinetics of aggregation.

This work sets out to investigate how clusterin and lysozyme interact with Aβ SO and provide new insights into how this may influence cellular uptake and trafficking.

1.4.1 Clusterin

Clusterin (Clu, also known as apolipoprotein J and SP-40,40) is ubiquitously expressed in the brain and peripheral tissues, where it functions as a chaperone, facilitates the regulation of cellular apoptosis, and serves as a complement regulating factor [172–174]. Upon translation, the chaperone is excreted into the extracellular space. Post-translational modifications of the single-chain Clu create a heterodimeric glycoprotein through internal cleavage. The resulting two 40 kDa subunits, α and β, are linked by a unique five-disulphide bond motif [175,176]. Roughly 17-27 % of the 80 kDA protein is glycosylated [177]. Due to the high levels of glycosylation paired with areas of intrinsic disorder, it has not been possible to fully unravel the structure of Clu with conventional methods such as NMR, mass spectrometry, or X-ray crystallography. Interestingly, Stewart and colleagues were able to show that deglycosylation of Clu neither affects its secondary structure nor its chaperone activity [178].

The physiological concentration of Clu ranges from 0.1-3.6 µg/ml in the CSF, 35-105 µg/mL in human blood plasma, and up to 2-15 mg/mL in seminal plasma [179–181]. Clu is moreover a constituent of a variety of other biological fluids, such as tears, saliva, breast milk, and urine [182]. In the brain, Clu mRNA has been identified in astrocytes, neurons, and the ependymal cells that line the ventricles, and it has been associated with lipid transport in the brain along with ApoE [183]. Clu displays high sequence homology (70-80 %) across a large number of mammalian species, which implies that the biological functions of Clu are highly conserved and essential to the organism [184].

In its role as an extracellular chaperone, Clu has been shown to preferentially bind to partially unfolded proteins, preventing their aggregation on the "off-folding" pathway [176,185]. Strikingly, Clu

has the capability to bind to and interact with both, Aβ1-40 and Aβ1-42 peptides, alter Aβ aggregation, and increase Aβ clearance from the extracellular space [98, 186]. These earlier observations were supported by results from a large-scale GWAS, which identified CLU as a risk factor of late-onset AD [81]. While Clu weakly associates with Aβ monomers, it has a higher binding affinity for SO than for fibrils [168, 187, 188]. Interestingly, a multi-centre patient study of subjects with AD of different severity identified Clu as an indicator of baseline disease severity and a predictor of fibrillar Aβ burden. These findings were reproduced in an APP/PS1 transgenic mouse model [189]. In line with these reports, it has been shown that Clu-depleted plasma displays a high susceptibility to protein aggregation *in vitro* [190].

The exact function of Clu is still unknown, however, given its elevated expression at fluid-tissue interphases, it is suspected that Clu plays a role in cell membrane protection from fluids such as bile, urine, gastric, and pancreatic juices [175]. Convergent genetic, cellular, and molecular data furthermore associate Clu with aggregate uptake by targeting misfolded proteins for receptor-mediated endocytosis and intracellular lysosomal degradation [168]. Additionally, it was shown that *in vitro*, Clu protects against Aβ1-40 neurotoxicity and prevents Aβ1-42 peptide aggregation suggesting a protective role of Clu in AD [169, 191].

1.4.2 Lysozyme

Lyoszme is a naturally occurring glycosidase (14.7 kDa), which takes part in the degradation of bacterial cell walls [170]. It is a globular protein consisting of 130 amino acids and belongs to the family of c-type lysozymes. As such, it is part of the innate immune system and exerts its anti-microbial, anti-inflammatory, and anti-oxidant activity in various tissues and fluids including the liver, spleen, milk, tears, saliva and the CSF [192–194]. Lys is secreted by epithelial cells, macrophages, astrocytes, as well as microglia [193].

Besides its anti-microbial activity, several lines of research have surfaced that suggest a protective role for the biomolecule Lys in AD. *In vitro* studies carried out by Luo et al. demonstrated that Lys inhibits Aβ1-40 aggregation via binding to the monomeric form of Aβ1-40, while it has also been shown to prevent the aggregation of Aβ17-42 [171, 195]. The over-expression of Lys in a Drosophila melanogaster model of AD was shown to reduce Aβ cytotoxicity, which was manifested by increased survival and locomotor activity of the AD flies [196]. Moreover, the level of Lys in the cortex and hippocampus of transgenic AD mice was shown to correlate with the plaque-pathology in these areas, while Lys is upregulated in human brain tissue and in the CSF from AD patients [197]. Recent

internalisation studies in the neuroblastoma cell line SH-SY5Y by Sandin et al. (unpublished work) demonstrated that Lys inhibits the uptake of oligomeric Aβ1-42 and prevents cell death when added post-oligomerisation [198]. These experiments formed the basis for the studies outlined in Chapter 5 with the aim of determining whether Lys displayed similar effects when interacting with microglia cells.

As neuroinflammation is regarded as a key contributor to the progression of AD, it is important to gain a broader understanding of the interactions between toxic aggregate species and the players of innate immunity. In particular, studies of such interactions will provide insights into the question of "When does the neuroinflammatory response to intruders becomes a chronic problem?" and it will ultimately inform the development of effective interventions.

1.5 Objectives and outline of the thesis

This thesis reports a comprehensive study of the influence of extracellular biomolecules on Aβ1-42 SO internalisation and trafficking by microglial cells. Different imaging techniques including confocal microscopy and flow cytometry are used with the aim to elucidate how the chaperone clusterin and antimicrobial enzyme lysozyme influence the Aβ1-42 SO-microglia interaction. Uptake and trafficking behaviour in the absence and presence of aforementioned biomolecules are studied at disease-relevant concentrations. Mammalian microglia cells were chosen for this line of experiments as a model system to further explore how Aβ1-42 SO confer cellular toxicity at different time points and how this process is affected by the presence of the different biomolecules.

Following the review of the relevant literature in this chapter, Chapter 2 outlines essential materials and methods used in this work. In Chapter 3, Aβ1-42 is characterised and suited controls are established. In Chapter 4, the uptake and trafficking of Aβ1-42 SO by microglia cells in the absence and presence of Clu and its effect on the microglial pro-inflammatory response are investigated. In Chapter 5, the uptake and trafficking of Aβ1-42 as well as the effect of Lys on these processes are explored with special emphasis on membrane interaction. Finally, in Chapter 6, topics for future work are discussed and conclusions are drawn.

2

MATERIALS AND METHODS

All chemicals and reagents were purchased from Sigma Aldrich (Dorset, UK) unless otherwise specified.

2.1 Aβ1-42 oligomer formation

2.1.1 HiLyte™ Fluor 488- or TAMRA-labelled Aβ1-42 preparations

Human Aβ1-42 labelled with HiLyte™ Fluor-488 and 5-Carboxytetramethylrhodamine (TAMRA) were purchased from AnaSpec Inc. (Fremont, CA, USA). The fluorophore-labelled Aβ1-42 was dissolved in 1 % ammonium hydroxide (NH_4OH) (final peptide concentration of 2 mg/mL) and diluted to 0.5 mg/mL in low-salt phosphate buffer (LSPB; 10 mM Na_2HPO_4, 10 mM NaCl, pH 7.4). The peptide solution was then aliquoted into working volumes of 10 µL, flash frozen in liquid nitrogen and stored at -80° C for later use. For oligomer formation, aliquots were thawed and incubated for 12 h at 4° C.

2.1.2 Unlabelled Aβ1-42 preparation

Unlabelled Aβ1-42 peptide (1 mg; AnaSpec Inc.) was dissolved in 1 mL of trifluoracetic acid (TFA) while kept on ice. The peptide solution was then sonicated for 30 s using a Bandelin SONOREX™ bath sonicator and the sample was flash frozen in liquid nitrogen. The TFA was subsequently removed by lyophilisation (12 h, room temperature (RT)). The lyophilised sample was then dissolved in 1 mL of cold 1,1,1,3,3,3,-Hexafluoro-2-propanol (HFIP) and incubated (10 min, on ice). Upon incubation, the peptide solution was divided into aliquots, dried by rotary evaporation using a Savant™ SpeedVac™ Concentrator (Fisher Scientific UK Ltd., Loughborough, UK), and stored at -80° C for later use. Two 10 µL samples were sent to the Department of Biochemistry (Cambridge, UK) for

quantitative amino acid analysis to confirm peptide concentration. Alternatively, the peptide concentration was determined using the colometric Pierce® bicinchoninic acid (BCA) Protein Assay Kit (Fisher Scientific UK Ltd., Loughborough, UK), which enables the detection of Cu^{2+} reduction to Cu^{1+} by protein in an alkaline medium. BCA reacts with the reduced (cuprous) cation yielding a purple-colored reaction product (BCA/copper complex) which is water soluble and shows a strong linear absorbance at 562 nm with increasing protein concentration.

For oligomer formation, the lyophilised peptide was dissolved in dimethyl sulfoxide (DMSO; Thermo Fisher Scientific, Paisley, UK) to a concentration of 5 mM. The peptide in DMSO was subsequently diluted with LSPB to reach a final concentration of 100 µM. Samples were incubated for 12 h at 4° C for soluble oligomer (SO) formation.

2.1.3 Recombinant Aβ1-42 preparation

Recombinant Aβ1-42 was prepared as described by Walsh and colleagues [199]. The lyophilised samples of recombinant Aβ1-42 used in this report were kindly provided by Ewa Klimont (University of Cambridge, UK).

2.1.4 Transmission electron microscopy (TEM)

To verify that oligomer formation took place, samples were prepared for transmission electron microscopy (TEM). After completion of the oligomer formation reaction, oligomer samples were diluted 1:7 in LSPB, and samples (5 µL) were applied to Formvar-coated copper grids (TAAB Laboratories Equipment Ltd., Aldermasten, UK) (2 min, RT). The samples were carefully removed using Whatman™ filter paper (GE Healthcare, Little Chalfont, UK) followed by deionised water (dH_2O) washes (2x, 2 min each). The samples were then stained with 2 % weight/volume (w/v) uranyl acetate in dH_2O (2 min, RT) and left to dry for imaging.

Image analysis was performed on a Philips FEI™ Technai G2 TEM (Cambridge Advanced Imaging Centre, University of Cambridge, UK) using the SIS Megaview II Image Capture system (Olympus, Muenster, Germany).

2.1.5 Sodium dodecyl sulphate (SDS) polyacrylamide gel electrophoresis (PAGE)

Each batch of newly prepared Aβ1-42 was moreover tested for its ability to form oligomers via sodium dodecyl sulphate (SDS) polyacrylamide gel electrophoresis (SDS-PAGE) using pre-cast Novex® NuPAGE® 4-12 % Bis-Tris protein gels (Thermo Fischer Scientific) according to the manufacturer's protocol with the appropriate standard protein ladders. Proteins were transferred from the gel to a

polyvinylidene difluoride (PVDF) membrane via an iBlot® gel transfer device using the default settings (Thermo Fisher Scientific). Upon transfer, the PVDF membrane was blocked in 1 % (w/v) bovine serum albumin (BSA; Jackson ImmunoResearch Europe Ltd., Suffolk, UK) in phosphate buffered saline (PBS; 18 h, 4° C) with gentle agitation and then washed with 0.05 % (v/v) Tween20 (NBS Biologicals Ltd., Huntingdon, UK) in PBS (3x, 10 min each). Primary and secondary antibodies used for staining were prepared in 0.5 % (w/v) BSA in 0.05 % (v/v) Tween20 in PBS. The membrane was incubated (18 h, 4° C) with gentle agitation in anti-amyloid β antibody, clone W0-2 (Millipore Ltd., Livingston, UK, MABN10, 1:1000) and washed with wash buffer (3x, 10 min each) followed by incubation with an appropriate Alexa Fluor (AF) secondary antibody (Thermo Fisher Scientific, 1:5000, 2 h, RT). The membrane was then washed with wash buffer (3x, 10 min each) and imaged with a Typhoon variable-mode imager (GE Healthcare) at 500 V.

2.1.6 Aβ aggregation kinetics

Fibril formation of 2 µM recombinant, monomeric Aβ1-42 was investigated using the well-established thioflavin-T (ThT)-based kinetics assay [200]. Aβ1-42 samples were prepared in the absence and presence of lysozyme (Lys) or clusterin (Clu) at ratios of 2:1, 1:1, 1:2 and 1:5 molar equivalents (Aβ-to-Lys) or 10:1 molar equivalents (Aβ-to-Clu). Samples were prepared in triplicates in 20 mM sodium phosphate buffer, pH 8, with 200 µM EDTA at 37° C using Eppendorf® LoBind microcentrifuge tubes for preparation on ice. Samples were carefully transferred to a 96-well half-area plate of black polystyrene with a clear bottom and polyethylene glycol (PEG) coating (Corning 3881, Corning Inc. Life Sciences, St. Davids, UK) and ThT fluorescence was measured under quiescent conditions using bottom-optics in a plate reader (Fluostar Omega or Fluostar Optima from BMG Labtech, Aylesbury, UK). The reaction was initiated by incubating the plate at 37° C, excitation was performed at 440 nm and the emission intensity was recorded at 480 nm.

2.2 Clusterin preparation

2.2.1 Unlabelled clusterin

Human clusterin (Clu) was provided by Prof. Mark Wilson (University of Wollongong, Australia) and it was purified in his laboratory as described by Wilson and Easterbrook-Smith [201]. Briefly, clusterin was purified from human serum by affinity chromatography using monoclonal antibody G7 (MAb G7). Tandem G7 and 41D monoclonal anti-Clu immunoaffinity columns were first washed with PBS containing 0.1 % (w/v) azide (PBS/Az) followed by 0.1 % (v/v) Triton™ X-100 in PBS

before being re-equilibrated in PBS/Az. Next, the columns were washed with 200 mM sodium acetate in 500 mM NaCl, pH 5, prior to eluting the bound protein using 2 M guanidine hydrochloride (GdnHCl) in PBS. The eluate was dialysed against 20 mM Tris/Az, pH 8.0, loaded onto a fast flow column and the bound protein was collected in 2 mL fractions applying a continuous 0-0.7 M NaCl gradient delivered over 80 min. The purity of the collected fractions was assessed by SDS-PAGE and Western blot analysis by our Australian colleagues. Purified Clu was subsequently dialysed against PBS/Az for storage.

Prior to use, the azide added for storage was removed via dialysis in 1 L PBS (12 h, 4° C) using Slide-A-Lyzer® MINI Dialysis Units (Thermo Fisher Scientific). The clusterin concentration was determined on a NanoDrop 2000 (Thermo Fisher Scientific) using an extinction coefficient of 37525 $M^{-1}cm^{-1}$ at 280 nm upon which the sample was aliquoted, flash frozen in liquid nitrogen and stored at -20° C for later use.

2.2.2 Labelled clusterin

Clusterin was labelled with N-hydroxysuccinimidyl ester forms of AF-647, which was kindly provided by Dr. Ana Bernardo-Gancedo (University of Cambridge, UK). For the labelling reaction, clusterin (at approximately 0.7 mg/mL) was incubated (1 h, RT) with a 10-fold molar excess of the functionalised fluorophore (added from a 10 mM stock in DMSO). After incubation, any unconjugated dye was removed by buffer exchange into PBS using a PD-10 column. The final protein concentration and labelling efficiency were assessed on a NanoDrop 2000 at 280 nm using an extinction coefficient of 250,000 $M^{-1}cm^{-1}$. The labelled clusterin was aliquoted and stored at -20° C for later use.

2.3 Lysozyme preparation

Lysozyme was expressed in Pichia pastoris and purified with the help from Dr. Ana Bernardo-Gancedo as described by Johnson et al. [202]. Specifically, the wild-type human lysozyme gene was inserted into a pPIC9 expression vector followed by transformation into P. pastoris GS115 by electroporation. The cells were subsequently plated on regeneration dextrose agar plates to produce single-clone colonies. Colonies were screened for lysozyme activity with a hydrolase activity assay using Micrococcus lysodeikticus as described by Lee and Yang [203].

Protein expression was initiated by inoculating buffered minimal glycerol (BMG) precultures with P. pastoris cells containing the lysozyme gene. Precultures were incubated for 36 h at 30° C with orbital

shaking in order to increase aeration. Aliquots (2 mL) of the preculture cell suspension were then used to inoculate 200 mL of BMG medium in 2 L Erlenmeyer flasks. The cultures were subsequently incubated for 28 h (30° C and 230 rpm) upon which they were centrifuged in sterile centrifuge bottles at 1500g for 5 min. The supernatant was discarded and the cells were resuspended in 400 mL of buffered minimal methanol (BMM) and incubated (30° C and 230 rpm) to induce protein expression. Methanol (2 mL) was added to the culture every 24 h for a total of 72 h. The methanol-containing cultures were then centrifuged (1500g at 4° C for 5 min) and the supernatant was stored at 4° C, filtered (0.45 mm pore size), and purified using a cation-exchange (Poros 20 HS) column (Applied Biosystems, UK) on a Biocad 700E system (Applied Biosystems, UK). Lysozyme was eluted from the column by a linear gradient of NaCl solution (0-1M) and fractions were subsequently analysed by SDS-PAGE, dialysed against water and lyophilised. Lysozyme concentration was determined by measuring the absorbance at 280 nm using E1% for 1cm path length = 25.5.

2.4 Dot blot assay

For the dot blot assay, Aβ1-42 SO were prepared as previously described and applied to a Whatman™ nitrocellulose membrane (GE Healthcare). The membrane was blocked (2 h, RT) in 1 % (w / v) BSA/PBS and the membrane was incubated with primary and secondary antibodies prepared in 0.5 % (w/v) BSA in 0.05 % (v/v) Tween20 in PBS. The membrane was incubated (18 h, 4° C) with gentle agitation in anti-amyloid β antibody, clone W0-2 (Millipore Ltd., Livingston, UK, MABN10, 1:1000) and washed with wash buffer (3x, 10 min each) followed by incubation with an appropriate Alexa Fluor (AF) secondary antibody (Thermo Fisher Scientific, 1:5000, 2 h, RT). The membrane was then washed with wash buffer (3x, 10 min each) and imaged with a Typhoon variable-mode imager (GE Healthcare) at 500 V.

2.5 Cell cultures

All cells were cultured in Greiner T-75 tissue culture treated flasks at 37° C in a humidified atmosphere of 5 % carbon dioxide (CO_2) and 95 % air.

2.5.1 EOC 13.31 microglial and LADMAC cells

The microglia cell line EOC 13.31 (ATCC® CRL-2468™) and LADMAC cell line (ATCC® CRL-2420™) were purchased from the American Type Culture Collection (Manassas, VA, USA). LADMAC cells were cultured for 10 days in Eagle's Minimum Essential Medium (EMEM) supplemented with 1 %

(v/v) of 200 mM L-glutamine (Thermo Fisher Scientific), 1 % (v / v) of 100 mM sodium pyruvate, and 10 % (v/v) fetal bovine serum (FBS) purchased from PAA (GE Healthcare). The conditioned medium was then collected, centrifuged (5000 rpm, 4° C) in a Hettich Rotina 38R centrifuge (DJB labcare, Newport Pagnell, UK), filtered through a 0.2 µm filter and stored at -20° C for later use as an EOC supplement. New flasks were seeded at 2x 10^5 cells/mL.

EOC 13.31 cells were cultured in Dulbecco's Modified Eagle Medium (DMEM; Thermo Fisher Scientific) enriched with 20 % (v/v) conditioned LADMAC medium, and 10 % (v/v) FBS. When confluent, medium was discarded and cells were gently removed from the flask using a Corning® Costar® cell scraper (Corning Inc., St. Davids, UK) prior to splitting at a 1:5 ratio for continued growth.

2.6 Aβ1-42 oligomer cell treatment protocols

2.6.1 3-[4,5-dimethylthiazol-2-yl]-2,5- diphenyltetrazolium bromide (MTT) assay

To verify that the treatment conditions previously used by Sharon Hook in SH-SY5Y cells were also suitable for EOC 13.31, cells were incubated with different concentrations of Aβ1-42 SO. A 3-[4,5-dimethylthiazol-2-yl]-2,5- diphenyltetrazolium bromide (MTT) assay was performed. The MTT assay measures cellular metabolic activity, which can be an indicator for proliferation, viability, and cytotoxicity. MTT is a water-soluble tetrazolium salt. Living cells with active metabolism convert the dissolved MTT to an insoluble formazan product inducing a colour change from yellow to purple. The measured absorbance is indicative of the concentration of converted dye equating to metabolic activity [204].

EOC 13.31 cells were plated in triplicates at a density of 20,000 cells/well in a 96-well plate and incubated in culture medium (24 h, 37° C). Cells were then exposed to 1 µM, 5 µM, and 10 µM Aβ1-42 (30 min, 37° C) in serum-free medium. Cells were treated with 0.1 % (v/v) Triton™ X-100 as a positive control, (10 min, 37° C) and with medium + LSPB (corresponding to the LSPB concentration of the 1 µM Aβ1-42 SO condition) as a negative control. MTT stock solution (5 mg/mL) was added to each well at 1/10th the original culture volume and incubated (4 h, 37° C). Next, the cells were incubated (1 h, 37° C) in 100 µL stop solution (20 % (w/v) SDS, 50 % (v/v) N,N-dimethylformamide, pH 4.7) and absorbance was measured at 570 nm with background subtraction at 690 nm using a CLARIOstar® multimode microplate plate reader. Cellular metabolic activity is expressed as the mean SD of n = 3 biological repeats. Statistical significance was determined using an unpaired t-test where *, $P < 0.05$; **, $P < 0.005$; ***, $P < 0.0005$, ****, $P < 0.00005$.

2.6.2 Cell treatment protocol for Aβ1-42 and clusterin

HiLyte™ Fluor 488-labelled Aβ1-42 oligomers were prepared as described in Section 2.1.1 and 1 µM SO were added to the cells unless otherwise stated. All experiments were performed at a SO-to-clusterin submolar ratio of 10:1 in serum-free cell medium for 30 min at 37° C. For the clusterin pre-treatment condition, cells were exposed to clusterin for 30 min, after which SO were added for an additional 30 min and subsequently washed (2x) with PBS. For the negative control (no-treatment condition), cells were incubated for 30 min in serum-free medium with LSPB (reflecting the amount of LSPB introduced in the Aβ1-42 SO condition).

2.6.3 Cell treatment protocol for Aβ1-42 and lysozyme

TAMRA-labelled Aβ1-42 SO were generated as stated in section 2.1.1 and 1 µM SO were added to the cells unless otherwise stated. All experiments were performed at a SO-to-lysozyme molar ratio of 1:2. Cells were exposed to the respective treatment conditions for 1.5 h in serum-free cell medium at 37° C, followed by PBS washes (2x). The cells were subsequently incubated in serum-free cell medium for another 30 min. For the lysozyme pre-treatment condition, cells were exposed to lysozyme for 30 min prior to the SO treatment described above. For the negative control (no-treatment condition), cells were incubated for 30 min in serum-free medium with LSPB (reflecting the amount of LSPB introduced in the Aβ1-42 SO condition).

2.7 Fluorescent staining and imaging

2.7.1 Cell preparation for fluorescent staining

The oligomer uptake experiments in the presence and absence of clusterin were performed in the microglia cell line EOC 13.31. EOC 13.31 cells were counted with a Countess™ automated cell counter (Bio-Rad, Hemel Hempstead, UK) and plated on ethanol-cleaned, fibronectin-coated 22x22 mm coverslips (Thermo Fisher Scientific Gerhard Menzel, Braunschweig, Germany) at a density of 200 cells/mm^2. The coverslips were placed in Corning® Costar® 6-well plates (Corning Inc.) for incubation in culture medium (24 h, 37° C). Next, cells were fast-washed (1x) with Dulbecco's Phosphate Buffered Saline (DPBS) and treated with serum-free culture medium containing 1 µM HiLyte™ Fluor 488-labelled Aβ1-42 oligomers and 0.1 µM clusterin (30 min, 37° C) where applicable. Alternatively, cells were treated with serum-free culture medium containing 0.5 µM TAMRA-labelled Aβ1-42 oligomers and 1 µM lysozyme (1.5 h, 37° C), followed by 2 PBS washes and incubation in serum-free

cell medium for 30 min.

2.7.2 Staining protocols for selected immunofluorescent antibodies and dyes

Cells were fast-washed in DPBS (1x) and fixed with 3.7 % (v/v) paraformaldehyde (PFA) solution (Thermo Fisher Scientific) in PBS (15 min, 37° C). After fixation, cells were washed in PBS (3x) and permeabilised with 0.2 % (v/v) Triton™ X-100/PBS (5 min, RT) followed by PBS washes (3x). Cells were blocked in 1 % (w/v) BSA (Jackson ImmunoResearch Europe Ltd.) in PBS (30 min, RT). The primary and secondary antibodies used for staining were prepared in 0.5 % (w/v) BSA in 0.05 % (v/v) Tween20 (NBS Biologicals Ltd.) in PBS and include the lysosomal-associated membrane protein 1 (LAMP1) (Abcam, Cambridge, UK, ab24170, 1:500) and cathepsin D (Abcam, ab72915, 1:200) as well as the fluorescent stain Hoechst (Thermo Fisher Scientific, 1:7000). Cells were incubated with the primary-antibody solution (1 h, RT) and washed (3x) with wash buffer (0.05 % v/v Tween20 in PBS) followed by incubation with the respective secondary antibody (2 h, RT). Once the secondary incubation was completed, cells were washed with wash buffer (3x). All fluorescent secondary antibodies used were labelled with Alexa Fluor dyes (Thermo Fisher Scientific, 1:500).

For incubation with the membrane stain, wheat germ agglutinin (WGA) (Thermo Fisher Scientific), a 1:500 (v/v) dilution of WGA in Hank's Balanced Salt Solution (HBSS) (Thermo Fisher Scientific) was applied to oligomer- and clusterin-treated cells (10 min, 37° C). Cells were then washed with HBSS (2x), fixed with PFA as described above, washed with HBSS (3x), and stained with Hoechst (5 min, RT).

For visualisation of acidic organelles, cells were incubated (30 min, 37° C) with LysoTracker® Red DND-99 (Thermo Fisher Scientific, L7528, 1:20,000) diluted in pre-warmed (37° C) serum-free culture medium together with the respective oligomer and clusterin treatment. Cells were then fixed with PFA and stained with Hoechst as described above.

2.7.3 Confocal microscopy and image processing

Coverslips were mounted on microscope slides (Corning Inc.) using 10 µL ProLong® Gold Antifade Mountant (Thermo Fisher Scientific). Images were acquired on a Leica TCS SP8 (Cambridge Advanced Imaging Centre, University of Cambridge, UK) using a 63x HCX PL APO CS NA1.4 oil objective and LAS X software (Leica Microsystems, Wetzlar, Germany). A typical 2D frame scan acquired in this work consist of 512x512 pixels. Whenever two or more dyes were used in the sample, care was taken to move detection and emission windows of respective dyes as far apart as possible,

while sequential scanning was used to acquire images.

To determine the corrected total cell fluorescence (CTCF) of microglial cells upon exposure to HiLyte™ Fluor-488 Aβ1-42 SO, acquisition settings were established using the positive control (SO-exposed cells). Once established, the settings were kept constant between samples to allow for later quantitative comparability. The exposure time, gain and offset were adjusted to use the entire dynamic range of the detectors. Importantly, image saturation was controlled for using the autohistogram display of the microscope.

Images were further processed with ImageJ software (National Institute of Health, Bathesda, USA) producing overlaid images of the different channels. To determine the intensity of the labelled oligomers within the cells, an outline was drawn around each cell. Area, mean fluorescence, and integrated density were then measured and the corrected total cell fluorescence (CTCF) was calculated using the following equation [205]:

CTCF = integrated density - (area of selected cell $\times$ *mean fluorescence of background readings)*

Fluorescence was compared across cell lines as per the Mann-Whitney test, where *, $P < 0.05$; **, $P < 0.005$; ***, $P < 0.0005$. Data points represent $n \geq 31$ cells pooled from n = 3 independent experiments. To ensure proper visibility of immunofluorescent stains in the printed version of this report, all shown images have been uniformly contrast enhanced post analysis.

For the morphology analysis, the top and bottom planes of WGA-stained microglia cells were manually identified based on visibility of the WGA stain. Once the cell boundaries had been determined, the first and last position of the z-stack were set accordingly and images were acquired based on optimal step size calculated by the image acquisition software. The total number of acquired planes was then divided by 2 to identify the centre plane, which was used to score cells based on "elongated", "intermediate", and "rounded" morphology.

Colocalisation of fluorescently labelled Aβ1-42 SO and lysotracker, LAMP1 or Cathepsin D, was analyzed using the Coloc2 plugin for ImageJ. Prior to colocalisation analysis, background subtractions were performed for the channels of interest. ROIs were selected on a per-cell basis and Costes randomization test was set to 100. The degree of colocalisation is illustrated based on Pearson's correlation coefficient, which estimates the degree of overlap of the red and green fluorophores [206]. Pearson's correlation coefficient has range of "+1" (perfect correlation) to "−1" (perfect but negative

correlation) with 0 denoting the absence of a relationship and was chosen here given it is unaffected by additive offset. A minimum of n = 10 cells were analyzed per treatment condition from n = 3 independent experiments. Data were tested for normality and treatments were compared to the "SO only" condition via an unpaired t-test where *, $P < 0.05$; **, $P < 0.005$; ***, $P < 0.0005$, ****, $P < 0.00005$.

2.8 Enzyme-linked immunosorbent assay (ELISA) to assess TNFα release

To assess the effects of Aβ1-42 oligomers in the presence and absence of clusterin on the release of selected cytokines by microglia cells, enzyme-linked immunosorbent assays (ELISAs) were carried out. Specifically, Ready-Set-Go!® ELISA kits (eBioscience, Ltd., Altrincham, UK) sensitive to mouse tumor necrosis factor alpha (TNFα) and mouse interleukin 1-beta (IL-1β) were used hereinafter.

EOC 13.31 cells were counted with a Countess™ automated cell counter and plated on Corning® Costar® 96-well plates (Corning Inc.) in culture medium at a density of $2x10^4$ cells/well (24 h, 37° C). Cells were fast-washed with DPBS and treated with either 2 µM Aβ1-42 oligomers diluted in serum-free culture medium (for oligomer preparation see section 2.1.2), 0.2 µM clusterin, 2 µM oligomers and 0.2 µM clusterin simultaneously (8 h or 24 h, 37° C), or they were pretreated with 0.2 µM clusterin (30 min, 37° C) upon which oligomers were added (7.5 h or 23.5 h, 37° C). The same experiment was carried out using 4 µM oligomers and 0.4 µM clusterin respectively. Known to induce a strong immune response in normal mammalian cells, the endotoxin lipopolysaccharide (LPS) was included at a concentration of 25 ng/mL as a positive control for cytokine release. For the negative control, cells were incubated in serum-free culture medium (8 h or 24 h, 37° C). Each treatment was performed in triplicates. Once the incubation was completed, the medium of the triplicates was combined and centrifuged (14,000 rpm, 15 min, 4° C). The supernatant was collected, flash frozen in liquid nitrogen, and stored at -80° C until further use.

For the ELISA, Nunc Maxisorp® 96-well plates were used. The ELISA was carried out according to the manufacturer's protocol. To increase the effectiveness of the washes, the maximum amount of recommended washes and wash times were applied at all times. Absorbance was measured on a CLARIOstar® multimode microplate plate reader (BMG LABTECH Ltd., Aylesbury, UK) at wavelengths of both 450 nm and 570 nm. The 570 nm reading was then subtracted from the 450 nm reading prior to data analysis. The concentration of released TNFα was compared to the SO + Clu condition using a two-sample t-test. Data represent n = 3 ± SD replicates. The results are representative of n = 2 experiments. **, $P < 0.005$.

2.9 Flow cytometry

The interaction of different Aβ1-42 aggregation forms with EOC 13.31 cells in the absence and presence of clusterin or lysozyme was quantified by flow cytometry. The cells were removed from the tissue culture flask by gentle scraping. Cells were then counted with a Countess™ automated cell counter (Bio-Rad), seeded in serum-free EOC medium (see section 2.4) at a density of 0.5x 10^6 cells in a Corning® Costar® 12-well plate (Corning Inc.) and incubated for 24 h at 37° C.

Upon incubation, the medium was changed to serum-free EOC medium containing either recombinant mouse low density lipoprotein receptor-related protein-associated protein 1 (LRPAP) protein (0.25 µM, RD Systems, Abingdon, UK), Fucoidan (100 µM) or an equal volume of LSPB as a negative control (30 min, 37° C). Cells were washed with PBS (2x) and treated with either 2 µM HiLyte™ Fluor Aβ1-42 monomers, SO, or 2 µM TAMRA-labelled Aβ1-42 monomers, or SO in the presence and absence of clusterin (10:1 Aβ1-42-to-clusterin molar ratio) or lysozyme (1:2 Aβ1-42-to-lysozyme molar ratio) for 0.5 h and 1.5 h respectively, unless otherwise stated. After incubation, cells were washed with PBS (2x), collected into Eppendorf® tubes by gentle scraping and stored on ice until analysis with an Attune NxT Flow Cytometer (Thermo Fisher Scientific). The gating was set around control cells that had not been exposed to Aβ-TAMRA. Further assessment followed using the software FlowJo™ v10.6.0 (BD Life Sciences, Franklin Lakes, NJ, USA). Analysis of microglial cells exposed to TAMRA-labelled SO in the absence and presence of Lys was carried out on data from n = 3 independent experiments. A Kruskal-Wallis test was performed, where *, $P < 0.05$ is considered statistically significant. For the flow cytometry analysis of microglial cells exposed to TAMRA-labelled SO in the absence and presence of Lys and the receptor inhibitors LRPAP and Fucoidan, data are expressed as the percentage of the CTRL condition. Data of $n \geq 2$ independent experiments were analysed using multiple t-tests to compare the inhibitor effects to the CTRL group of respective treatment conditions, where *, $P < 0.05$; **, $P < 0.005$; ***, $P < 0.0005$.

2.10 Immunoprecipitation assay

To assess whether lysozyme and Aβ1-42 formed stable complexes under different aggregation conditions, Dynabeads™ His-Tag Isolation and Pulldown beads, as well as Dynabeads™ M-270 Streptavidin beads were used (Thermo Fisher Scientific). An Invitrogen DynaMag™-Spin magnet was used to separate beads from solutions throughout the experiment. All reactions were performed in

Eppendorf® LoBind microcentrifuge tubes. Aggregated Aβ1-42 solutions (10 µM, 100 µL total volume) were prepared and incubated with lysozyme at a 1:2 (Aβ-to-lysozyme) molar ratio (37° C or RT where indicated, 1.5 h). The immunoprecipitation assay was performed according to the manufacturer's protocol. Briefly, the Dynabeads™ were resuspended and aliquoted into 50 µL working volumes. Aliquots were incubated with 5 µg His-tagged anti-lysozyme camelid antibody cAbHul-6 (kindly provided by Dr. Mireille Dumoulin, University of Liege, Belgium [207]) in 1x binding/wash buffer (prepared as 2x buffer: 100 mM sodium phosphate pH 8.0, 600 mM NaCl, 0.02 % (v/v) Tween-20) for 5 min RT with gentle agitation. After incubation, Dynabeads™ were washed 4x with 300 µL of the 1x binding/wash buffer and then incubated with 100 µL Aβ1-42/lysozyme solution prepared in 1x pull down buffer (prepared as 2x buffer: 6.5 mM sodium phosphate pH 7.4, 140 mM NaCl, 0.02 % (v/v) Tween-20) at RT for 10 min with gentle agitation. Dynabead™/protein solutions were washed four times with 300 µL 1x binding/wash buffer. To elute the protein complex, the beads were incubated in 50 µL urea (8 M) for 5 min at RT with gentle agitation. Beads were then removed using a magnet and eluted samples were analysed by western blotting (see section 2.1.5).

2.11 qPCR

EOC 13.31 cells were cultured until confluent and subsequently seeded in 6-well plates (Corning Inc.) at a density of 5x 10^5 cells/well. Cells were incubated in culture medium (24 h, 37° C), washed with DPBS, and treated with different concentrations of LPS in serum-free medium for 6 h and 24 h. Upon treatment, cells were washed with DPBS and 350 µL of the lysis buffer RLT Plus (QIAGEN, Manchester, UK) was added to each well. Cell treatment was performed in triplicates and subsequently, lysates were pooled, transferred to Eppendorf® tubes, and stored at -20° C for later analysis. RNA isolation was performed in collaboration with Zhen Du in Prof. Laura Itzhaki's Group (Department of Pharmacology, University of Cambridge, Cambridge, UK) using the RNeasy® Plus Micro Kit (QIAGEN) and all steps were performed according to the manufacturer's protocol. Subsequent qPCR was kindly performed by Zhen Du (Department of Pharmacology, University of Cambridge). The results are exploratory and representative of n = 1 experiment. To avoid amplification of genomic DNA, primers were designed so that they hybridize to different exons. The primer (origin) sequences and concentrations were as follows:

mouse TNFalpha forward: 117.4 µg, 17.6 nmol (HPLC purified)
5′ - GGTGCCTATGTCTCAGCCTCTT - 3′

mouse TNFalpha reverse: 89.3 µg, 12.4 nmol (HPLC purified)
5′ GCCATAGAACTGATGAGAGGGAG 3′

2.12 Membrane disruption assay

The membrane disruption assay was carried out as described by Flagmeier et al. [208]. Briefly, the extent of Aβ1-42 aggregate-induced Ca^{2+} entry into individual lipid vesicles was measured by means of change in fluorescence using total internal reflection fluorescence microscopy (TIRFM). The vesicles were composed of 1-palmitoyl-2-oleoyl-sn-glycero-3-phosphocholine (POPC) and biotinylated POPC (at a ratio of 100:1) filled with the Ca^{2+}-sensitive Cal-520 dye, which allows for detection of picomolar concentrations of Aβ1-42 oligomers. A total of 16 fields of view using a computer-controlled automatic microscope stage were imaged. The fluorescence signal before and after adding the samples was measured. In order to quantify the influx of Ca^{2+}, the cation-transporting ionophore ionomycin was added, which permits Ca^{2+} entry to saturation. The maximum fluorescence intensity was subsequently measured and the percentage of Ca^{2+} influx was determined using the formula:

$(F_{aggregate}\text{-}F_{blank})*100/\ (F_{ionomycin}\text{-}F_{aggregate})$, where F is the fluorescence.

Statistical analyses were carried out using GraphPad Prism version 8 (GraphPad Software, La Jolla, USA). The ROUT test was applied to identify and remove outliers from the datasets. The datasets were then tested for normality using the Shapiro-Wilk test and subsequently analysed using a one-way ANOVA with Dunnett's multiple comparisons test. Statistical significance is indicated by an asterix, where ****, $P < 0.00005$.

2.13 Statistical analysis

All data are expressed as a mean ± standard deviation (SD) unless otherwise indicated. Statistical analyses were carried out using OriginPro 9.3 (OriginLab Corporation, Northampton, MA, USA) or GraphPad Prism (La Jolla California USA). Datasets were tested for normality using the Shapiro-Wilk test. If datasets were not consistently normally distributed, the nonparametric Mann-Whitney test was applied to test for significant differences unless otherwise indicated. If datasets were normally distributed, the two-sample-t test was used unless otherwise stated. $P < 0.05$ was considered statistically significant. *, $P < 0.05$; **, $P < 0.005$; ***, $P < 0.0005$.

3

FORMATION AND CHARACTERISATION OF Aβ1-42 OLIGOMERS

3.1 Introduction and objectives

3.1.1 ADDLs for the study of Aβ SO toxicity

Over the last decades, increasing scientific evidence has emerged that links soluble oligomeric forms of the Aβ1-42 peptide, known as amyloid-derived diffusible ligands (ADDLs), to the neurodegenerative processes associated with AD. However, the accurate biophysical characterisation of ADDL preparations is impeded by the strong tendency of Aβ to self-associate, while factors such as ionic strength, temperature, and pH add additional complexity to the study of their behaviour. The challenges of studying the structure-toxicity relationship of Aβ SO is inherent to these characteristics - Aβ SO are transient in nature and readily convert into other conformations during amyloid oligomerisation and fibrillation, which results in a heterogeneous population of polymorphic, metastable Aβ SO.

ADDLs were first described in the context of a seminal study that demonstrated the spontaneous assembly of Aβ into small, soluble oligomeric species and shortly after their discovery, it was shown that these ADDLs could act as neurotoxins without the presence of amyloid fibrils [82]. Since their first association with neurotoxic events and the description of their formation by incubating Aβ1-42 in F12 media at low temperatures, the protocol has been refined leading to the ability to reproducibly generate two main conformers, namely SO (generated using low ionic strength solutions, such as F12 media or 10 mM phosphate with 10 mM NaCl and incubation at low temperature) and protofibrillar aggregates, which are larger in size (using higher ionic strength buffers, such as PBS with incubation at 37° C) [82, 132, 135]. A benefit of studying synthetic Aβ1-42 oligomers is that they are pure in the sense that no contaminating factors are present, which may not be the case when using oligomers

extracted from cells, tissues or biological fluids. Moreover, they have been the subject of extensive characterisation, making ADDLs a suited tool for the study of the effects of SO in AD [136]. However, it shall be pointed out that the Aβ1-42 oligomers produced using these protocols can continue aggregating during experiments and these techniques do not produce a homogeneous preparation of one oligomer species, but rather a mixture of oligomers in equilibrium. Effects of oligomer presence discussed herein can therefore not accurately be ascribed to a particular oligomeric species. Despite this limitation, observations between experimental variables can advance our understanding of the effect of presence and timing of Aβ SO as well as the effect of biological molecules and chaperones on these processes.

3.1.2 The use of HiLyte™ Fluor-488-labelled Aβ1-42 and TAMRA-labelled Aβ1-42 SO for SO visualisation

For experimental conditions that rely on visualisation of SO interaction with microglial cells, commercially available fluorescently-labelled Aβ1-42 peptides were used to form oligomers. Starting from HFIP-treated N-terminal fluorophore-labelled Aβ1-42 peptide, SO were formed under commonly used oligomer-forming conditions (see Section 2.2.1). Compared to amine-reactive conjugates, this method offers the advantage of not having to purify oligomers from free dye, while labelled peptide can be stored for oligomer formation as needed.

Herein, HiLyte™ Fluor-488 label and 5-Carboxytetramethylrhodamine (TAMRA) label were used where specified. HiLyte™ Fluor-488-labelled Aβ1-42 peptide has an absorbance / emission peak at 503 / 528 nm. The spectrum of HiLyte™ Fluor-488 closely resembles that of fluorescein (FITC), while it is more photostable [209]. TAMRA-labelled Aβ1-42 peptide has an absorbance / emission peak at 544 / 572 nm. The chemical structures of respective fluorophores are shown in Figure 3.1.

A) HiLyte™ Fluor 488

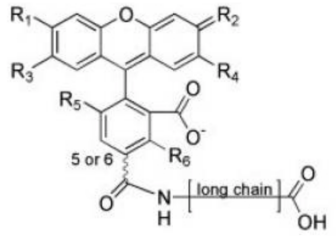

B) 5-Carboxytetramethylrhodamine

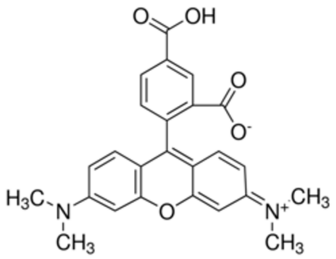

Figure 3.1: Chemical structures of HiLyte™ Fluor-488 and TAMRA. Figure adapted from [210].

While optical techniques are a powerful tool for the investigation of Aβ1-42 SO interactions with cells and other biomolecules, one major drawback is their need for fluorescence and the required modification of the original peptide system through fluorophore attachment. Even though the N-terminus is considered to be a loose end of the primary peptide structure and as such believed to not strongly contribute to its aggregation mechanisms nor structure formation, there are experimental studies that suggest otherwise [211, 212]. Using time-resolved and single-molecule fluorescence spectroscopy along with AFM and TEM, Waegele and colleagues demonstrated that the sizes of Aβ1-40 oligomeric species varied significantly depending on the chosen fluorophore, likely attributable to net-attractive, hydrophobic fluorophore-peptide interactions. At the same time, it was shown that amongst the fluorophores under investigation, HiLyte™ Fluor-488 displayed relatively low net-attractive interactions with the Aβ1-40 peptide making it a more suited labelling candidate compared to other fluorophores such HiLyte™ Fluor-647 [212]. Chafekar et al. reported that labelled oligomer and fibril preparations that were formed from a mixture of 2:1 unlabeled Aβ1-42-to-TAMRA labelled-Aβ1-42 showed comparable morphology to unlabelled assemblies as indicated by EM [213]. Mixtures of unlabelled-to-labelled Aβ1-42 at different ratios have been commonly employed in order to reduce the effects of fluorophore molecular structures on Aβ assembly and function [214, 215]. Here, we use 100 % HiLyte™ Fluor-488-labelled as well as TAMRA-labelled Aβ1-42 peptides in accordance with previous studies performed by our group in order to allow for comparability. However, we acknowledge the likely impact of the properties of fluorophores on transient Aβ aggregates, which

needs to be considered in the interpretation of obtained experimental data discussed in this work.

3.2 Identification of stable oligomeric species by SDS-PAGE and TEM

In a first step, it was established that the experimental conditions used in the formation of Aβ1-42 SO do indeed result in the desired Aβ1-42 species that should be clearly distinguishable from monomeric Aβ1-42 (see Fig. 3.2). As oligomeric preparations have been reported to result in SDS-stable Aβ species of different sizes, SDS-PAGE followed by Western blot were carried out using the anti-Aβ antibody W02. According to the manufacturer, this antibody binds residues 4-10 of human Aβ and has been shown to detect monomeric as well as oligomeric Aβ species [216]. Western blot analysis of the different monomer and SO preparations showed different-sized Aβ1-42 species for SO (lanes (B) and (C)) with predominantly monomeric and dimeric species, and to a lesser extent, also trimeric (12-16 kDa) species. The monomer preparation (lane A), yielded solely monomeric Aβ1-42 species (4 kDa), even though the signal was quite faint. Here, we show that our experimental conditions for Aβ1-42 SO preparation can generate Aβ1-42 species of higher molecular weight than monomeric Aβ1-42 and that the anti-Aβ antibody reliably detects Aβ1-42 species of different molecular weights.

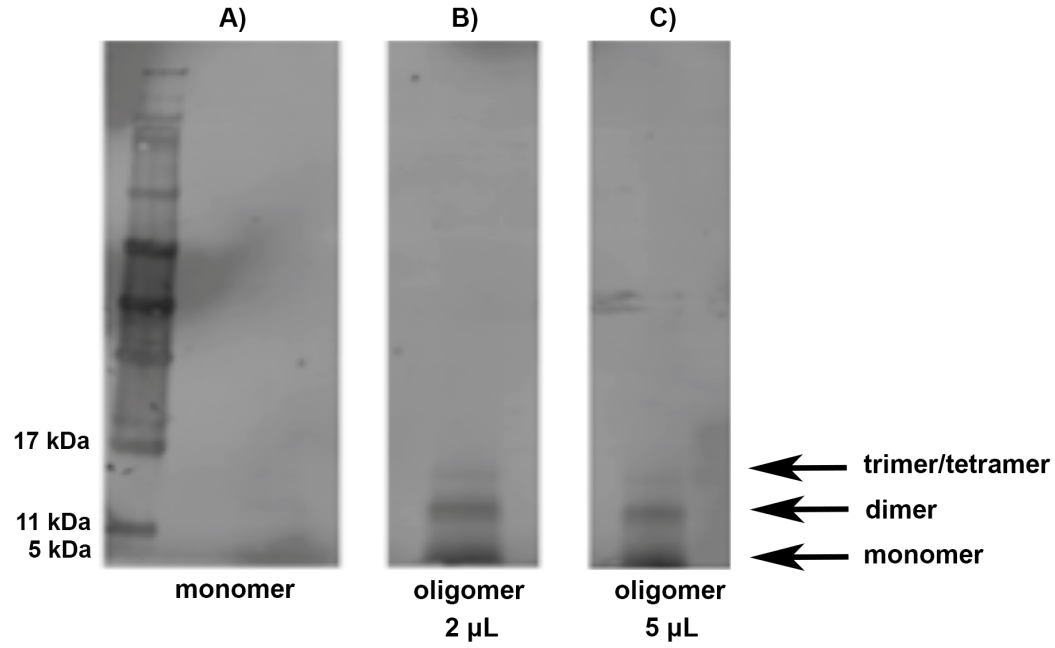

Figure 3.2: Aβ1-42 SO formed *in vitro*. Western blot analysis of unlabelled Aβ1-42 monomers (A), and different concentrations of SO: 2 µL sample (B) and 5 µL sample (C). Peptides were transferred to a PVDF membrane and incubated with the W02 anti-Aβ antibody.

Because SDS-PAGE can be prone to artefacts, the generation of Aβ1-42 SO was additionally confirmed by TEM. Briefly, TEM is a microscopy technique that applies a beam of high energy electrons,

which are transmitted through and interact with an ultra-thin specimen. Depending on the density of the material under investigation, the electrons are scattered in unique patterns, while some will disappear from the beam. Those electrons that hit the screen at the bottom of the microscope are aggregated to form an image. Due to its favourable electron scattering properties, the the stain uranyl acetate is commonly used with this technique in order to increase the contrast of the image. TEM is particularly suited for the visualisation of Aβ species as it allows for image acquisition at high resolution revealing information on size and width of the samples.

TEM preparations of unlabelled Aβ1-42 SO, HiLyte™ Fluor-488-labelled Aβ1-42, and TAMRA-labelled Aβ1-42 SO samples (see Fig. 3.3 (A, II), (B, I) and (B, II) each showed small aggregates of circular, doughnut-like, shape roughly 10-20 nm in diameter. There was no apparent difference in morphology between the labelled and unlabelled SO preparations apart from more background noise in the unlabelled condition likely induced during the handling of the grid. Figure 3.3, (A, I) shows Aβ1-42 monomers and (A, III) fibrils characterised by an elongated and twisted morphology of 100-200 nm in length. These were included to demonstrate that we can selectively generate the different Aβ1-42 species of interest, in our case predominantly SO, whose morphological characteristics compare to reports in the literature [135, 217].

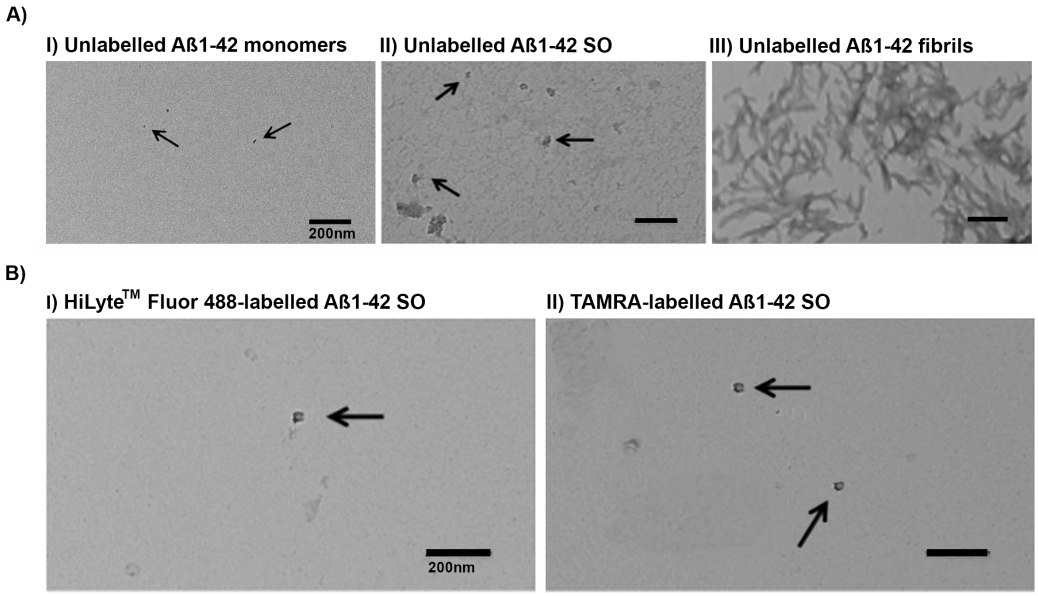

Figure 3.3: TEM images of unlabelled and labelled Aβ1-42 species. TEM grids were coated with 5 µL unlabelled Aβ1-42 monomers (A, I), unlabelled Aβ1-42 SO (A, II), and unlabelled Aβ1-42 fibrils (A, III) or with 5 µL HiLyte™ Fluor-488-labelled Aβ1-42 SO (B, I), and TAMRA-labelled Aβ1-42 SO (B, II). Monomeric and oligomeric species are indicated by arrows. Scale bar = 200 nm.

In order to further establish antibody specificity of the W02 mouse anti-Aβ1-42 monoclonal antibody that was used for the detection of Aβ1-42 SO throughout this project, a dot blot analysis of

different concentrations of unlabelled Aβ1-42 SO (A), HiLyte™ Fluor-488-labelled Aβ1-42 (B), and TAMRA-labelled Aβ1-42 SO (C) samples was carried out. It could be shown that increasing sample concentrations of respective Aβ1-42 SO yielded a concentration-dependent increase in antibody binding (see Fig. 3.4) with negligible background staining.

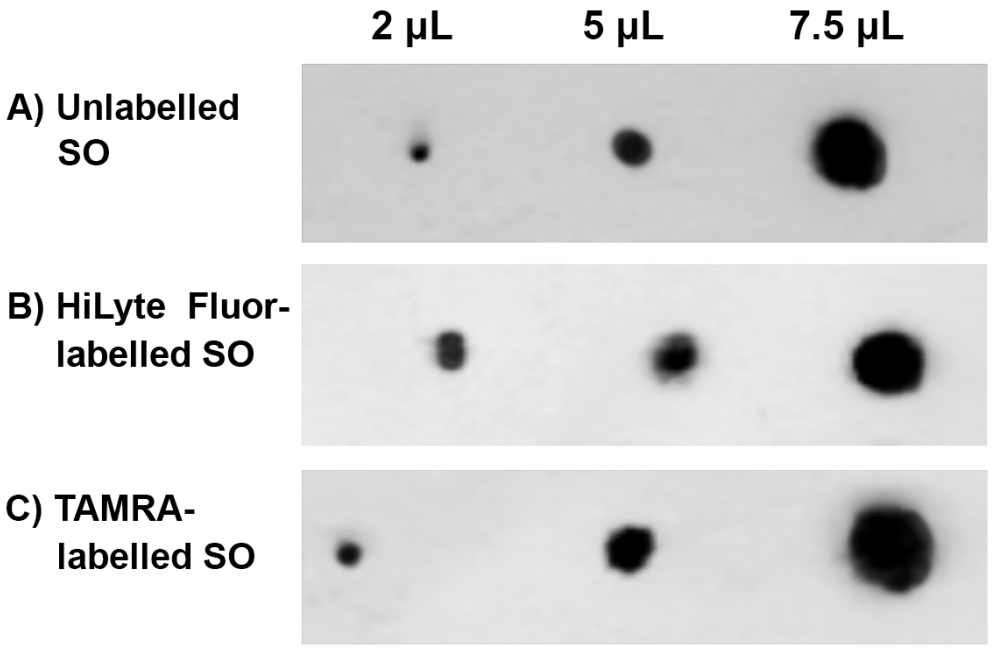

Figure 3.4: Dot blot analysis of different concentrations of unlabelled Aβ1-42 SO (A), HiLyte™ Fluor-488-labelled Aβ1-42 (B), and TAMRA-labelled Aβ1-42 SO (C) samples stained with the anti-Aβ1-42 W02 (1:1000) antibody.

3.3 Assessing the suitability of EOC 13.31 cells as a microglial cell model

While primary microglial cells most closely resemble *in vivo* microglia, their use is limited by the difficulty of obtaining pure cell populations. Additionally, their limited lifespan as well as availability, rapid phenotypic changes, and partly missing cell-to-cell interactions combined with the challenges of adequately culturing primary microglia made this cell line infeasible for the scope of this work. Immortalised cell lines are, in theory, homogeneous, genetically identical populations facilitating the generation of consistent and reproducible data [218]. Their high proliferation capacity and indefinite lifespan therefore make them a robust model for the study of molecular processes. However, a major drawback to using immortalised cell lines is the loss of their exact phenotypes upon establishment of immortality by which they could potentially lose relevant attributes compared to "normal" cells. Previous work of our group along with reports in the literature have suggested the suitability of the murine microglial cell line EOC 13.31 as a model system for the study of Aβ interaction with mi-

croglia. EOC 13.31 is a spontaneously immortalised microglial cell line that has been derived from individual agar-cloned microglial precursors residing in the brain. The cell line differs from other commonly used microglial cell lines in that it has not been produced by deliberate virus transformation or oncogene transfection [219]. The colony-stimulating factor-1 dependent EOC cells are highly proliferating and possess the ability to secrete several different cytokines that contribute to neuroinflammation as well as reactive species, including nitric oxide [220]. A systematic PubMed database analysis of different microglial cell lines has further shown that the properties of EOC microglial cells are largely comparable to those of primary microglia (primary cultures involve the isolation of cells directly from donor tissue) (see Table 3.1, albeit noticeably fewer published studies (18) reported the use of EOC 13.31 as compared to e.g. BV2 microglial cells (142) [220]). Cheng-Chung Wei and colleagues later evidenced that EOC 13.31 microglial cells release TNFα, interleukin-1β, interleukin-6, and inducible nitric oxide synthase in response to Aβ1-42 exposure as shown by real-time PCR of respective mRNA expression [221].

Table 3.1: Overview of microglial properties of selected cell lines. Table adapted from Stansley et al. [220]. *Limited data available.

Properties	**Primary**	**BV2**	**N9**	**EOC 13.31**
MAC-1	+	+	+	+
LPS stimulation	+	+	+	+
IL-1β release	+	-	+	N/A
TNF-release (following LPS)	+	+	+	+
Phagocytosis	+	+	+	+
Peroxidase	-	-	-	-
Non-specific esterase	+	+	+	+
Glial fibrillary acidic protein	-	-	-	-
Galactocerebroside	-	-	-	-
NO production	+	+	+	+
Aβ-induced IL-1β	+	+	+	N/A
Aβ-induced TNFα*	+	+	+	+
Aβ phagocytosis	+	+	+	N/A

The demonstrated EOC responsiveness to Aβ1-42, the ability to release several neuroinflammatory cytokines, as well as the possibility of building on previous experience from work within our group and hence, comparability of experimental data, has encouraged the use of EOC 13.31 cells as a model system for the study of the modulating effects of Clu and Lys on Aβ1-42 SO toxicity. Because cell cultures have the potential to change with time due to selective pressures in the culture environment and genetic instability, the EOC 13.31 microglial cells were passaged for a maximum of 25 times.

Prior to investigating how Clu and Lys affect the interactions of SO and microglial cells, the experimental treatment conditions were tested and optimised.

3.3.1 Determining effective Aβ1-42 SO treatment conditions

First, an MTT metabolic activity assay was carried out to assess the effect of different Aβ1-42 SO concentrations on cell toxicity. Aβ1-42 SO samples ranging from 1-10 µM were added to the cells for 30 min (the incubation time intended to be used throughout this project) in serum-free medium, followed by the steps outlined in the standard MTT protocol (see Section 2.6.1). Briefly, MTT is a water-soluble tetrazolium salt. Living cells with active metabolism convert the dissolved MTT to an insoluble formazan product inducing a colour change from yellow to purple. The measured absorbance is indicative of the concentration of converted dye equating to cellular metabolic activity [204]. The test was used here in order to ensure that the used concentration of 1 µM showed an observable effect on the cells (measured as % reduction of metabolic activity), while simultaneously ensuring that it did not cause cell metabolism to halt. Treatment with Aβ1-42 SO resulted in a concentration-dependent reduction of metabolic activity of the EOC 13.31 cells, where 10 µM SO resulted in 95 % reduced activity compared to the no-treatment control, while the majority of cells (72 %) remained metabolically active when treated with 1 µM SO. Since it is the aim of the study to elucidate the effect of Clu and Lys on Aβ1-42 SO interactions with microglial cells, it needed to be verified that the Aβ1-42 SO concentration used was high enough to induce a response, while it was low enough to remain physiologically relevant and to not induce cell death. Derived from these results and previous reports of effective Aβ1-42 SO treatment conditions, a concentration of 1 µM (based on monomer concentration) was chosen for the next set of experiments [222].

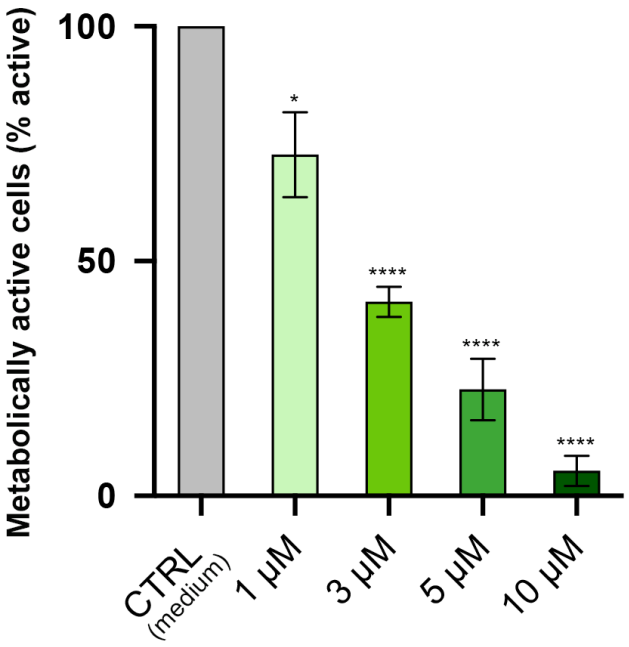

Figure 3.5: MTT metabolic activity assay to determine effective Aβ1-42 SO treatment concentrations. EOC 13.31 were treated with 1, 3, 5, and 10 µM Aβ1-42 SO for 30 min. An MTT assay was carried out to determine metabolically active cells, represented as the normalised % of the non-treated cells (CTRL). Cells were treated in triplicates. Cellular metabolic activity is shown as the mean SD of n = 3 biological repeats. Statistical significance was determined using an unpaired t-test where *, $P < 0.05$; **, $P < 0.005$; ***, $P < 0.0005$, $P < 0.00005$.

3.3.2 Exploring and optimising microglial imaging techniques

Next, EOC 13.31 microglial cells were incubated with either 1 µM HiLyte™ Fluor-488-labelled Aβ1-42 SO for 0.5 h or with TAMRA-labelled Aβ1-42 SO for 1.5 h at 37° C in order to determine whether confocal microscopy enabled the detection of microglial morphology and SO. The following experiments are based on the assumption that HiLyte™ Fluor-488-labelled as well as TAMRA-labelled Aβ1-42 SO cause the same degree of toxicity as was observed for unlabelled Aβ1-42 SO at given concentrations, however, this assumption has not been further tested herein. In addition to validate the chosen imaging conditions, the following study further aimed to determine whether the chosen time-frames of 0.5 h and 1.5 h were sufficient to show internalisation. The experimental conditions for the Clu studies outlined in Chapter 4 were chosen based on previous findings of SO interactions with SH-SY5Y cells by Hook, while the treatment concentration, incubation time, and TAMRA-dye for the Lys studies were chosen based on unpublished work by Sandin et al. and are outlined in more detail in Chapter 5 [198,222]. Moreover, the membrane stain wheat germ agglutinin was tested here, both, in its 488 (for TAMRA experiments) and 633 (for HiLyte™ Fluor experiments) versions in order to determine its suitability as a cell membrane marker and thus, a morphology marker.

Both treatment conditions enabled the visualisation of labelled Aβ1-42 SO, while WGA enabled the

visualisation of the microglial morphology, though the 488 version proved to be more suited for our quantitative analysis of intracellular fluorescence. Because WGA 633 did not produce as "sharp" of a contour as seen for WGA 488, brightfield images were used to quantify cell-internal fluorescence in the experiments that used HiLyte™ Fluor-488-labelled SO.

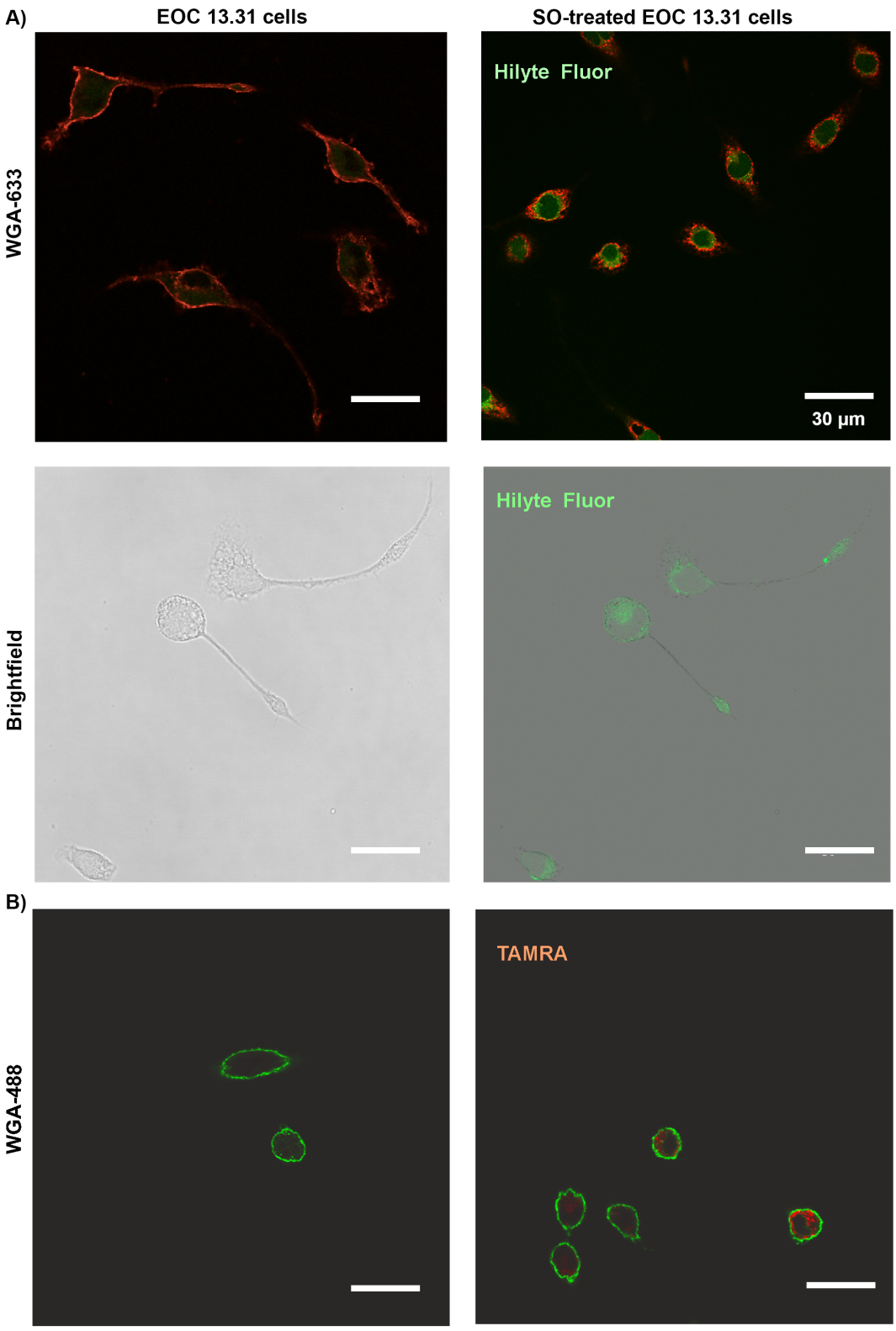

Figure 3.6: Exploratory confocal microscopy study of HiLyte™ Fluor-488 (A) and TAMRA-labelled (B) Aβ1-42 SO treatment of microglial cells. EOC 13.31 cells were incubated with either 1 µM HiLyte™ Fluor-488) or 0.5 µM (TAMRA) labelled SO for 0.5 h and 1.5 h respectively. The membrane stain WGA was furthermore tested for the use of morphology studies and compared to brightfield images (middle panels). Images are representative of n = 4 biological repeats.

Lastly, a flow cytometry study was performed to further investigate SO and EOC 13.31 interactions in given experimental conditions. The study design was optimised with the aim of gaining insights into the size distribution of the microglial cell line (especially since its medium is conditioned with LADMAC medium, which, even though filtered, could lead to impurities from this cell line). Representative scatter plots of untreated (A) and treated (B) EOC 13.31 cells are displayed in Figure 3.7, which indicate that our experimental conditions yield two distinct populations. The larger-sized population corresponds to the EOC 13.31 microglia, while the smaller-sized population likely represent LADMAC cells (see A and B, Panel I.). Cells were therefore selected based on size and the laser intensity was adjusted based on the control (untreated) condition. Representative measurements of cell-associated fluorescence are shown in Panel III. with corresponding cell percentages in this condition. It can be clearly seen that TAMRA-labelled SO associate with the cells, which confirms our observations from the confocal microscopy study. Noticeably, the flow cytometry study yielded two peaks for the TAMRA+ condition with the second, smaller peak likely due to an artefact from the LADMAC medium or due to cell clumping which had not been fully excluded by prior gating. Given that confocal images do not show evidence for a second cell population (i.e. LADMAC), the latter explanation seems more likely. Further investigation is needed to identify the origin of the second peak with certainty.

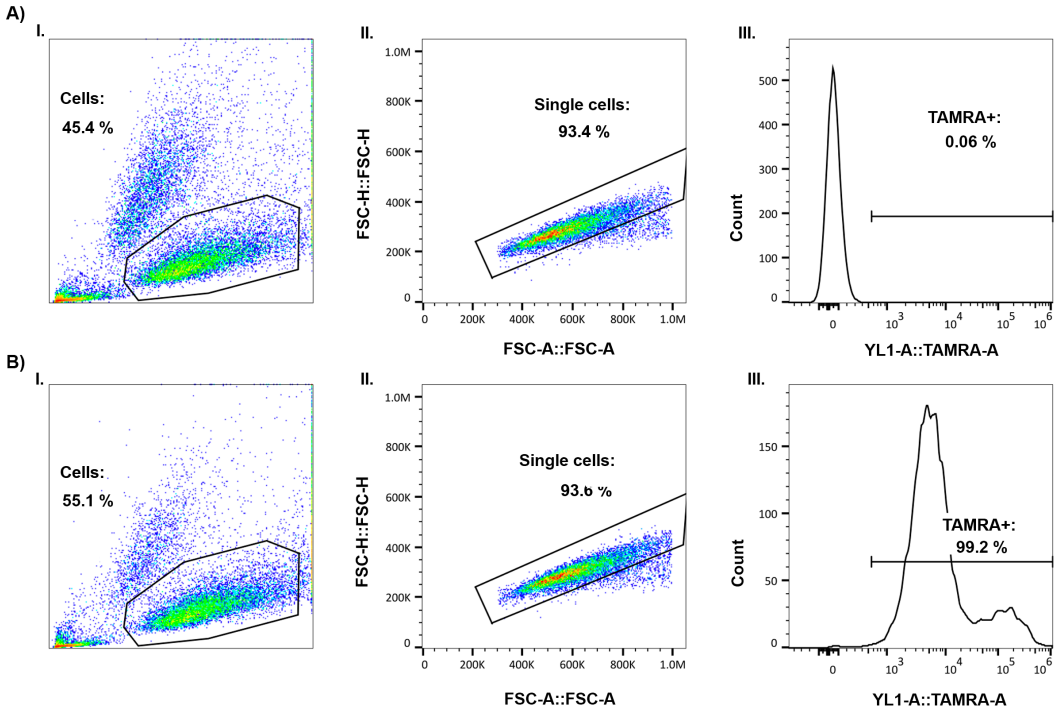

Figure 3.7: Representative images of a flow cytometry analysis of EOC 13.31 microglial cells in the absence (A) and presence (B) of TAMRA-labelled Aβ1-42. Cells were incubated with 0.5 µM SO for 1.5 h at 37° C. Microglial subpopulations were selected (I) and from those, single cells were further selected (II), whose fluorescence intensity was subsequently measured (III). The flow settings were adjusted based on the control group (medium only) and kept constant across all the experiments. Scatter plots are representative of n = 3 biological repeats.

3.4 Summary and discussion

In this Chapter, it was our aim to establish and optimise experimental conditions to meet the following requirements: (I) the ability to visualise fluorescently labelled Aβ1-42 SO, (II) the ability to observe SO internalisation, (III) ensuring that chosen incubation times showed an effect on microglial cells, while maintaining metabolic health, and (IV) the ability to reliably assess cellular morphology. Here, the spontaneously immortalised murine microglial cell line EOC 13.31 was chosen based on published data that highlight the presence of characteristic microglial attributes, which closely resemble those of primary microglial cells [220]. By limiting the number of cell passages, precautionary measures were taken to minimise the effect of changes in phenotype and genotype over time. Of particular importance in choosing an adequate microglial cell model was the demonstrated ability of EOC 13.31 cells to respond to Aβ stimulation [221]. While also BV2 as well as N9 microglial cells have been found to respond to Aβ stimulation, EOC 13.31 were the chosen cell line for this thesis given previous work of our group that formed the basis for certain experimental conditions and allowed for comparability. Despite previously addressed research suggesting the suitability of EOC 13.31 for the study of the modulating effects of Clu and Lys on Aβ1-42 SO toxicity, this cell line has not been used extensively within the scientific community, which limits the interpretation and comparability of obtained results with the work of other groups. One such example is the observed second peak in our flow cytometry analysis of TAMRA-labelled Aβ1-42 SO (see Fig. 3.7), which, to our knowledge, has not been reported before and cannot be explained herein with certainty. Given that confocal images do not show evidence for a second cell population (i.e. LADMAC), the second peak is likely due to cell clumping which had not been fully excluded by prior gating. The limitation of using a less common cell line therefore needs to be considered when interpreting experimental results.

In this work, ADDLs were used, which have been previously characterised in the literature [136]. We were able to show by TEM as well as SDS-PAGE that SO of roughly 10-20 nm in diameter could be robustly generated using established protocols (see Fig. 3.2 and Fig. ref{TEM). It shall be pointed out that, using these protocols, ADDLs can continue aggregating during experiments, while the employed techniques produce a mixture of oligomers in equilibrium; the herein observed effects of SO can hence not be accurately ascribed to a particular oligomeric species but need to be interpreted in their entirety.

For visualisation of Aβ1-42 SO, commercially available HiLyte™ Fluor-488-labelled as well as TAMRA-labelled Aβ1-42 peptides were used to form oligomers. Fluorescently-labelled SO could be successfully visualised by confocal microscopy and flow cytometry (see Fig. 3.6 and Fig. 3.7) and SO inter-

nalisation could be further observed (see Fig. 3.6). In order to further explore observed interactions of HiLyte™ Fluor-488-labelled SO with EOC 13.31 that had been previously made in our group, experimental conditions were largely kept consistent to enable comparison of obtained results. We therefore use 100 % HiLyte™ Fluor-488-labelled or TAMRA-labelled Aβ1-42 peptides for all experiments that involve fluorophore-labelled SO. Even though research by Waegele and colleagues suggests that due to its relatively low net-attractive interactions with the β-peptide, HiLyte™ Fluor-488 is a more suited labelling candidate than other fluorophores, it likely still impacts transient Aβ aggregates [212]. If comparability to previous work were not of consideration herein, it would be advisable to generate SO from a mixture of at least 50% unlabeled-to-labelled Aβ1-42 to reduce the effects of fluorophore molecular structures on Aβ assembly and function and to validate proper monomer, SO, and fibril formation using established methods [213–215]. Incubation times and concentrations of Aβ1-42 SO that have been previously used by our group as well as by Sandin et al. could be shown to yield detectable results, while maintaining metabolic health (see Fig. 3.5) [198,222]. Those experiments that involved fluorophore-labelled Aβ1-42 SO are based on the assumption that the HiLyte™ Fluor-488 as well as TAMRA labels have no effect on the degree of toxicity as observed for unlabelled Aβ1-42 SO at given concentrations. This assumption requires further testing in the future.
It was moreover demonstrated that microglial morphology could be visualised using WGA stain. WGA 488 was found to be better suited for our quantitative analysis of intracellular fluorescence compared to WGA 633, which did not produce contours that were "sharp" enough for proper detection by confocal microscopy. Hence, brightfield images were used for analysis of cell-internal fluorescence in the experiments that used HiLyte™ Fluor-488-labelled SO.

Equipped with validated and partly optimised experimental protocols within the constraints of ensuring comparability with the works of Hook et al. as well as Sandin et al., we next investigated the effects of the biomolecules Clu and Lys on uptake and trafficking of Aβ1-42 SO by EOC 13.31 microglia.

4

CLUSTERIN

4.1 Introduction and objectives

With increasing scientific evidence suggesting a link between the extracellular chaperone clusterin (Clu) and AD, a growing body of research is attempting to elucidate exactly how Clu affects the interactions between Aβ1-42 and cells. In the past, Clu has been shown to alter Aβ aggregation as well as its clearance. Interestingly, Clu has been ascribed a neuroprotective role, while it has also been shown to reduce Aβ clearance, thereby promoting toxicity [215, 223–226].

Using PDAPP transgenic mice that develop age-dependent Aβ accumulation in the absence of Clu, DeMattos and colleagues demonstrated that Clu along with apoE regulates soluble Aβ levels prior to Aβ deposition [223]. With a modified approach of their well-established clearance technique in mice, Bell et al. showed that binding of synthetic Aβ1-42 to native human plasma-derived Clu enhances the Aβ1-42 clearance rate across the blood-brain barrier by 83% [224]. Mulder and colleagues, on the contrary, found that Aβ clearance by primary microglia cells is reduced in the presence of Clu [226].

Previous work of our group showed that Clu prevents SO from binding to the cell surface of the neuroblastoma cell line SH-SY5Y (4.1). It further appeared that the effect of Clu on SO-cell interaction differed by cell type. Using flow cytometry, which assesses the total amount of aggregates associated with the cells, differences were observed between SH-SY5Y cells (drastically decreased association of SO with cells upon simultaneous exposure to SO + Clu) and EOC 13.31 microglia cells (less pronounced effect of Clu on SO interaction with cells when exposed to SO + Clu simultaneously, however, increased SO association with cells when pre-exposed to Clu prior to SO addition) as shown in Fig. 4.1.

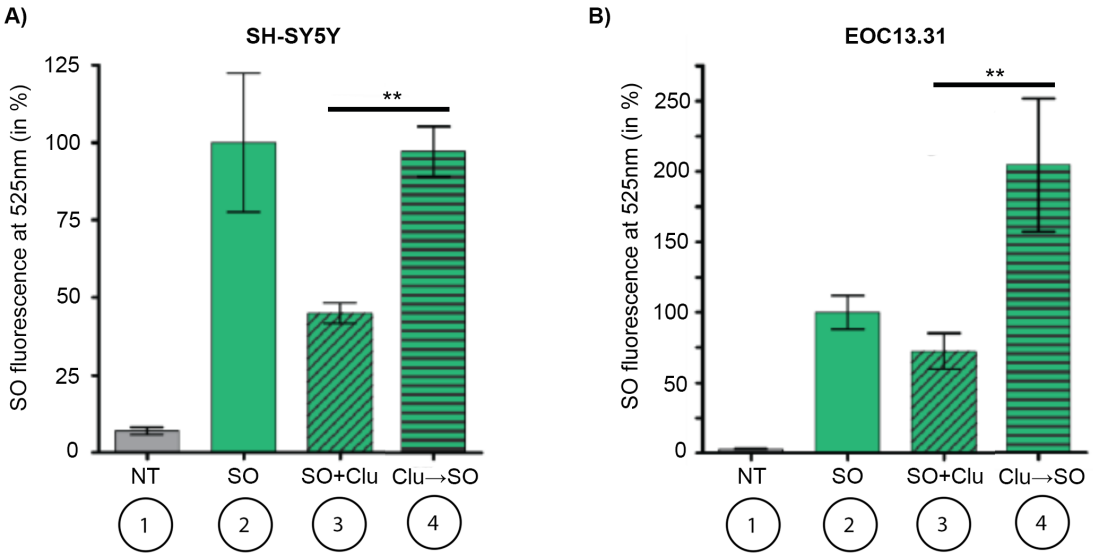

Figure 4.1: Previous work of our group, displayed here, has shown that the order of Clu addition influences interactions with EOC 13.31 but not SH-SY5Y cells [222]. In SH-SY5Y cells, SO + Clu results in less associated fluorescence as measured by flow cytometry, while adding Clu prior to introducing SO shows no effect (A). For EOC 13.31 cells, the decrease in fluorescence is less pronounced for SO + Clu, however, adding Clu before SO results in an increase in associated fluorescence (B).

The data suggest that the role of Clu in SO interactions with microglia is complex and that unlike in SH-SY5Y cells, preventing the interaction of SO with the cell membrane may not be the only predominate mechanism. Flow cytometry, which was used here to assess Aβ1-42 SO association with cells, is a laser-based technique commonly used to detect and measure physical and chemical characteristics of cell populations and particles. A cell sample is suspended in a fluid and injected into the instrument. Cells then flow in single file in front of a laser and different parameters of the cell morphology as well as fluorescent labels on the cell can be measured as they pass the detection apparatus. It is important to note, however, that flow cytometry measures fluorescence of the cell as a whole and is therefore not suited to distinguish between external and internal fluorescence.

While it is widely acknowledged that microglia play a critical homeostatic role in both, neuroinflammation and phagocytic mechanisms, studies of their effectiveness in the context of Aβ clearance have yielded disparate results. *In vivo* imaging studies in a mouse model of AD by Bolmont et al. showed that microglia migrate to amyloid plaques and internalise Aβ, which was further shown to localise in lysosomal compartments [227]. On the contrary, it has also been demonstrated that eliminating microglia from the brains of an AD mouse model does not impact Aβ plaque deposition nor amyloid-associated neuritic dystrophy [228]. A possible explanation for the ambiguous results regarding the role of microglia in Aβ clearance has been provided by Yamamoto and colleagues, who suggest that the phagocytic ability of microglia might be directed by pro- and anti-inflammatory

cytokines [229]. This ambiguity underlines the importance of further investigating the microglial response mechanism to Aβ1-42.

The work in this chapter focuses on the interaction of Aβ1-42 SO and microglia cells with particular interest in the effect of Clu on SO uptake and intracellular trafficking. Furthermore, the effect of SO and Clu on microglia activation and its inflammatory response in the form of cytokine release are studied. Advancing the understanding of microglial interactions with SO and possible modes of intervention, i.e. extracellular chaperones, could provide important information for the development of strategies to reduce Aβ1-42 toxicity. To date, our knowledge of the precise *in vivo* effects of Clu on microglia cells and overall AD progression are inconclusive, which further underlines the need for differentiated experimental investigations into the role of Clu.

4.1.1 Experimental setup

In Chapter 3, Aβ1-42 SO were formed using unlabelled Aβ1-42, HiLyte™ Fluor-488 labelled Aβ1-42, and TAMRA-labelled Aβ1-42. Experimental conditions that had been previously established within our group were tested and further optimised with the aim to ensure observability of Aβ1-42 internalisation, while enabling comparability with previously obtained data.
In this Chapter, HiLyte™ Fluor-488 labelled Aβ1-42 SO, as well as unlabelled SO, are used to investigate their interactions with microglial cells in the absence and presence of Clu. The murine microglia cells EOC 13.31 were the chosen cell model for SO and Clu interaction at a 10:1 Aβ1-42 SO-to-Clu submolar ratio. Our studies focused specifically on the population of microglia that showed internalisation of SO to determine how Clu affects the overall uptake and trafficking of SO in this cell line. Two conditions were used for comparison; incubation with only labelled SO and incubation with a mixture of SO + Clu (Fig. 4.2, 2 and 3). To evaluate if effects were due to unbound Clu, as opposed to the combined SO + Clu treatment, a third condition was also investigated in which cells were pre-incubated with Clu prior to SO exposure (Fig. 4.2, 4). A no-treatment condition (serum-free medium + solvent) was included throughout the experiments as a negative control (Fig. 4.2, 1).

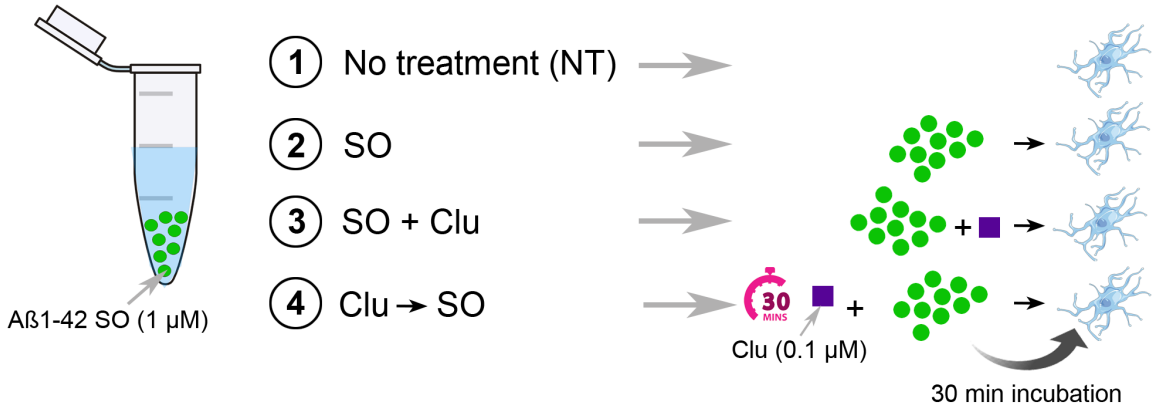

Figure 4.2: Schematic overview of experimental design. Note: Items displayed are not drawn to scale.

An incubation time of 30 min for pre-incubation of cells with Clu and for SO exposure, respectively, was chosen here in line with previous experiments conducted by Hook (compare Fig.4.1).

4.2 Assessment of cell fluorescence upon SO and Clu treatment

It was examined whether the presence of Clu has an impact, not only on cell interaction, but more specifically, on the internalisation of Aβ1-42 SO in microglia using confocal microscopy. EOC 13.31 were incubated with HiLyte™ Fluor-488 labelled Aβ1-42 SO for 30 min in the presence and absence of Clu. To determine the corrected total cell fluorescence (CTCF) of microglial cells upon exposure to HiLyte™ Fluor-488 Aβ1-42 SO, acquisition settings were established using the positive control (SO-exposed cells). Once established, the settings were kept constant between samples to allow for later quantitative comparability. The exposure time, gain and offset were adjusted to use the entire dynamic range of the detectors. Importantly, image saturation was controlled for using the auto-histogram display of the microscope. The corrected total cell fluorescence (CTCF) was subsequently calculated with ImageJ (Fig. 4.3 A) using the following formular:

$$CTCF = integrated\ density - (area\ of\ selected\ cell \times mean\ fluorescence\ of\ background\ readings)$$

The CTCF, as represented by the mean, is significantly higher in the SO + Clu treatment condition compared to untreated as well as Clu pre-treated cells. While these findings suggest that Clu enhances internalisation, Hook had previously reported that Clu pre-exposure had the largest effect on the interaction of SO with microglia, as opposed to the simultaneous SO + Clu exposure as observed here. This apparent discrepancy may be due to the use of two different imaging techniques

(flow cytometry assessing overall SO-cell association vs. confocal microscopy assessing internalised SO). To further investigate whether this observations can be ascribed to SO and Clu interacting with one another upon administration to the cells, microglia cells were treated with both, labelled Clu (shown in red) and labelled SO (shown in green) while using the same treatment conditions as described above (Fig. 4.3 B). Colocalisation is observed in the overlaid images when both, SO and Clu are present, irrespective of when Clu was administered. Yet, qualitatively it appears that the extent of colocalisation is greater when SO and Clu are administered simultaneously. As previously mentioned, cells were selected based on whether they displayed SO interaction. The data therefore provide a snapshot of those microglia cells that have internalised SO and the effect of Clu on this internalisation. It should be pointed out, however, that the observed trends for the effect of Clu on SO internalisation are not significant when compared to SO alone. It is possible that this observation might be due to a selection bias introduced by the screening for those cells that have internalised SO. While the experimental design enabled the assessment of SO internalisation on a cellular level, it did not allow for the assessment of the total number of SO-associated cells in a controlled manner as was done in the flow cytometry experiments. Taken together, these studies suggest that the exposure to Clu and the timing of this exposure alters the interaction of microglia cells with Aβ1-42 SO. To better understand this observed trend, an investigation of SO trafficking by microglia followed.

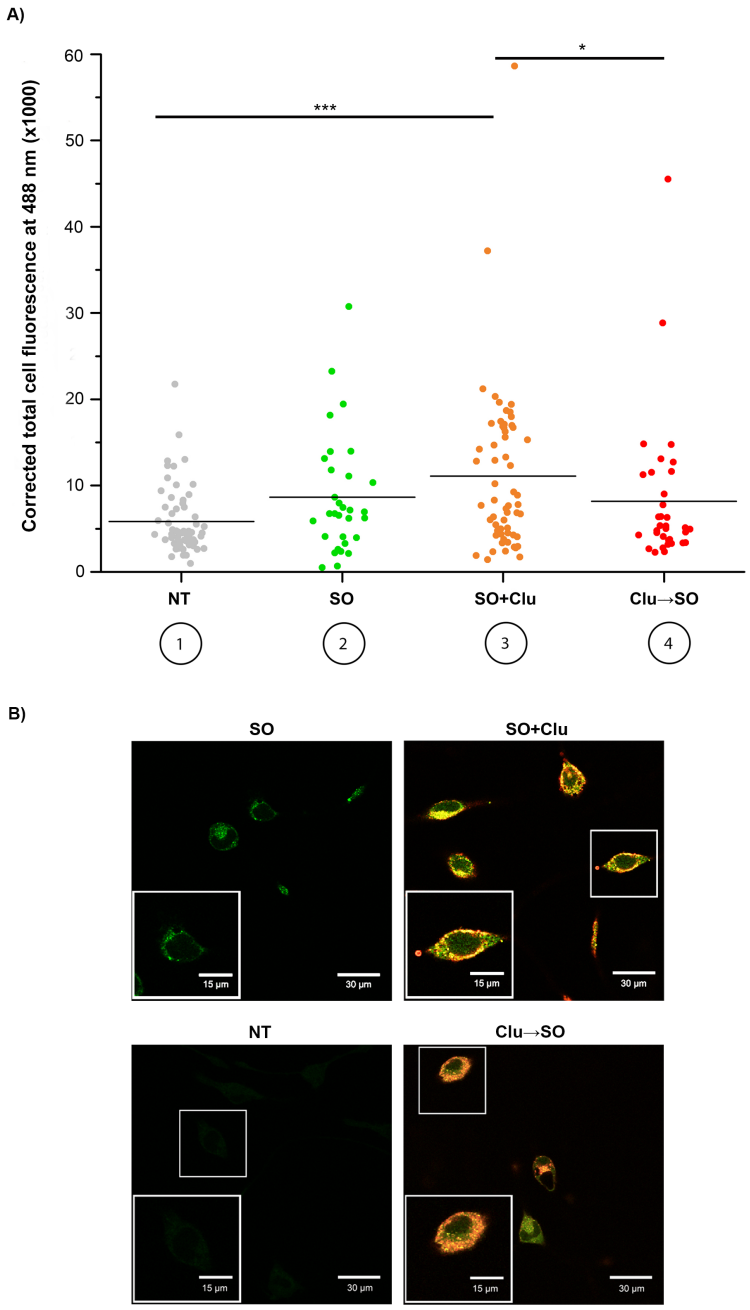

Figure 4.3: CTCF of EOC 13.31 microglia cells upon different treatments (A, 1-4), as well as representative images of microglia cells in the respective treatment conditions (B). EOC 13.31 cells were treated with 1 µM labelled Aβ1-42 SO (A, 2), SO + Clu (A, 3) or remained untreated (A, 1) for 30 min, 37° C. Alternatively, cells were pretreated with 0.1 µM Clu (A, 4) for 30 min, 37° C followed by SO for another 30 min, 37° C. The cell fluorescence was measured in ImageJ and compared across cell lines as per the Mann-Whitney test. Data points in (A) represent $n \geq 31$ cells pooled from n = 3 independent experiments. The mean of each group is marked by a black line. The representative images of EOC 13.31 show SO treatment (green) and Clu (red). Scale bars = 10 µm (inset) or 30 µm. *, $P < 0.05$; **, $P < 0.005$; ***, $P < 0.0005$. Panel (B) was contrast-enhanced post-analysis for better visualisation of fluorescence.

4.3 Colocalisation study of SO-treated cells

Having observed SO internalisation by EOC 13.31 cells (Fig. 4.3), it was next examined whether the intracellular trafficking of SO follows the endosomal/lysosomal pathway and whether it is affected by the presence of Clu. Colocalisation patterns of SO with lysotracker (Fig. 4.4) were therefore assessed, which stains acidic compartments of the late edosomal/lysosomal pathway [230–232]. Colocalisation was analysed using the Coloc 2 plugin of ImageJ and are expressed and the degree of colocalisation is expressed as Pearson's correlation coefficient, where "+1" means perfect correlation and "−1" perfect but negative correlation with 0 denoting the absence of a relationship. Colocalisation analysis revealed that SO and lysotracker colocalised, to different degrees, in all three treatment conditions (Fig. 4.4, B) forming a ring-like structure in close proximity to the cell membrane. The presence of Clu resulted in a higher degree of colocaliation with pretreatment showing the most significant increase, albeit the respective means (shown as a black line) indicate only moderate overall colocalisation (mean PCC = 0.4 for Clu then SO).

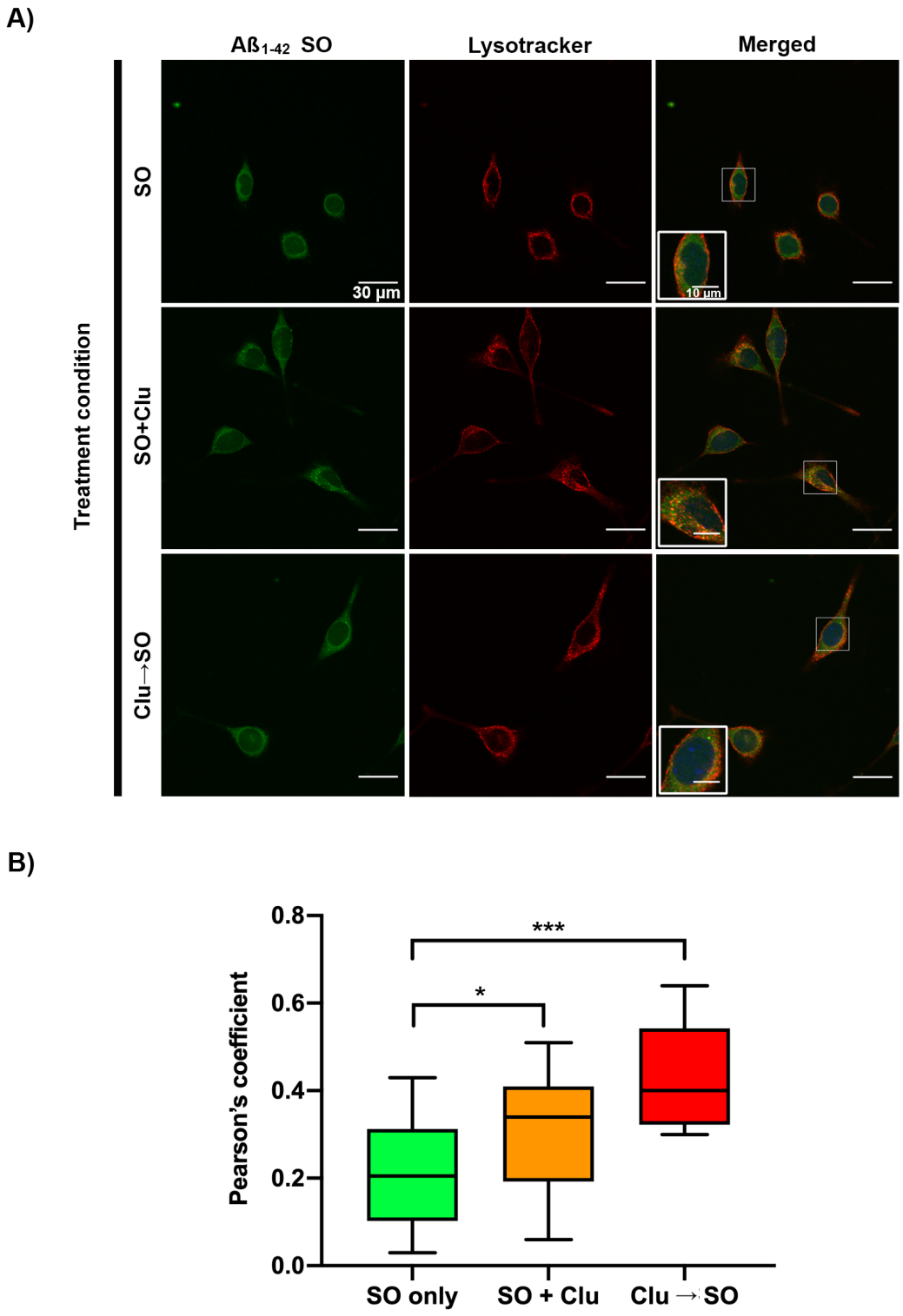

Figure 4.4: SO colocalisation study of microglial cells stained with lysotracker in different treatment conditions (A). EOC 13.31 cells were treated with 1 µM labelled Aβ1-42 SO (green), SO + Clu, or pretreated with 0.1 µM Clu for 30 min, 37° C, followed by SO treatment for an additional 30 min, 37° C. Cells were simultaneously treated with lysotracker (red) followed by counterstaining of the nuclei with Hoechst (blue). Images represent n = 3 independent experiments. Scale bars = 10 µm (inset) and 30 µm. The degree of colocalisation of Aβ1-42 SO and lysotracker was assessed with the ImageJ Coloc 2 plugin and is shown as the Pearson correlation coefficient of n = 3 experiments for respective treatment conditions, where *, $P < 0.05$; **, $P < 0.005$; ***, $P < 0.0005$ (B). Images were contrast-enhanced post-analysis for better visualisation of fluorescence.

Next, the possible colocalisation of SO and LAMP1, a lysosomal-associated membrane protein that is involved in maintaining lysosomal acidity was investigated using the same treatment conditions as described before (Fig. 4.5) [233]. To avoid the possibility of Aβ1-42 degradation in the lysosome and therefore false negative results, the microglial cells were pre-treated with the lysosomal inhibitor chloroquine, which acts via inhibition of the acidification of the endosome-lysosome system and has made its way into the clinic primarily used for the treatment of malaria [234].

While the overall degree of colocalisation was lower than observed for lysotracker (mean PCC = 0.29 for SO + ClU), increased punctated SO accumulation throughout the cytoplasm was noticed that differed from the ring-like distribution of SO previously detected (compare Fig. 4.4 and Fig. 4.5). Moreover, the highest degree of colocalisation was oberseved for the SO + Clu condition, whereas pretreatment with Clu resulted in almost no colocalisation (mean PCC = 0.1).

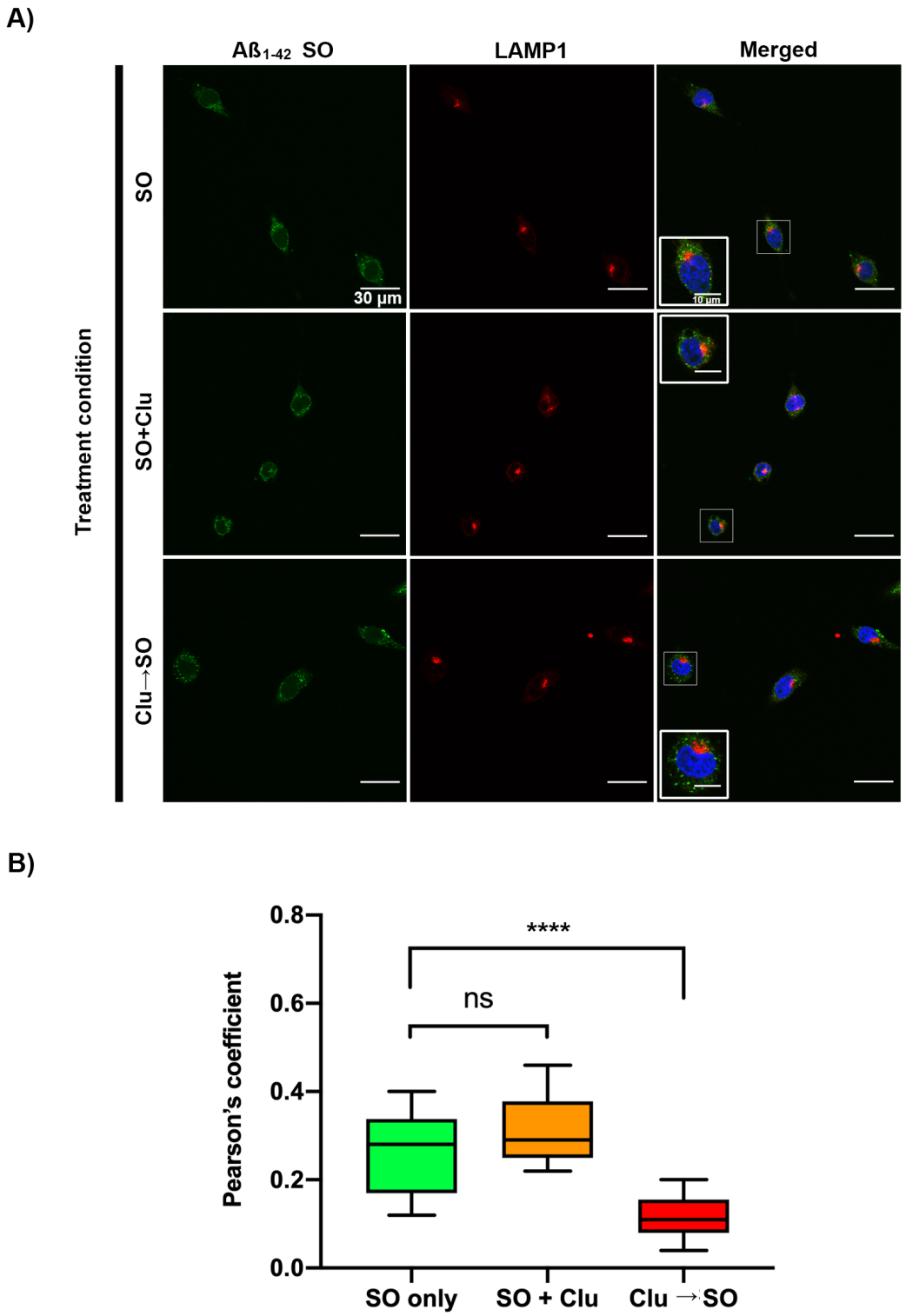

Figure 4.5: SO and LAMP1 colocalisation study of microglial cells in different treatment conditions. Representative images of EOC 13.31 cells treated with 200 µM chloroquine for 1 h at 37° C prior to SO (green) and Clu exposure as described before. Cells were stained with anti-LAMP1 (red) followed by counterstaining of the nuclei with Hoechst (blue). Images represent n = 3 independent experiments. Scale bars = 10 µm (inset) and 30 µm. The degree of colocalisation of Aβ1-42 SO and LAMP1 was assessed with the ImageJ Coloc 2 plugin and is shown as the Pearson correlation coefficient of n = 3 experiments for respective treatment conditions, where *, $P < 0.05$; **, $P < 0.005$; ***, $P < 0.0005$, ****, $P < 0.00005$ (B). Images were contrast-enhanced post-analysis for better visualisation of fluorescence.

An additional set of experiments was carried out to assess whether Aβ1-42 colocalises with the lysosomal aspartic endopeptidase cathepsin D (Fig. 4.6). In this study, Aβ1-42 showed the highest degree of colocalisation in the SO + Clu treatment condition (mean PCC = 0.47), while SO only and pretreatment with Clu show very limited colocalisation (mean PCC $\leq$ 0.2).

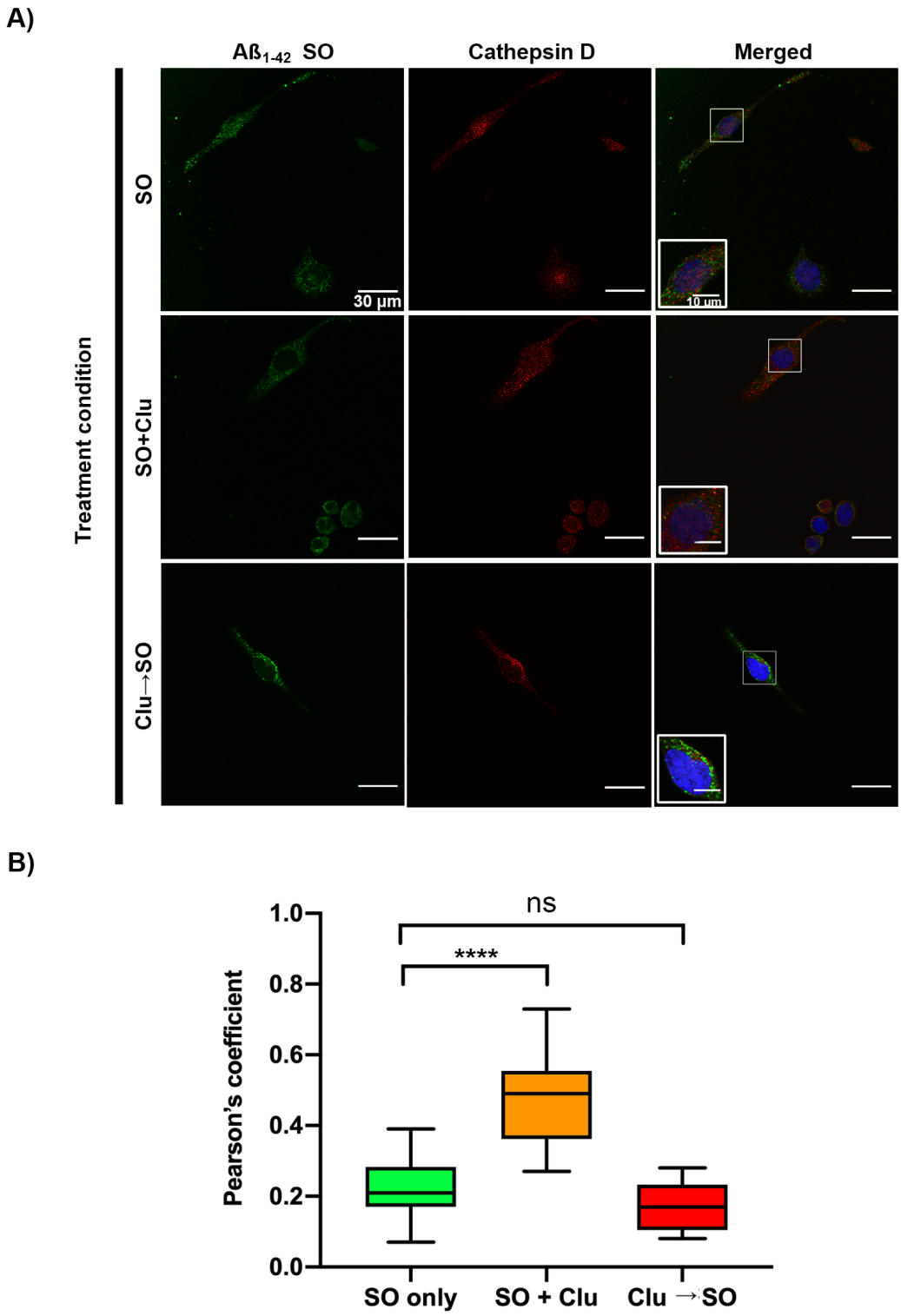

Figure 4.6: SO colocalisation study of microglial cells stained with anti-Cathepsin-D in different treatment conditions. EOC 13.31 cells were treated with 1 µM labelled Aβ1-42 SO (green), SO + Clu, or pretreated with 0.1 µM Clu for 30 min, 37° C, followed by SO treatment for an additional 30 min, 37° C. Cells were simultaneously stained with Cathepsin-D antibody (red) followed by counterstaining of the nuclei with Hoechst (blue). Images represent n = 3 independent experiments. Scale bars = 10 µm (inset) and 30 µm. The degree of colocalisation of Aβ1-42 SO and Cathepsin D was assessed with the ImageJ Coloc 2 plugin and is shown as the Pearson correlation coefficient of n = 3 experiments for respective treatment conditions, where *, $P < 0.05$; **, $P < 0.005$; ***, $P < 0.0005$, ****, $P < 0.00005$ (B). Images were contrast-enhanced post-analysis for better visualisation of fluorescence.

4.4 Morphology study of microglia cells under different SO and Clu treatment conditions

As outlined earlier, it is well established that microglial cells undergo a morphological shift upon activation. To determine the effects of SO and Clu treatments on microglial morphology and concomitantly, their activation, confocal microscopy was used to analyse the shapes of treated EOC 13.31 cells after 30 min incubation. Confocal images of microglial cells were taken at a set interval between the first and last planes of focus (each representing a single optical slice within the cell) to ensure that the morphological features of the microglial cells were fully captured. The respective centre planes were then mathematically determined and the cellular morphology of respective 2D images were analysed (see Section 2.7.3). Representative images of "elongated", "intermediate", and "rounded" cells are shown in Fig. 4.7. Elongated cells were characterised by their neurite-like processes that tend to branch out, which is typical for non-activated microglia [235]. Round cells, on the contrary, represent activated microglia and display an amoeboid morphology with retracted processes [236]. Cells were defined as intermediate if they displayed less pronounced extensions, yet, could not be described as fully rounded.

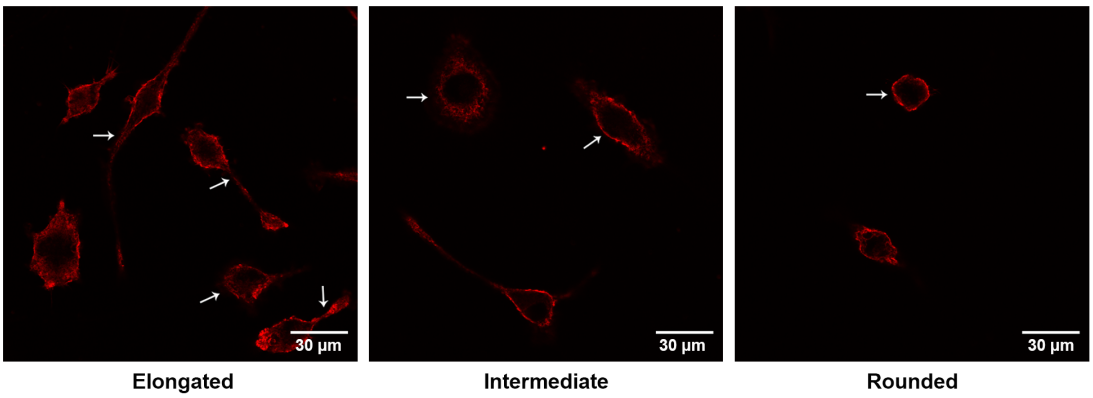

Figure 4.7: Microglial activation induces a morphological shift from an elongated to a rounded shape. Representative images of EOC 13.31 cell morphologies from n $\geq$ 3 experiments observed upon SO and Clu exposure as indicated by arrowheads. Cell membranes were stained with WGA. Scale bars = 30 µm. Images were contrast-enhanced post-analysis for better visualisation of fluorescence.

The percentages of "elongated", "intermediate", and "rounded" cells upon SO, SO + Clu, and Clu→SO treatments as well as their respective average area are shown in Table 4.1. As a known activator of microglial cells, lipopolysaccharide (LPS) was included as a positive control, which resulted in a distinguishable depletion of elongated "resting" cells (Table 4.1). When untreated, the majority of cells were elongated (65 %), while roughly a quarter of the cells (24 %) showed an activated, rounded morphology. Similarly, the majority of cells adapted a "resting" morphology in the SO

(70 %) as well as the Clu→SO (65 %) conditions suggesting that these treatments had little effect on microglial activation at this short incubation time. The largest decrease in elongated "resting" cells was observed in the SO + Clu treatment condition (52 % elongated cell population), which is comparable to the amount of elongated "resting" cells in the LPS condition (54 %). It shall be noted that the data represent a snapshot of a dynamic process with cells labelled as "intermediate" likely undergoing activation, which suggests that overall, simultaneous addition of SO + Clu may have a similarly activating effect on the cells as the LPS control.

Table 4.1: Quanitification of microglial activation upon SO exposure in different treatment conditions. EOC 13.31 cells were treated with SO, SO + Clu, Clu→SO, and LPS for 30 min, 37° C and the cell morphologies were qualitatively categorised as "elongated", "rounded" or "intermediate". Percentages of total cell counts from n $\geq$ 3 experiments are shown here. The average cell area $\pm$ SD was measured using ImageJ and compared to the "elongated" group within the same treatment condition applying the Mann-Whitney or two-sample t-test. *, P < 0.05; **, P < 0.005; ***, P < 0.0005.

	Cell morphology [%]			**Area of the cell [µm^2]**		
	elongated	intermediate	rounded	elongated	intermediate	rounded
Treatment [n]						
NT [37]	65	11	24	952 $\pm$ 399	536 $\pm$ 58	623 $\pm$ 154*
LPS-treated [24]	54	25	21	1285 $\pm$ 684	935 $\pm$ 257	532 $\pm$ 170*
SO [30]	70	10	20	882 $\pm$ 355	555 $\pm$ 210	456 $\pm$ 136**
SO + Clu [59]	52	5	43	1152 $\pm$ 542	740 $\pm$ 204	672 $\pm$ 248***
Clu→SO [34]	65	18	18	1302 $\pm$ 682	757 $\pm$ 120*	573 $\pm$ 120***

These findings support the internalisation results, which imply increased SO internalisation when Clu and SO are simultaneously administered (Fig. 4.3). In addition to evaluating microglial activation based on qualitative categorisation, the average area of the different cells was measured and compared within each treatment condition (Table 4.1). The round cells were significantly smaller than the elongated cells in all treatment conditions underlining a noticeable change in morphology.

4.5 Cytokine release of microglia cells upon SO and Clu treatment

In the aforementioned studies, it has become evident that the addition of Clu and importantly, its timing, impact SO uptake and cell morphology. In a next step, the release of inflammatory cytokines TNFα and IL-1β as well as the anti-inflammatory cytokine IL-10 was examined. It has been previously shown that microglia activation by Aβ peptides can cause the release of pro-inflammatory

cytokines in a concentration-dependent manner [237, 238]. Here, it is investigated whether these observations can be replicated using EOC 13.31 and whether Clu influences this process.

4.5.1 ELISA analysis of TNFα release after Aβ1-42 exposure

To better understand how Clu affects the observed microglial activation over an extended period of time, ELISA assays were performed to determine the concentration of the released inflammatory cytokines, TNFα (Fig. 4.8) and IL-1β (data not shown), upon SO and Clu treatment. Cytokine release measurements were determined after extended incubations for 24 h (37° C). SO treatment of EOC 13.31 induced the highest TNFα release (133 pg/mL, (Fig. 4.3, 2) after 24 h, which was significantly higher than the TNFα released by SO + Clu (110 pg/mL, (Fig. 4.3, 3), while TNFα release in Clu-pretreated cells (61 pg/mL) was significantly lower compared to simultaneous treatment.

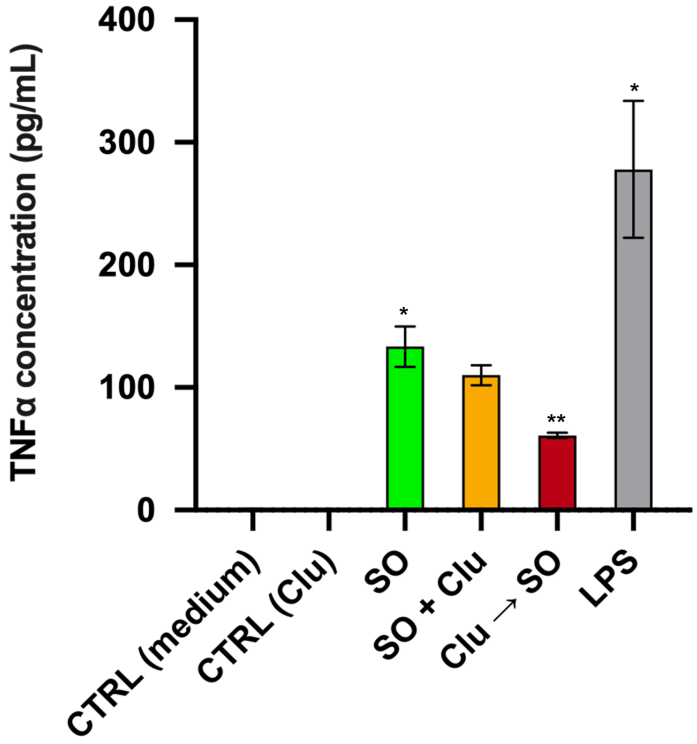

Figure 4.8: TNFα release of microglia cells treated with SO in the presence and absence of Clu. EOC 13.31 cells were treated with 4 µM Aβ1-42 SO (2), SO + Clu (3) or remained untreated (1) for 24 h, 37° C. Alternatively, cells were pretreated with 0.4 µM Clu (4) for 30 min followed by SO for 23.5 h, 37° C. The concentration of released TNFα was measured via ELISA and compared to the SO + Clu condition using a paired t-test. The bars represent n = 3 ± SD replicates. The results are representative of n = 2 experiments. **, $P < 0.005$.

The observed trend in the ELISA assay is surprising not only because the SO + Clu cell population, which had been previously identified as the population with the highest proportion of activated cells, did not release the largest amount of TNFα as would have been expected, but also because

the amounts of released TNFα measured here are 10-30-fold lower than what has been observed elsewhere using similar treatment controls and/or the same ELISA assay protocol (see Table 4.2) [221, 239–242]. However, it shall be pointed out that due to the low quantities of TNFα release and associated difficulty of obtaining meaningful ELISA readouts, the data discussed herein are not fully conclusive and need to be confirmed.

Table 4.2: Overview of selected TNFα ELISA measurements and associated experimental conditions based on a literature search. *TNFα concentrations are estimated based on histogram representations of data.

Author	Microglia cell line	Stimulant	Stimulant concentration	Incubation time [h]	TNFα release* [pg / mL]
Yao et al. [239]	BV2	AnaSpec Aβ1-42 SO	20 µ/mL	24	38
Jian et al. [240]	BV2	GL Biochem Aβ1-42 SO	0 µM	24	280
			2.5 µM	24	210
			5 µM	24	190
			10 µM	24	600
			20 µM	24	590
Floden and Combs [241]	Postn. brain-derived	Amer. Peptide Aβ1-42 SO	0 µM	24	120
			5 µM	24	205
			10 µM	24	260
			20 µM	24	210
	Adult brain-derived	Amer. Peptide Aβ1-42 SO	0 uM	24	140
			5 µM	24	220
			10 µM	24	290
			20 µM	24	510
Cheng-Chung Wei et al. [221]	EOC 13.31	AnaSpec Aβ1-42 SO	10 µM	24	3500
		LPS	100 ng/mL	24	4700
Korneev et al. [242]	BMDM	LPS	10 ng/mL	5	2800

It appears that Aβ1-42 SO-induced TNFα release greatly varies between studies even though higher amounts of Aβ1-42 SO (between 10-20 µM) have been shown to elicit higher quantities of released TNFα. While our data combined with findings reported in the literature suggest that Aβ1-42 SO can induce TNFα release in EOC 13.31 microglial cells, further investigation is needed in order to substantiate our observations. The experimental conditions would likely need to be adjusted by increasing the Aβ1-42 SO concentration and it could be worth considering using the RD Systems ELISA kit that has been commonly used by others.

The repeated assessment of IL-1β release yielded measurements below the quantifiable cytokine threshold of 16 pg/mL. In order to determine whether the presence of Clu may exert a protective role by means of stimulating anti-inflammatory cytokine release, the supernatant levels of the anti-inflammatory cytokine IL-10 were measured next. However, similarly to the problems experienced with the IL-1β assay, the measurement of IL-10 release was also below the quantifiable threshold of 32 pg/mL for the assay kit. Additionally, it was tested whether a shorter incubation (8 h) would increase the measurable cytokine release, which resulted in even less quantifiable results (data not

shown). Therefore, alternative methods to investigate cytokine production were explored by means of qPCR.

4.5.2 qPCR analysis of TNFα mRNA content

Since the study of cytokine release upon EOC 13.31 stimulation produced ambiguous results, it was explored whether qPCR would be better suited for the given experimental design. An exploratory study of the effect of exposure to different concentrations of LPS, a known inducer of microglial inflammation and used as a positive control in the previous experiment, was carried out next. In particular, the effect of LPS (0 ng/mL, 25 ng/mL, 50 ng/mL, and 75 ng/mL) on TNFα mRNA levels upon cell exposure for 6 h and 24 h were studied. After 6 h LPS incubation, the mRNA levels increased in a concentration-dependent manner up to a 2-fold increase at an LPS concentration of 75 ng/mL (the highest LPS concentration used in this study). Interestingly, the mRNA levels decreased compared to the control condition when exposed to LPS for 24 h, with the lowest amount of mRNA measured in the highest LPS treatment condition. While there appears to be an effect of LPS on TNFα expression levels, the effect on EOC 13.31 is weaker than anticipated based on the literature, where a fraction of the used LPS concentration (10 ng/mL) induced a much larger relative change in mRNA levels ($\geq$3-fold) [243].

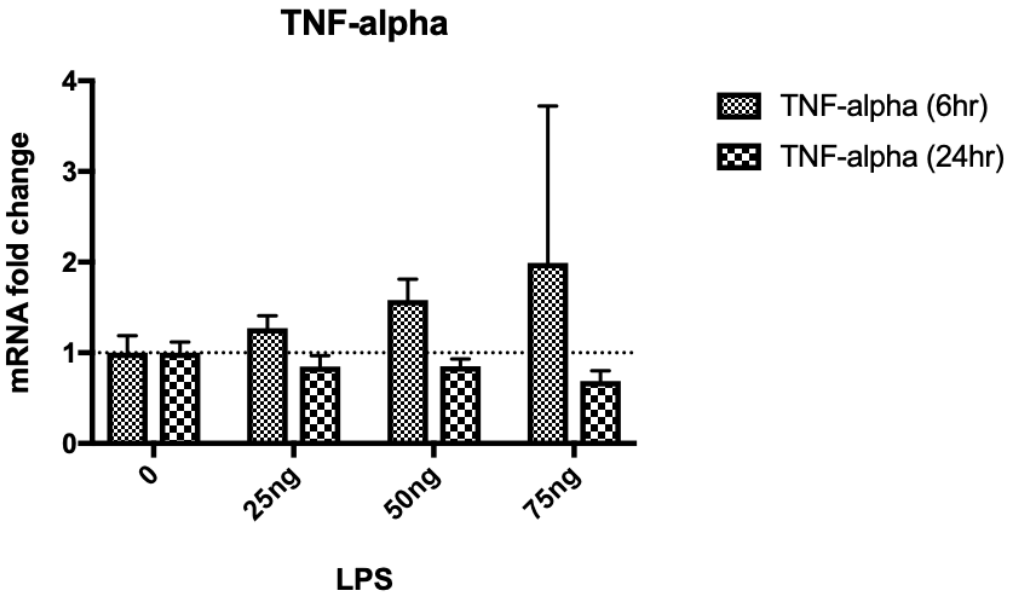

Figure 4.9: Relative TNFα mRNA levels upon LPS treatment (analysis kindly conducted by Zhen Du, Department of Pharmacology, University of Cambridge). EOC 13.31 cells were treated with 25 ng, 50 ng, and 75 ng LPS for 6 h and 24 h respectively. The levels of mRNA were subsequently measured by qPCR. The bars represent n = 1 ± SD replicate. The results are exploratory and representative of n = 1 experiment.

4.6 Summary and discussion

In this Chapter it has been shown that EOC 13.31 cells internalise synthetic Aβ1-42 SO and that this process is influenced by Clu. The experiments suggest that simultaneous addition of SO + Clu stimulates increased oligomer uptake with concomitant microglial activation as morphologically indicated by a shift from elongated to rounded cells. Moreover, it appeared that SO colocalise with selected messengers of the late endosomal-lysosomal pathway which is impacted by the presence of Clu as well as its timing. Qualitatively, an increase in SO accumulation throughout the cytoplasm upon lysosomal inhibiton independent of Clu treatment was noticed. After extended incubation times, this initially increased oligomer uptake seen in the the presence of Clu may have contributed to the reduced pro-inflammatory response as measured by TNFα release. Albeit exploratory, the cytokine release studies suggests that Clu may play a protective role in Alzheimer's disease (subject to further investigation), while posing questions about the exact effect that Clu exerts on SO at different incubation times.

The hypothesis that the effect of Clu on SO interaction might differ depending on cell type under investigation arose from an initial flow cytometry study (see Fig. 4.1). In the study, the highest amount of SO-microglia association was observed for the Clu pre-treated cells, however, it fell short to distinguish between internalised and membrane-associated SO. The confocal imaging study that followed

was able to provide insights into the effect of Clu on SO internalisation. Here, the highest uptake was observed in the SO + Clu treatment condition. While the flow cytometry results had initially led to the hypothesis that the treatment condition showing the highest degree of SO interaction, namely Clu→SO, would also equate to the highest degree of SO internalisation, the results herein suggest otherwise. A possible reason for the observed increased fluorescence in the Clu pre-treatment condition of the flow study might be SO retention on the cell membrane facilitated by the prolonged presence of Clu. Another, albeit less likely explanation for the comparatively reduced CTCF might be due to expedited degradation of SO within the cells when pre-exposed to Clu. The simultaneous addition of SO + Clu, on the contrary, appears to promote SO internalisation. It is moreover possible, that it slows down trafficking and degradation inside the cell leading to an accumulation of intracellular SO. The colocalisation studies that followed indicated that in the presence of Clu, SO show greater colocalisation with lysotracker, while SO also appear to colocalise with cathepsin D when SO + Clu are administered simultaneously. The overall weak colocalisation with LAMP1 may be due to the time point of 30 minutes chosen for our investigation and would need observing over an extended period for further analysis. It is possible that Aβ1-42 SO and Clu form a complex when administered simultaneously, thereby facilitating its uptake and further processing by microglial cells. It has been previously shown that, *in vitro*, Aβ1-40 complexes with Clu in a concentration-dependent manner. It was further shown that while Aβ1-40 alone does not bind to the low-density lipoprotein receptor LRP-2, Clu in complex with Aβ1-40 bridges the interaction of Aβ with the receptor and promotes its internalisation and subsequent degradation in lysosomes [244, 245]. The discovery of a genetic variant of triggering receptor expressed on myeloid cells 2 (TREM2) that increases the risk of AD in humans 3-4-fold has not only provided strong evidence for the involvement of microglia in AD, but it has also pointed at receptor-mediated Aβ internalisation as a possible route of Aβ-microglia interaction [246, 247]. It has since been shown that TREM2 expression is able to enhance phagocytosis of Aβ1-42 oligomers as well as inhibit Aβ-induced proinflammatory responses in microglial cells [248, 249]. Strikingly, it has been reported that Clu is a ligand of TREM2, whose interaction can increase the Aβ uptake by microglia cells providing a potential route of internalisation of the SO + Clu complex observed in this study [250]. While the underlying cause remains elusive, these findings along with our confocal imaging data suggesting increased SO internalisation in the presence of Clu could be explained by an increased SO uptake via receptor-mediated endocytosis, which may be facilitated by the complexation with Clu.

It would be interesting to further investigate the role of different receptors, including TREM2 as well as their involvement in cytokine release in the herein outlined experimental conditions. However,

given the experienced difficulties with the ELISA assay, alternatives should be explored. A lot of the studies that report significant cytokine release, including TNFα, use murine BV2 microglia cells and / or an Aβ SO concentration of at least 10 µM [240, 251]. Interestingly, Jian and colleagues observe an initial decline in TNFα with levels below the control condition when cells were exposed to 2.5 µM and 5 µM Aβ1-42 SO, respectively. These findings, if replicable, would suggest that the herein chosen Aβ1-42 SO concentration might be below the activation threshold for an inflammatory response. It remains to be determined whether a higher, non-physiological, Aβ1-42 SO concentrations would still provide relevant knowledge furthering our understanding of AD disease progression.

It was furthermore observed that simultaneous administration of SO + Clu induced a change from "resting" to more "activated" microglia, which was assessed based on microglial morphology and average cell area. In microglia, a morphological shift from a ramified state featuring small, round cell bodies with many branching processes to an ameboid state with retracted processes and enlarged cell bodies is indicative of microglial activation [252]. This complex, multistage process results in the release of cytokines, such as the aforementioned TNFα [253]. Conspicuously, the rounded cells were significantly smaller than the "resting", elongated cells, which is contrary to observations reported in the literature [236, 254]. Most studies, however, compare the size of the cell bodies only, not taking into account the protrusions as was done here. Our results indicate that EOC 13.31 microglia display a clearly distinguishable morphology when activated.

Upon internalisation, the SO were shown to colocalise with lysotracker, a marker of acidic compartments in the late endosomal/lysosomal pathway. Colocalisation with LAMP1 and Cathepsin D appeared to be overall more affected by the timing of Clu exposure. This study offers a snapshot of the SO trafficking after a 30-minute treatment. It is likely that detectable Aβ accumulation in the lysosome occurs at a later point in time as has been reported previously [213, 255]. The presence of Clu may enhance SO uptake and thereby also the intracellular trafficking of the oligomers. It remains a goal to develop a more quantitative method of categorising microglial morphology and their activation state to enable a more objective assessment. Moreover, an investigation into how different concentrations of Aβ1-42 SO influence the morphological shift and how this concentration then translates into cytokine release would be of interest in the future. The findings herein are based on investigations using synthetic Aβ1-42. A comparison of the results discussed herein with the behaviour of recombinant Aβ1-42 would further facilitate our understanding of the interaction of Aβ1-42 SO and microglia. The following chapter sets out to explore the influence of another biomolecule, namely lysozyme, on the interaction of EOC 13.31 with Aβ1-42 SO.

5

LYSOZYME

5.1 Introduction and objectives

In the previous chapter, the interactions between the extracellular chaperone Clu and microglia cells have been investigated, along with their effect on neuroinflammatory responses. Employing confocal microscopy, it appears that Aβ1-42 SO and Clu colocalise and that Clu exerts a largely protective effect on Aβ1-42 SO-microglia interactions even though further experiments are needed to confirm these initial findings. While it is still unknown whether inflammation is a driver, a contributor, or an epiphenomenon of AD, recent years have brought forward new links between endogenous proteins of the immune system and Aβ. One such protein, lysozyme (Lys), is a major player of innate immunity (see Section 1.4.2) that is over-expressed in five different AD mouse models, while elevated levels of Lys have also been measured in the CSF of AD patients [197, 256]. The experimental foundation for studies that followed was provided by Lou and colleagues, who showed that *in vitro*, human Lys can prevent amyloid aggregation of the Aβ1-40 peptide at a 1:1 ratio [171]. Unlike Clu, which is a potent inhibitor of Aβ1-42 aggregation at sub-molar ratios, the amount of Lys needed to perturb Aβ1-42 aggregate formation is therefore significantly higher. Helmfors and colleagues later demonstrated that Lys colocalises with Aβ1-42 in plaques of AD patients and, following investigation of a Drosophila model of AD, they further reported that neuronal co-expression of Lys and Aβ1-42 reduced the formation of soluble and insoluble Aβ species, prolonged survival, and improved the activity of Aβ1-42 transgenic flies [196]. The concentrations and treatment durations used herein were chosen based on the aforementioned study by Lou et al. as well as unpublished work by Sandin et al., who observed that the uptake of TAMRA-labelled Aβ1-42 by SH-SY5Y cells was significantly reduced with the highest degree of reduction measured at a 1:2 Aβ1-42-to-Lys molar ratio [198]. These observations laid the foundation for a research collaboration and informed the chosen cell treatment conditions used herein.

Given its role during inflammatory events and scientific evidence pointing at a protective role of Lys in different AD models, this Chapter uses a number of biophysical and biochemical, as well as fluorescence microscopy techniques to elucidate how Lys interacts with Aβ1-42 SO and how this interaction influences Aβ1-42 SO uptake by microglia cells. Ultimately, it is the aim to understand whether the biomolecule Lys can modify the toxic effect of Aβ1-42 SO by changing its cellular internalisation. By comparing these findings with the insights derived from the Clu studies, we further aim to explore how the respective *modi operandi* translate into toxicity or the alleviation thereof. To date, the number of studies looking into the influence of Lys on microglia in the context of AD are very limited. However, a better understanding of the underlying processes that govern Lys and Aβ1-42 SO interaction with respect to microglia will help to shed light on how inflammation contributes to AD and thereby further facilitate the search for effective interventions.

5.1.1 Experimental setup

In this Chapter, TAMRA-labelled, HiLyte™ Fluor-488 labelled SO, as well as unlabelled Aβ1-42 SO are used to investigate oligomer interactions with microglial cells in the absence and presence of Lys. As this thesis is largely focused on Aβ1-42 interaction with microglia, synthetic Aβ rather than recombinant Aβ was used. Recombinant Aβ is preferentially expressed in E. coli given the simplicity of its expression system and availability of well-characterised genomic data, which greatly facilitate the vector design. However, the outer membrane of E. coli, like that of most Gram-negative bacteria, contains the potent proinflammatory molecule lipopolysaccharide (LPS) [257]. The removal of endotoxins from recombinantly expressed proteins require considerable effort and methodological constraints impair endotoxin removal in their entirety posing the risk of trace contamination [258–260]. In order to study the aggregation kinetics of Aβ1-42 and accompanying effects of the presence of Lys as well as Clu, recombinant Aβ as opposed to synthetic Aβ is used (see Fig. 5.2). These experiments typically require access to very homogeneous Aβ peptides as preformed seeds or small impurities of synthetic Aβ (despite the TFA and HFIP treatments) can have a great impact on the aggregation behavior [261]. Given the thioflavin T kinetics assay is a cell-free assay, possible endotoxin contamination is of lesser concern in this experiment, which further encouraged the use of recombinant Aβ in this set of experiments. However, the use of two different types of Aβ, namely synthetic and recombinant, need to be considered in the interpretation of results.

As in the previous Chapter, all cell experiments were carried out with the murine microglia cell line EOC 13.31. Here, a 1:2 Aβ1-42 SO-to-Lys molar ratio is used to better reflect the physiological conditions encountered by SO. Previous studies demonstrated, using electron microscopy, that the

TAMRA label did not affect oligomer formation, a quality control step that is also employed here [262]. Upon exposure of the microglial cells to TAMRA-labelled Aβ1-42 SO for 1.5 h in serum-free medium, the cells were washed twice with PBS to remove any unbound constituents. The cells were subsequently incubated in growth medium for 0.5 h to enable uptake of Aβ1-42 SO attached to the plasma membrane and then washed twice with PBS prior to further analysis.

Based on unpublished studies with SH-SY5Y cells and Aβ/Lys, the conditions for cell incubation were as follows: I) incubation with only labelled SO, II) incubation with a mixture of SO + Lys, and III) pre-incubation with Lys prior to SO exposure (Fig. 5.1, 2, 3, and 4). An additional co-aggregation condition was included in some experiments with the aim of investigating whether incubation of Lys and Aβ1-42 during oligomer formation had an effect on cellular interaction [198]. This condition is referred to as "SO/Lys co-aggregated" hereinafter (Fig. 5.1, 4). Incubation times and Aβ-to-Lys ratio were chosen based on previous work [171, 198].

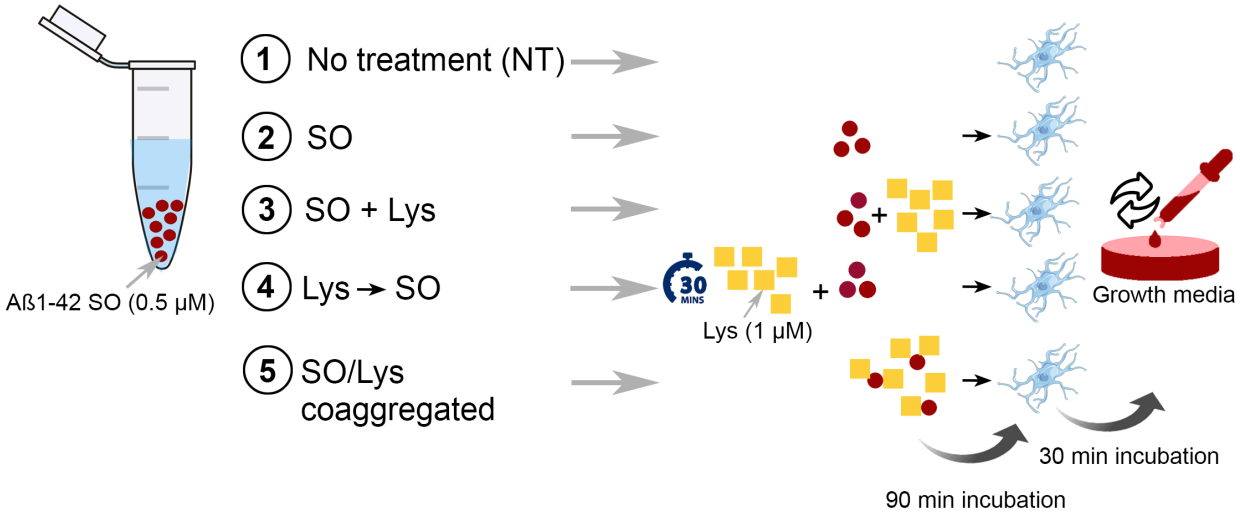

Figure 5.1: Schematic overview of experimental design. Note: items displayed are not drawn to scale.

5.2 Aβ1-42 aggregation kinetics with different lysozyme concentrations

In order to gain a better understanding of the effect that the biomolecule Lys exerts in the mechanism of co-aggregation, exploratory kinetic assays were performed using the benzathiole dye ThT that enables the monitoring of Aβ aggregation *in situ*. Here, a well-established kinetics assay using recombinant Aβ1-42 was performed to monitor the effects of Lys [200]. Vassar and Culling were first to describe the use of ThT as a potent fluorescent marker of amyloid in histology [263]. The quantification of amyloid fibrils in vitro by spectrophotometrically detecting the fluorescence emission of

ThT was first demonstrated by Naiki et al., who observed linearity between fibril concentration and emission intensity [264]. Since then, ThT has become one of the most widely used gold standards for selectively identifying and analysing formation of amyloid fibrils, both *in vivo* and *in vitro* [265]. Despite its extensive use for over 6 decades, the mechanism by which ThT recognises and binds peptide self-assemblies remains elusive. Proposed mechanisms are ThT interaction with β-sheet structures, the formation of ThT micelles binding to the grooves of the twisted protofibrils or fibrils, as well as a channel within the β-sheets of amyloid fibrils as site where ThT binds with its long axis parallel to that of the fibrils [266–268].

As previously mentioned, this method was chosen over aggregation assays with the synthetic Aβ as it has been reported that trace contaminants of the synthetic peptides may alter the aggregation kinetics, despite the TFA and HFIP treatments. Aβ monomers were incubated at 37° C in the absence and presence of Lys at a 2:1, 1:1, 1:2, and 1:5 Aβ1-42-to-Lys molar ratio (Fig. 5.2, A). For comparison, a 10:1 Aβ1-42-to-Clu condition was included as a positive control, as it is well known that submolar ratios of Clu can completely inhibit Aβ aggregation over the time scale of these assays (Fig. 5.2, B) [269]. Addition of the dye ThT enabled the monitoring of the formation of cross-β structured fibrils as indicated by an increase in fluorescence emission at 480 nm.

Figure 5.2 displays the aggregation profiles of Aβ1-42 in the absence and presence of Lys (A) and Clu (B) over time. The typical sigmoidal shape of the "Aβ1-42 only" curve is indicative of an accelerating aggregation reaction, suggesting contribution of secondary processes. The data, albeit exploratory, indicate that Lys might interfere with Aβ1-42 aggregation in a concentration-dependent manner, however, unlike Clu, Lys is not very effective at submolar ratios and 5-fold molar excess is needed to completely inhibit aggregation over this time scale. With respect to our SO-interaction studies, the data suggest that the 1:2 Aβ-to-Lys ratio is within the effective range of Lys inhibition. These observations are in line with previous findings reported by Helmfors et al., whose ThT analysis showed that the presence of Lys significantly slowed Aβ1-42 aggregation kinetics at a 1:1 ratio between Aβ1-42 and Lys, while no change in the ThT signal was detected for lysozyme alone. In her study, TEM images captured 24 h after aggregation initiation further confirmed fibril formation by the aggregated Aβ1-42 sample, whereas no fibrils were detected for the lysozyme samples [197].

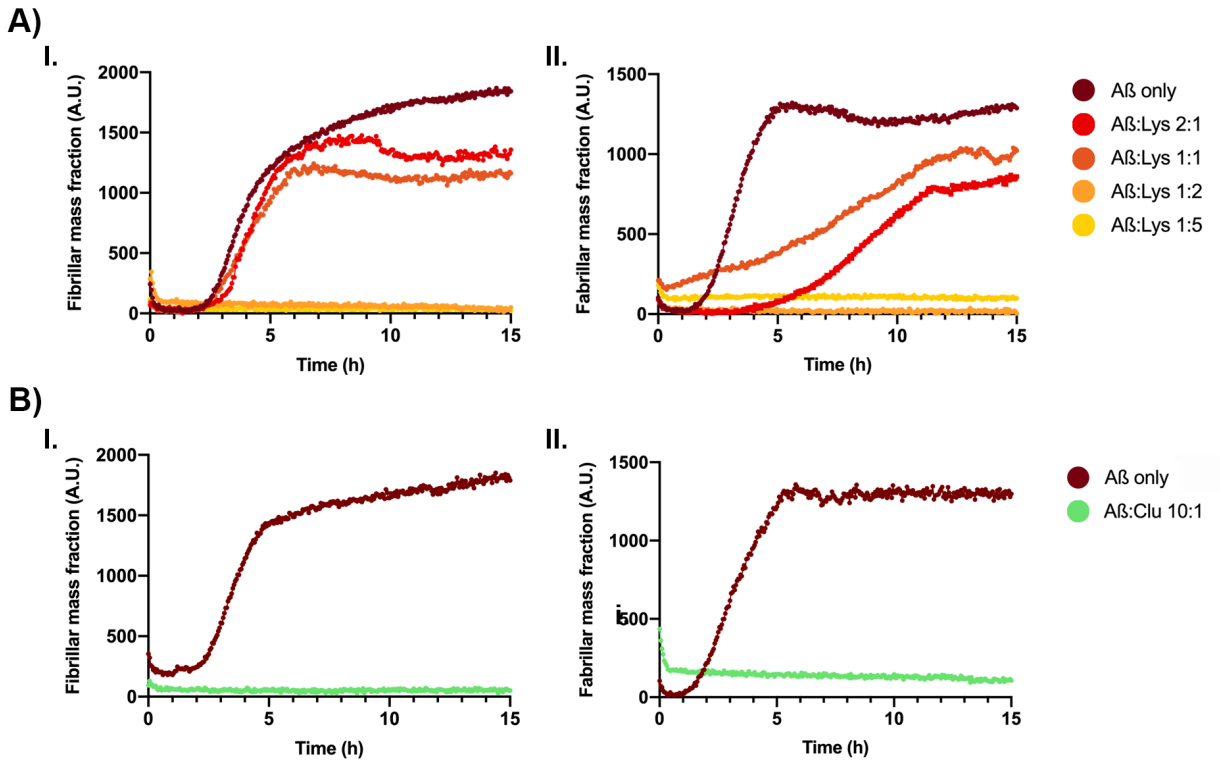

Figure 5.2: Aggregation kinetics of Aβ1-42 monomers with different concentrations of Lys. Aβ1-42 (2 µM) was incubated in the absence and presence of Lys at a 2:1, 1:1, 1:2, and 1:5 molar ratio of Aβ1-42-to-Lys as well as a 10:1 submolar ratio of Aβ1-42-to-Clu. Graphs I. and II. are derived from n = 2 independent experiments.

The herein presented results provide preliminary findings on the effect of Lys on Aβ aggregation. While a reduction in ThT fluorescence is often interpreted as an indication of the Aβ self-assembly process, additional repeats as well as control experiments, such as TEM analysis of resulting Aβ species and the quantification of resulting Aβ monomers need to be performed in order to be able to confirm Helmfors's previous findings and rule out fluorescence self-quenching through binding of ThT to the amyloid fibrils as reported by Lindberg et al. [270].

5.3 Study of Aβ1-42 and Lys interactions

Preliminary findings of the kinetics study along with reported results by Helmfors et al. suggest that Lys has the ability to inhibit Aβ1-42 SO aggregation in a concentration-dependent manner [197]. However, the underlying molecular processes of Aβ1-42 SO and Lys interactions and the role that exposure times play with regards to these interactions are not well understood. The following experiments therefore set out to investigate how the exposure of Aβ1-42 SO to Lys affects uptake by microglia and whether the timing of Lys exposure modifies the microglial response. First, the ques-

tion whether Aβ1-42 and Lys form a complex when administered simultaneously was addressed experimentally.

In order to answer this question, an immunoprecipitation (IP) technique using a His-tagged anti-Lys antibody as the bait was chosen. This antibody fragment, cAbHuL-6, has a strong affinity for human Lys in the native state and it has been used for ELISA pull-down assays for quantifying Lys in Drosophila lysate [207,271]. Briefly, IP enables the immobilisation of an antibody for a target protein (in this case, Lys) in a complex. Initially, the anti-Lys antibody cAbHuL-6 was immobilised on a magnetic Dynabead™ coated with cobalt-based immobilised metal affinity chromatography (IMAC) chemistry, which selectively binds histidine-tagged proteins (in this case, cAbHuL-6). Lys that had been pre-incubated with Aβ1-42 SO was then applied to the beads and the bound protein was eluted after several wash steps (Fig. 5.3, A). Next, a Western blot analysis on the eluted protein was carried out probing for Aβ1-42 SO. In theory, a band should only appear in those treatment condition that included both, Lys and Aβ1-42 SO as any non-specific binding would have been removed during the wash steps (see Fig. 5.3, A). The treatment conditions were the same as outlined in Section 5.1.1 with an Aβ1-42 SO-to-Lys molar ratio of 1:2 and an incubation time of 1.5 h at 37° C (Fig.5.3, H).

Figure 5.3 illustrates the reiteration of the IP assay carried out to optimise protocol parameters. Figure 5.3, B) shows the initial trial using 10 µM Aβ1-42 SO and 20 µM Lys, which resulted in high background noise and indistinguishable bands. A first attempt to reduce the extent of non-specific binding/noise was made by exchanging the eluent, SDS loading buffer (LB), for 8 M urea, and by increasing the Tween® concentration in the wash buffer, which was used for the remaining experiments. Iterations C) and D) investigated whether the temperature (37° C vs RT) during the 1.5 h incubation of Aβ1-42 SO and Lys affected their interactions. No detectable difference was observed between the two conditions, and hence, the remaining experiment were all conducted at 37° C in line with the incubation conditions of the other studies. While the use of urea and an increased concentration of Tween® in the wash buffer improved the signal quality, the visible bands in the Aβ1-42 monomer and SO conditions indicate that the experimental conditions resulted in non-specific binding of Aβ1-42 SO. Reiteration E) therefore aimed to identify an Aβ1-42 SO concentration that by itself, would not result in non-specific binding. At the same time, trial F) was carried out to determine the minimum detectable Lys concentration that resulted in a clear signal. Here, an anti-Lys primary antibody was used for protein visualisation. The results in Fig. 5.3, E) clearly demonstrate that if the Aβ1-42 SO concentration exceeds 0.5 µM, the SO is sticking to the cAbHuL-6 resin even when Lys is absent. Lys, on the other hand, showed a concentration-dependent signal, as would have been

expected (Fig. 5.3, F). However, all concentrations above 1 µM resulted in a lot of background noise. Given we were able to avoid non-specific binding when using 0.5 µM SO, the complex formation was investigated at a reduced concentration of 0.5 µM SO and 1 µM Lys (Fig. 5.3, G). Despite the various protocol adaptations, the non-specific binding of Aβ1-42 could not be prevented and the elution of complexed Aβ1-42 and Lys was not successful. The presented results (or the lack thereof) are likely attributable to experimental challenges due to the stickiness of Aβ1-42 rather than a lack of complex formation. A last attempt was made by using streptavidin-coupled Dynabeads® M-280 and biotinylated anti-Aβ antibody kindly provided by Sam Ness (University of Cambridge) as the bait. The experiment was conducted as outlined before, however, this time, an anti-Lys antibody was used for primary incubation to detect any Lys that, if in complex with Aβ1-42, would have been "pulled down" by the elution buffer. Because the experiment did not yield any visible bands despite the use of enhanced chemiluminescence (ECL) Western blot detection methods, data have been omitted.

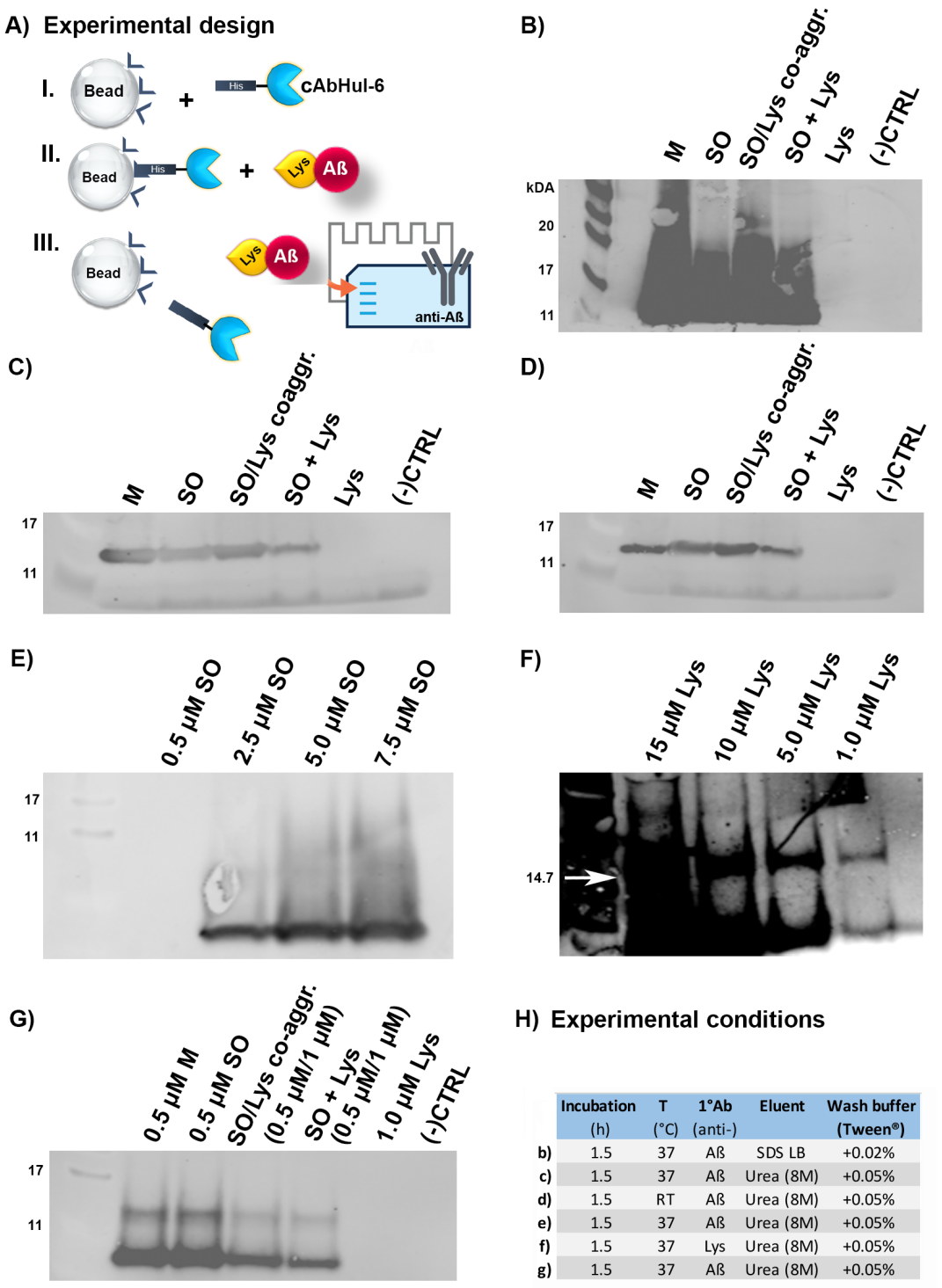

	Incubation (h)	T (°C)	1°Ab (anti-)	Eluent	Wash buffer (Tween®)
b)	1.5	37	Aß	SDS LB	+0.02%
c)	1.5	37	Aß	Urea (8M)	+0.05%
d)	1.5	RT	Aß	Urea (8M)	+0.05%
e)	1.5	37	Aß	Urea (8M)	+0.05%
f)	1.5	37	Lys	Urea (8M)	+0.05%
g)	1.5	37	Aß	Urea (8M)	+0.05%

Figure 5.3: Western blot analysis of eluates from a series of IP assays testing different incubation temperatures, elution buffers, as well as Aβ1-42 and Lys concentrations. A) Overview of experimental design; B) 10 µM Aβ1-42 at a 1:2 molar Aβ1-42-to-Lys ratio eluted with SDS LB and probed with anti-Aβ antibody (W02); C) 10 µM Aβ1-42 at a 1:2 molar Aβ1-42-to-Lys ratio eluted with 8 M urea at 37° C; D) 10 µM Aβ1-42 at a 1:2 molar Aβ1-42-to-Lys ratio eluted with 8 M urea at RT; E) Different concentrations of Aβ1-42 only; F) Different concentrations of Lys only probed with an anti-Lys antibody; G) 0.5 µM Aβ1-42 at 1:2 molar Aβ1-42-to-Lys ratio; H) Overview of experimental conditions. M represents monomeric Aβ1-42, (-)CTRL is a buffer control. Panels B, C, D, E, and G were probed with an anti-Aβ primary antibody and Panel F was probed with an anti-Lys primary antibody.

Even though we were unable to clearly demonstrate the complex formation of Aβ1-42 and Lys, aforementioned results point at a protective role of Lys in AD, which is in line with the findings of others [171, 195–197]. While most of the earlier studies were either performed *in situ* or in animal models, our knowledge of the modifying effect of Lys on the interaction of Aβ1-42 and microglia cells is limited. Given the importance of both, microglial cells and Lys in the innate immune response, the following set of experiments aims to enhance our understanding of whether and how the presence of Lys affects Aβ1-42 uptake by microglial cells, which could have important implications for neuroinflammation in AD.

5.4 Assessment of cell fluorescence upon SO and Lys treatment

Similar to the experimental design outlined in Chapter 4, Section 4.2, Aβ1-42 SO uptake by microglia cells was analysed using confocal microscopy. After 2 h of total incubation time (treatment + growth media), the fluorescence present within the cells was assessed with ImageJ. Using the WGA-stained cell images, the boundaries of the outer cell membrane were selected based on which the total cell fluorescence was calculated. The corrected total cell fluorescence (CTCF) as represented by the mean, is highest in the SO + Lys treatment conditions. The "SO only" and pre-treated conditions display comparable CTCF, whereas the CTCF of the control conditions (media only, i.e. "NT", and "Lys only") was significantly lower than that of SO-treated cells. The overall trend is similar to the observations made in the Clu experiment with simultaneous Aβ1-42 SO and Clu exposure resulting in the highest amount of internalised SO. The effect of simultaneous Lys exposure seen here appears more pronounced compared to Clu.

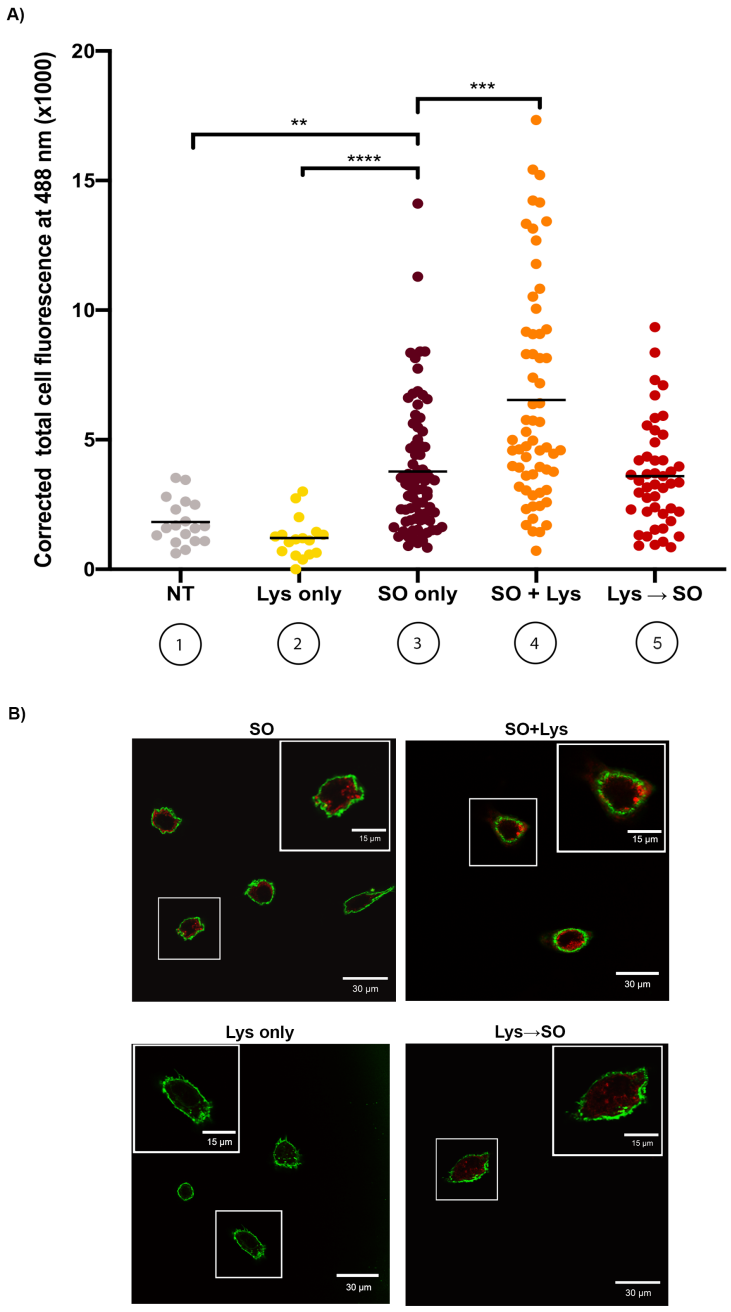

Figure 5.4: CTCF of EOC 13.31 microglia cells upon different treatments with SO and Lys (A, 1-5), as well as representative images of microglia cells in the respective treatment conditions (B). EOC 13.31 cells were treated with 0.5 µM TAMRA-labelled Aβ1-42 SO (A, 3), SO + Clu (A, 4), Lys only (A, 2) or media only (NT: A, 1) for 1.5 h, 37° C and subsequently incubated in growth medium for 0.5 h. Alternatively, cells were pretreated with 1 µM Lys (A, 5) for 0.5 h, 37° C followed by SO for another 1.5 h, 37° C and incubation in growth medium. The cell fluorescence was measured in ImageJ and compared across cell lines as per the Kruskall-Wallis test followed by Dunn's Multiple Comparisons test. Data points in A) represent n $\geq$ 17 cells pooled from n = 3 independent experiments. The mean of each group is marked by a black line. The representative images of EOC 13.31 show SO treatment (red) and Lys (unlabelled). The membrane stain WGA (green) was used to visualise the cell morphology. Scale bars = 10 µm (inset) or 30 µm. *, P < 0.05; **, P < 0.005; ***, P < 0.0005, ****, P < 0.00005. Images were contrast-enhanced post-analysis for better visualisation of fluorescence.

5.5 Morphology study of microglia cells under different SO and Lys treatment conditions

Next, the impact of the presence of Lys on microglia cells was assessed applying the same methodology as outlined in Chapter 4, Section 4.4. Confocal microscopy analysis of aforementioned cell treatment conditions revealed changes in microglia cell morphology. As morphological changes are related to microglia changing from a resting state to an activated form, a morphological response to SO and Lys treatments was observed and qualitatively analysed. The percentages of "elongated", "intermediate", and "rounded" cells as well as their respective average area are shown in Table 5.1. Representative images of the scored cell shapes are displayed in Fig. 5.5. Elongated cells were characterised by their neurite-like processes typical for non-activated microglia. Round cells with retracted protrusions represent activated microglia. Cells were defined as indeterminate if they displayed less pronounced extensions, yet, could not be described as round.

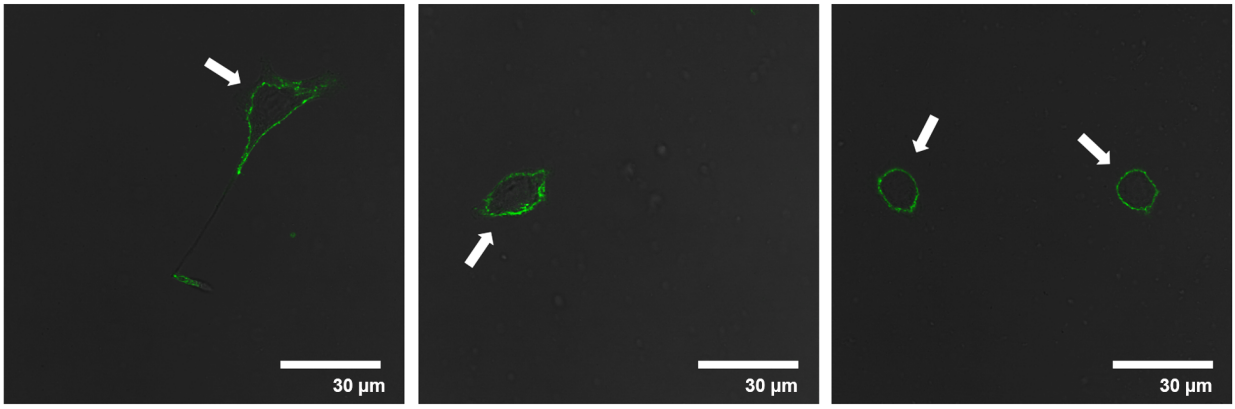

Figure 5.5: Morphological analysis of microglial activation. Microglial activation induces a morphological shift from an elongated to a rounded shape. Representative images of EOC 13.31 cell morphologies from n $\geq$ 3 experiments observed upon SO and Lys exposure as indicated by arrowheads. Cell membranes were stained with WGA. Scale bars = 30 µm. Images were contrast-enhanced post-analysis for better visualisation of fluorescence.

Additionally, the average area of the different cell morphologies was analysed with LPS treatment included as a positive control. As expected, the "Lys only" condition yielded the lowest fraction of "rounded" (activated) cells, while the "SO only" condition showed the highest. Strikingly, the simultaneous addition of SO + Lys yielded the highest fraction of "elongated" (resting) cells, even though this condition was shown to result in the largest amount of internalised Aβ1-42 SO (Fig. 5.1). These results imply that the presence of Lys may facilitate SO internalisation but masks the ability of the SO to elicit microglial activation.

Table 5.1: Quanitification of microglial activation upon SO exposure in different treatment conditions. EOC 13.31 cells were treated with SO, SO + Lys, Lys→SO, and LPS for 1.5 h, 37° C followed by a 30 min incubation in growth medium. Cell morphologies were qualitatively categorised as "elongated", "rounded", or "intermediate". Percentages of total cell counts from n $\geq$ 3 experiments are shown here. The average cell area $\pm$ SD was measured using ImageJ and compared to the "elongated" group within the same treatment condition applying the Welch's or one-sample t-test. *, P < 0.05; **, P < 0.005; ***, P < 0.0005.

	Cell morphology [%]			**Area of the cell [µm^2]**		
	elongated	intermediate	rounded	elongated	intermediate	rounded
Treatment [n]						
NT [31]	65	19	16	988 $\pm$ 302	564 $\pm$ 62	612 $\pm$ 147*
LPS-treated [28]	50	21	29	1285 $\pm$ 388	514 $\pm$ 018	934 $\pm$ 620**
Lys only [23]	78	18	4	1050 $\pm$ 245	393 $\pm$ 88	401 $\pm$ 0***
SO [78]	50	22	28	925 $\pm$ 410	666 $\pm$ 301	597 $\pm$ 239***
SO+Lys [63]	80	6	14	1027 $\pm$ 389	531 $\pm$ 81	606 $\pm$ 336**
Lys→SO [46]	61	22	17	944 $\pm$ 438	745 $\pm$ 355	507 $\pm$ 98***

5.6 Study of the effect of Lys on SO-microglia interactions with selected receptor inhibition

As indicated by the previous experiments, Lys likely slows down and may even prevent Aβ1-42 aggregation (see Fig.5.2), while it can also reduce microglia activation (see Fig. 5.5 and Table 5.1). Interestingly, the simultaneous addition of Lys and SO resulted in increased internalisation by microglia, while pre-incubation with Lys showed the same amount of internalisation as "SO only" but yielded less microglial activation according to the morphology data (28 % vs. 17 % of rounded cells). It is possible that the interaction of SO and Lys triggers a different, less damaging, route of internalisation. Using flow cytometry and selected receptor inhibitors, the following experiment aims to further investigate the interaction of SO with microglial cells at the membrane level. The treatment conditions for TAMRA-labelled SO remained the same as described in Section 5.1.1. Briefly, microglial cells were incubated with SO, SO + Lys, or pre-incubated with Lys for 0.5 h followed by 1.5 h incubation with SO. Upon treatment, the cells were incubated in growth medium for 0.5 h to remove non-specific binding. A "Lys only" and a "medium" condition were included as negative controls. Additionally, the effects of pre-incubation (0.5 h) with the receptor inhibitors LRPAP and Fucoidan were assessed.

LRPAP (LDL receptor-related protein-associated protein 1, also named RAP) is a ubiquitously expressed chaperone for LDL receptor family proteins. In the cell, LRPAP resides in the endoplasmic reticulum (ER), where it binds lipoprotein receptor-related protein 1 (LRP1). Together, they traffic to the Golgi apparatus, whose acidic environment causes dissociation of the complex [158]. When applied exogenously, LRPAP competitively inhibits LDL receptor family binding [272]. It binds to LRP1 on the cell surface, where it gets endocytosed and trafficked to the acidic endosome. Here, LRPAP and LRP1 dissociate and LRP1 recycles back to the cell surface [273]. LRP1 serves as a multifunctional receptor that controls the endocytosis of a variety of ligands, including Aβ, influences signaling pathways, and regulates gene expression through its intracellular domain [274]. Shibata et al. moreover reported that Aβ1-40 clearance was substantially inhibited by antibodies against LRP1 as demonstrated after intracerebral microinjections of Aβ1-40 in young mice [275].

Fucoidan is a bio-functional, sulfated polysaccharide extracted from marine sources like sea cucumbers and brown algea. Fucoidan has been the focus of many studies that revealed its anti-oxidant, anti-inflammatory, anti-tumor, anti-viral, and anti-coagulant properties [276–281]. Using a BV2 microglial cell model, Park and colleagues showed that Fucoidan was able to reduce the LPS-induced pro-inflammatory response of this cell line [282]. In the context of AD, Jhamandas et al. demonstrated that Fucoidan pretreatment of rat primary cultures exposed to Aβ1-42 resulted in an improvement of neuronal survival of cholinergic basal forebrain neurons and that Fucoidan did not interfere with Aβ1-42 aggregation [283]. In this experiment, both, LRPAP and Fucoidan, were included in order to investigate targeted receptor inhibition (LRPAP for LRP1 inhibition) and broader anti-inflammatory effects (Fucoidan as an inhibitor with broad effects).

The flow cytometry analysis revealed that monomeric Aβ1-42 displays the highest amount of association with microglial cells, followed by SO, then SO + Lys. The increased fluorescence in the monomeric condition may be explained by a rapid cellular uptake of Aβ1-42 monomers via endocytosis during the initial incubation, as was previously observed by Esbjoerner and colleagues [284]. Pre-incubation of microglia with Lys resulted in even less association and the least amount of cell-associated fluorescence was measured in the co-aggregation condition. These results are interesting as they are in contrast to the results of the SO internalisation study, where the highest amount of SO-associated fluorescence was measured in the SO + Lys condition, while pre-treatment of the cells with Lys did not reduce SO internalisation (see Fig. 5.4). As highlighted in Chapter 4, the confocal experiments were designed to measure the fluorescence of internalised SO, while flow cytometry does not distinguish between cell-associated and internalised SO. The fact that we observe different

trends in these two experiments implies that Lys might influence SO internalisation at the level of cell membrane interaction between SO and the microglia. It appears to alter cellular uptake by enhancing SO internalisation, especially when administered simultaneously with SO (SO + Lys yielded the third highest amount of cell-associated fluorescence, while this condition showed the highest degree of internalisation, as seen in Fig. 5.4, A) 3). SO, on the contrary, readily associates with the cells but it does not get internalised as rapidly as shown in the internalisation study (see Fig. 5.4, A) 2). While the pretreatment of microglia with Lys seems to overall prevent SO association with the cells as indicated by the low signal in the flow cytometry study, the reduced number of microglia-associated SO appear to get internalised more efficiently than SO (as indicated by comparable levels of internalised SO in the "SO only" and the Lys-pretreatment conditions, see Fig. 5.4, A) 2 and 4.

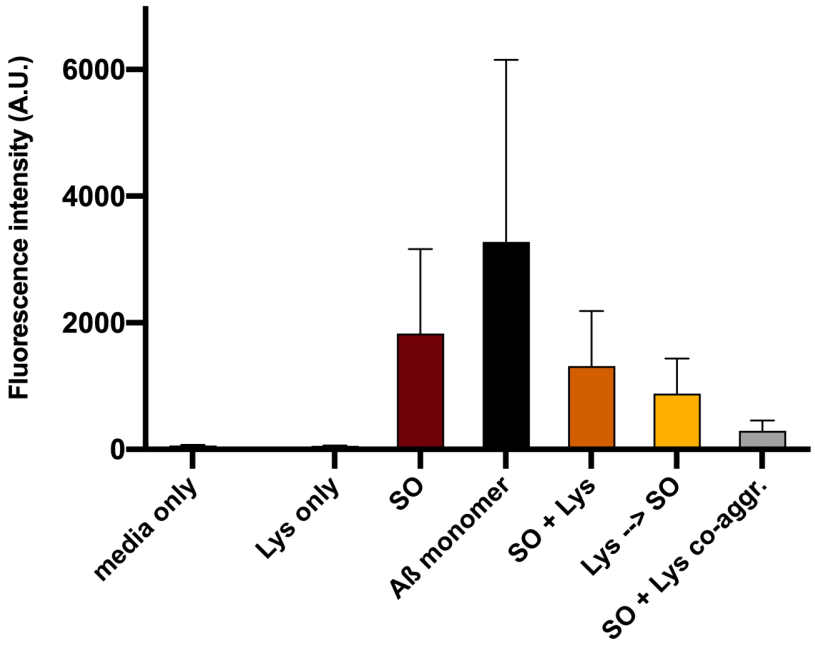

Figure 5.6: Flow cytometry analysis of microglial cells exposed to TAMRA-labelled SO in the absence and presence of Lys. The error bars represent the SD of n = 3 independent experiments. A Kruskal-Wallis test was performed, however, no statistically significant difference was detected.

The same experiment was carried out using inhibitors LRPAP and Fucoidan to determine whether LRP1 is involved in the uptake and to understand whether the different treatment conditions affect the route of internalisation, in which case we would expect to see a difference in the fluorescence pattern that we previously observed in our control experiment (see Fig. 5.7, A). The results are shown as percentages of the "CTRL" group (i.e. without inhibitor) of the respective treatment conditions. LRP1 inhibition yielded a slight increase in SO association with microglial cells across almost all conditions, while "Lys only" and pretreatment with Lys resulted in no change and a slight decrease, respectively. However, only the increase of microglial association with co-aggregated SO + Lys was

statistically significant. The treatment with Fucoidan, on the contrary, resulted in an overall reduction of SO association with microglia across all treatment conditions, with the SO + Lys condition as well as the co-aggregated SO + Lys condition showing statistical significance. Given that we aimed to understand early events of the interactions between microglia and SO, the same experiment was performed with a reduced (0.5 h) incubation time (see Fig. 5.7, B). LRP1 inhibition resulted in a statistically increased fluorescence in the SO + Lys condition as well as the co-aggregated SO + Lys condition. Incubation with fucoidan, again, resulted in a reduced fluorescent signal across all treatment groups, which was statistically significant in the SO, Aβ monomer, Lys then SO, and co-aggregated SO + Lys groups. The fact that LRP1 inhibition with LRPAP results in a significant increase in cell-association of co-aggregated SO + Lys reinforces our hypothesis that co-aggregation might yield a different Aβ1-42 species, which leads to a different mode of internalisation. An increase in association when LRP1 is inhibited might be attributable to receptor binding but blocked endocytosis of the receptor-ligand complex. However, at this point the available experimental data do not allow to draw sound conclusions. Fucoidan reduces the association of microglia and SO, which might be due to both, reduced binding and uptake to the cell. To further determine whether the observed interactions between SO and microglia are receptor-dependent, the same, short incubation (0.5 h) experiment was performed at 4° C with the rationale of slowing uptake and therefore only focus on cell surface interactions (see Fig. 5.7, C). Fucoidan appeared to have the same reducing effect on SO association with microglia as before, while the statistical significance is more pronounced in the SO and Lys pretreatment conditions. Overall, this trend suggests that Fucoidan exerts its reducing effect at the membrane level, possibly by preventing binding of the oligomers rather than at the receptor level. Noteworthy here is the reduction of SO association with microglia in the co-aggregated condition, which suggests that co-aggregated SO + Lys interacts with the LRP1 receptor at the membrane level, however, the underlying mechanisms need to be further explored.

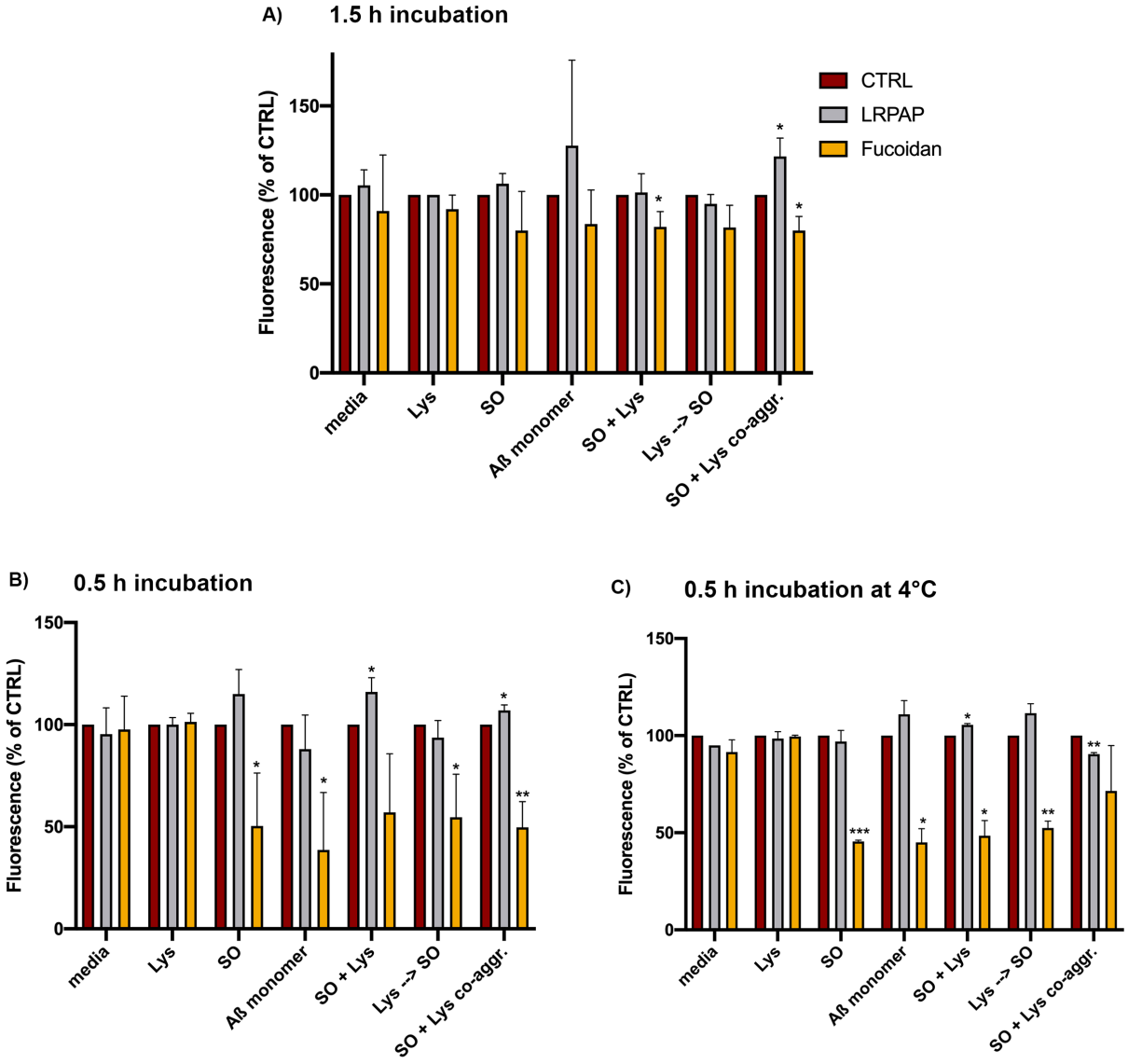

Figure 5.7: Flow cytometry analysis of microglial cells exposed to TAMRA-labelled SO in the absence and presence of Lys and the receptor inhibitors LRPAP (grey) and Fucoidan (yellow). Cells were incubated with the receptor inhibitors for 0.5 h prior to the respective SO treatment condition. The measured fluorescence is expressed as the percentage of the CTRL (red) condition. The experiment was carried out after 1.5 h incubation with the respective SO treatment (A), after 0.5 h incubation (B), and after 0.5 h incubation 4° C. The error bars represent the SD of n $\geq$ 2 independent experiments. Multiple t-tests were performed to compare the inhibitor effects to the CTRL group of respective treatment conditions, where *, P < 0.05; **, P < 0.005; ***, P < 0.0005.

5.7 Study of the impact of Lys on SO-membrane interactions

As mentioned previously, flow cytometry does not distinguish between cell-associated and internalised SO, however, given that we observe different trends in the flow cytometry study compared to the confocal microscopy study, Lys might influence SO internalisation at the level of cell membrane

interaction between SO and the microglial cells. While a large body of evidence in the literature suggests that endocytosis is critical in mediating Aβ1-42 toxicity, other studies also implicate that cellular toxicity of Aβ1-42 SO is partly attributable to their capacity to disrupt cellular membranes, thereby increasing membrane permeability [127, 132, 255, 285]. More specifically. it has been shown that Aβ can associate to the plasma membrane and induce the formation of pores, similar to pore-forming toxins, upon interaction with membrane lipids like GM1 and cholesterol. This results in increased permeability enabling the influx of small ions and larger molecules, which in return, may lead to an increase in intracellular Ca^{2+} concentration causing alterations in ionic homeostasis and ultimately cell death [286–288].

We therefore next investigated whether our chosen experimental SO conditions induce membrane permeabilisation and further elucidate whether Lys can modify Aβ1-42 SO membrane interaction, potentially underlining its previously observed cytoprotective effect. By using a membrane disruption assay, the responses to Aβ1-42 exposure can be investigated independent of possible receptor interactions. Furthermore, by reducing the number and complexity of different events, we aimed to provide additional insights on microscopic events that contribute to Aβ1-42 SO toxicity. Moreover, the experimental design allows to investigate the effects of Aβ1-42 SO at picomolar concentrations, which compares to the concentration of oligomers reported in human CSF [289].

In this experiment, membrane disruption was measured according to a protocol developed by Flagmeier et al. [208]. Briefly, membrane disruption was determined by Ca^{2+} entry into immobilised, nanosized vesicles filled with the calcium-sensitive dye Cal-520. Membrane disruption resulted in different extents of dye leakage allowing the binding of Ca^{2+} ions within the external media that, in return, induced an increase in fluorescence. We captured images of hundreds of individual vesicles per field of view via total internal reflection fluorescence microscopy (TIRFM) allowing the quantification of the change in fluorescence. Measured fluorescence was normalised to the Ca^{2+} influx upon addition of ionomycin. To assess the effect of Lys on Ca^{2+} influx, solutions containing 10 nM Aβ1-42 SO alone (Aβ SO), Aβ SO + Lys at molar ratios of 100:1, 10:1, 5:1, 1:1, and 1:10 (Aβ1-42-to-Lys) as well as Lys alone were added. Lys significantly reduced the membrane permeating effects of Aβ1-42 SO and the reduction of Ca^{2+} influx occurred in a concentration-dependent manner by as much as 87 % (Fig. 5.8, Aβ1-42 SO + Lys 1:10). At this ratio, the extent of Ca^{2+} influx was as low as that observed in the "Lys only" condition. Additionally, Aβ1-42 SO and Lys were co-aggregated at a ratio of 1:2, which significantly reduced the effect of Aβ1-42 SO on membrane disruption, however, the effect was less pronounced than Lys addition after Aβ1-42 oligomer formation. In this condition,

it is likely that the formation of oligomers in the presence of Lys result in a different morphology which may contribute to the change in membrane disruption capability. Moreover, the effect of the extracellular chaperone Clu on membrane permeation was tested and served as a positive control. Clu has repeatedly been reported to bind Aβ aggregates and it was previously shown to reduce Ca^{2+} influx into vesicles [208]. Here, a significant reduction in Ca^{2+} influx by as much as 88 % compared to Aβ1-42 SO was observed. We observed that Clu is a more potent inhibitor showing a comparable effect to the "SO + Lys 1:10" condition, however, at a much lower concentration.

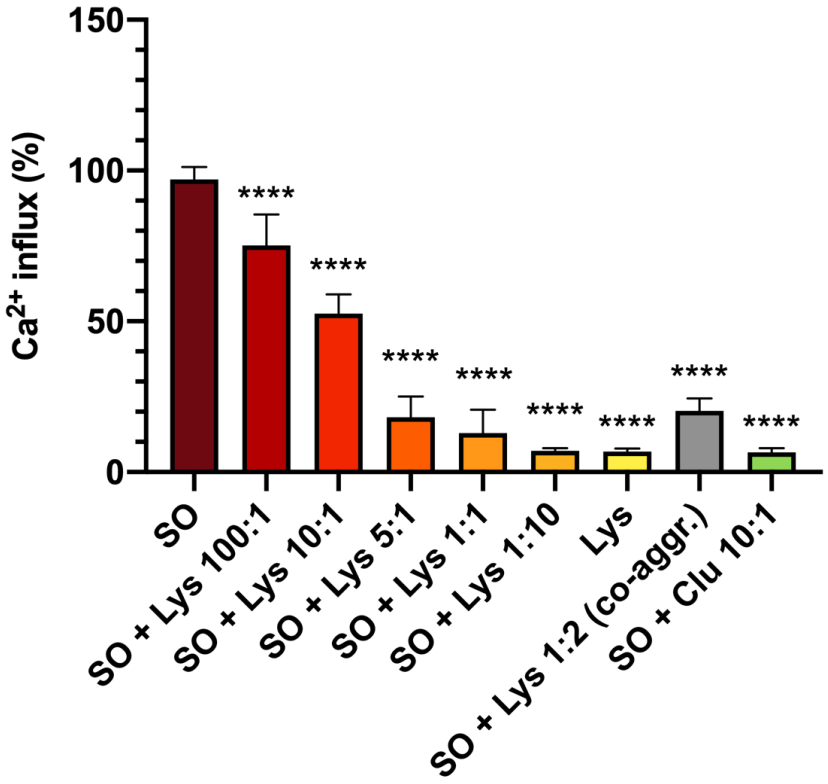

Figure 5.8: Study of the effect of different Lys concentrations as well as the chaperone Clu on Aβ1-42 SO induced Ca^{2+} influx. Error bars represent the SD of n = 3 independent experiments. All conditions were compared to Aβ SO using an ordinary one-way ANOVA with multiple comparisons, where ****, $P < 0.00005$.

5.8 Summary and discussion

The work in this Chapter investigated whether Lys could modify the toxic effect of Aβ1-42 on microglial cells by exploring the uptake and trafficking of Aβ1-42 SO in different Lys treatment conditions (simultaneous administration, pre-incubation with Lys, and co-aggregation of SO + Lys). Prior to exploring the effects of Lys in the cellular environment, it was investigated whether the Aβ1-42 SO-to-Lys molar ratio of 1:2 was within the effective range of Lys inhibition. Assuming that the reduction in ThT fluorescence is an indication of the inhibition of the macromolecular Aβ self-assembly process, preliminary results of the aggregation kinetics of Aβ1-42 in the presence of Lys suggest that Lys can extend the lag phase in a concentration-dependent manner and that a 1:2 molar ratio of recombinant Aβ1-42-to-Lys was sufficient to show an inhibitory effect (see Fig. 5.2). These observations are in line with previous findings reported by Luo et al., who showed that human lysozyme prevents Aβ peptide aggregation using ThT fluorescence assays and AFM imaging, combined with secondary structure characterisation by circular dichroism (CD) and NMR spectroscopy [171]. Molecular dynamics studies have moreover suggested a potential molecular interaction mechanism between lysozyme and the monomeric Aβ peptide [171]. The herein presented results provide preliminary findings on the effect of Lys on Aβ aggregation. While a reduction in ThT fluorescence is commonly interpreted as an indication for the Aβ self-assembly process, additional repeats as well as control experiments, such as TEM analysis of resulting Aβ species and the quantification of resulting Aβ monomers need to be performed in order to rule out fluorescence self-quenching through binding of ThT to the amyloid fibrils.

A pull-down assay was performed to further investigate the interaction of SO and Lys with the aim of demonstrating complex formation (see Fig. 5.3). The assay showed a lot of "false positive" signals, which were likely caused by non-specific binding of the Aβ1-42 to the cAbHuL-6 capture antibody or the Dynabeads® themselves. To overcome this problem, alternative assays would need to be explored. Kumita et al., for instance, used an ELISA based pull-down assay to detect clusterin-substrate complexes formed during aggregation, and this could be applied in the future for the Aβ-Lys complexes [290]. Alternatively, a proximity ligation assay or DNA-PAINT may be more suited for the investigation of complex formation. It has been previously reported, based on molecular docking simulations, that the N-terminus of Aβ1-40 binds to the active site of Lys; however, preliminary studies in our group did not show interactions between monomeric Aβ1-42 and WT Lys using 2D NMR techniques (personal communication, Dr. Minkoo Ahn), nor was Aβ1-42 able to inhibit Lys ac-

tivity (personal communication with Dr. Janet Kumita). Data on complex formation between Aβ1-42 and Lys therefore remain inconclusive and require further investigation.

While complex formation could not be shown here, the previous results taken together with previous findings hint at a sub-optimal experimental design rather than a lack of interaction between Aβ1-42 and Lys. Additional methods, such as a co-localisation study of fluorescently labelled SO and Lys, similar to the Clu study presented in Chapter 4, will need to be employed in order to further explore how and when SO and Lys interact. However, given the observed ThT fluorescence reduction during Aβ1-42 aggregation in the presence of Lys along with promising data from the literature, we carried on with our experimental conditions. The confocal microscopy study showed an increase in internalisation when SO and Lys were administered simultaneously. Confocal microscopy was the chosen method here due to its ability to obtain high-resolution images with all areas in focus throughout the field of view. It therefore enabled the detection and quantification of internalised SO. The observed trends across the different treatment conditions were similar to the effect that was seen when cells were treated with Clu. Strikingly, the increased uptake of SO + Lys was accompanied by the highest amount of elongated (resting) microglia (80 %). SO treatment and Lys pretreated cells showed the same amount of SO internalisation, while the concomitant microglial morphology suggested 11 % more activation (see Table 5.1). These findings suggest that the presence of Lys does not prevent SO internalisation per se but it may somehow reduce its activating (and potentially toxic) effects on microglial cells.

The results of the flow cytometry studies further suggest that Lys influences SO internalisation at the level of cell membrane interactions between SO and the microglia. SO showed the highest degree of membrane association in the flow study, while the confocal microscopy experiment indicated that the presence of Lys enhanced their internalisation. An enhancing effect on SO internalisation is also likely when the cells are pretreated with Lys as suggested by a relatively low degree of microglial association seen in the flow study and a comparatively high degree of internalisation in the confocal microscopy study (when compared to the "SO only" treatment condition). Interestingly, Fucoidan showed a significant reduction in SO-microglia association across all treatment conditions and irrespective of the presence of Lys. This effect was more pronounced at shorter incubation times and given the little effect that the reduction of temperature had on these results, it appears that the effect may have been receptor-independent. It would be interesting to further investigate whether the presence of Fucoidan prevents SO internalisation altogether, for example by confocal microscopy as was done with Lys and Clu. It is possible that during the longer incubation time of 1.5 h at 37° C,

the SO continue to aggregate and that the conformational change impacts the interaction with the membrane. Fucoidan has been shown to alter the properties of cell surfaces in the context of anti-viral studies, however, the underlying molecular mechanisms are not clear [291]. A similar effect on microglial cell membranes could explain the results observed here, however, these are merely speculations. Moreover, Fucoidan has been shown to inhibit nitric oxide (NO) synthesis in cells by down-regulating the expression of iNOS along with pro-inflammatory cytokines (TNFα, IL-6, IL-1β) [292]. While these results do not offer a direct explanation for the findings presented here, they can guide the direction for future experiments that would provide a better understanding of the downstream effects of SO, Lys, and Fucoidan in microglial cells.

The membrane permeabilisation assay provided further insights into the effects of Lys on Aβ SO at the membrane level. Here, we were able to show that synthetic Aβ1-42 SO can induce ion-permeable pores in synthetic membranes. The presence of Lys reduced membrane disruption in a concentration-dependent manner, though its effect was less potent than that observed for Clu. Given Clu is a chaperone with a high binding affinity for Aβ1-42, these findings do not come as a surprise [169]. When Aβ1-42 was co-aggregated with Lys, its ability to prevent membrane disruption was less potent. This was further indication that co-aggregation might result in a different species than addition of Lys post-oligomerisation of Aβ1-42. A recent study suggests that Aβ oligomers extract lipids from membranes, which causes membrane deformation and ultimately, membrane destabilization [293]. Future work could further investigate whether this study can be replicated with the Aβ1-42 SO used here and how Lys effects lipid extraction from membranes. While the experimental design allowed to investigate Aβ 1-42 SO-membrane interaction at physiologically relevant concentrations, the impact of SO requires additional investigation in the cellular context. Here, we used synthetic vesicles to demonstrate membrane permeabilisation, whereby we do not control for potential intracellular effects that may counteract membrane disruption.

Taken together, the results suggest that Lys may prevent Aβ1-42 aggregation and exert a protective effect on SO membrane interaction. The simultaneous administration seems to enhance SO uptake, without inducing microglial activation. Within the scope of our experiments, we observed an overall protective effect of Lys on the interactions between SO and microglia, which appears to take place at the membrane level. The search for receptor involvement in this process has not been exhaustive and could provide a molecular explanation for the observed processes. We acknowledge that the herein presented experiments partially involve different types of Aβ SO (recombinant Aβ for the kinetics assay and synthetic Aβ for the other experiments), the impact of which requires further exploration.

Moreover, some reultst are preliminary and provide guidance for follow-up studies to fully elucidate the effect of Lys on Aβ interaction with microglia cells.

6

DISCUSSION AND FUTURE WORK

6.1 Discussion

Over a century after its first mention in the scientific literature, AD remains one of the most prominent of the protein misfolding diseases. Despite extensive research over those years, the cause of the disease is still an enigma and remains a subject of controversy. The last decades have seen significant advances in our understanding of disease pathology adding the topic of neuroinflammation to the discussions around the Aβ and tau hypotheses. The once opposing schools of thought are now shaking hands and with united efforts, the search for effective treatments continues.

While the research focus has shifted to SO as the main toxic species in AD progression, the heterogeneity of aggregate morphology significantly contributes to the difficulty of studying how the pathogenic aggregates confer cellular dysfunction. Since the first description of the generation of ADDLs in the literature, many modifications have been made that improved our understanding of their characteristics as well as their physiological effects. Based on this knowledge, this thesis explored the internalisation of Aβ1-42 SO by a microglia cell line (EOC 13.31) in the absence and presence of the naturally occurring extracellular biomolecules, Clu and Lys, with the following aims: I) to validate SO formation of synthetic Aβ1-42, both, unlabelled as well as labelled with the dyes HiLyte™ Fluor-488 and TAMRA using different biophysical and biochemical techniques (Chapter 3), II) to investigate how the extracellular chaperone Clu alters the early events of uptake and trafficking of HiLyte™ Fluor-488-labelled Aβ1-42 SO by EOC 13.31 microglial cells, including studying morphological changes and microglial activation, along with pro-inflammatory cytokine release (Chapter 4), and III) to investigate the effect of the biomolecule Lys on the interactions of TAMRA-labelled Aβ1-42 and EOC 13.31 microglial cells (Chapter 5).

Findings and observations made throughout this thesis are summarized below, while it is stressed

that these observations have been made within the constraints of the experimental protocols used herein. Specifically, findings are limited to the study of synthetic Aβ1-42 (with the exception of the kinetics study, where recombinant Aβ was used). Moreover, observed interactions of Aβ1-42 SO and microglia are limited to EOC13.31 cells, while the interaction with other microglial cell lines is subject to further investigation. Experiments were moreover conducted under the assumption that labelled Aβ1-42 behaves similarly to unlabelled Aβ1-42 and that the impact of fluorophore molecular structures on Aβ assembly and function are negligible. Observations outlined below were made within 30 minutes of SO exposure to cells, which provides a snapshot of early events that occur upon Aβ1-42 exposure to EOC 13.31 microglia cells.
Within the scope of the experiments conducted within this thesis, the following observations were made:

1) Both, Clu and Lys appeared to increase SO internalisation by microglia when administered simultaneously.
2) Both, Clu and Lys may reduce Aβ1-42 SO toxicity, while Clu appears to be more potent *in vitro*.
3) Increased SO internalisation in the presence of Clu may contribute to microglial activation as indicated by a change in morphology, which was less pronounced in the presence of Lys.
4) Co-aggregation of Lys and SO may result in a new species with potentially different interaction patterns when exposed to EOC 13.31 microglia compared to Aβ1-42 SO.
5) Fucoidan appeared to reduce the association of SO with EOC 13.31, independent from the presence of Lys.

These findings are discussed in more detail below and their implications in the broader context of AD are highlighted.
Given experimental conditions, it was shown that EOC 13.31 microglial cells internalised Aβ1-42 SO and that this process was influenced by Clu, which significantly increased SO internalisation when administered simultaneously with SO. Simultaneous exposure of SO + Clu moreover resulted in a morphological shift from elongated cells to a rounded shape. which likely indicates microglial activation. The morphological features of the microglial cells upon activation are congruent with previous reports of microglial morphology in resting and activated states [236]. This activation, which appeared more pronounced when SO + Clu were administered simultaneously compared to pretreatment of Clu or SO alone may be due to increased SO internalisation as was observed in the confocal microscopy analysis. As the scoring of microglial morphology was done qualitatively, the assessment of the data was not fully objective. However, the quantitative assessment of microglial

that these observations have been made within the constraints of the experimental protocols used herein. Specifically, findings are limited to the study of synthetic Aβ1-42 (with the exception of the kinetics study, where recombinant Aβ was used). Moreover, observed interactions of Aβ1-42 SO and microglia are limited to EOC 13.31 cells, while the interaction with other microglial cell lines is subject to further investigation. Experiments were moreover conducted under the assumption that labelled Aβ1-42 behaves similarly to unlabelled Aβ1-42 and that the impact of fluorophore molecular structures on Aβ assembly and function are negligible. Observations outlined below were made within 30 minutes of SO exposure to cells, which provides a snapshot of early events that occur upon Aβ1-42 exposure to EOC 13.31 microglia cells.
Within the scope of the experiments conducted within this thesis, the following observations were made:

1) Both, Clu and Lys appeared to increase SO internalisation by microglia when administered simultaneously.
2) Both, Clu and Lys may reduce Aβ1-42 SO toxicity, while Clu appears to be more potent *in vitro*.
3) Increased SO internalisation in the presence of Clu may contribute to microglial activation as indicated by a change in morphology, which was less pronounced in the presence of Lys.
4) Co-aggregation of Lys and SO may result in a new species with potentially different interaction patterns when exposed to EOC 13.31 microglia compared to Aβ1-42 SO.
5) Fucoidan appeared to reduce the association of SO with EOC 13.31, independent from the presence of Lys.

These findings are discussed in more detail below and their implications in the broader context of AD are highlighted.
Given experimental conditions, it was shown that EOC 13.31 microglial cells internalised Aβ1-42 SO and that this process was influenced by Clu, which significantly increased SO internalisation when administered simultaneously with SO. Simultaneous exposure of SO + Clu moreover resulted in a morphological shift from elongated cells to a rounded shape, which likely indicates microglial activation. The morphological features of the microglial cells upon activation are congruent with previous reports of microglial morphology in resting and activated states [236]. This activation, which appeared more pronounced when SO + Clu were administered simultaneously compared to pretreatment of Clu or SO alone may be due to increased SO internalisation as was observed in the confocal microscopy analysis. As the scoring of microglial morphology was done qualitatively, the assessment of the data was not fully objective. However, the quantitative assessment of microglial

activation continues to be a scientific challenge given there are no morphological classification standards to date [146, 147]. In order to improve the assessment methodology and reduce the potential risk of bias in the present study, the cell morphology could additionally be scored by colleagues in order to calculate the representative mean of these assessments and provide an indication of the standard deviation.

It was further observed that, *in situ*, Clu is a potent inhibitor of synthetic membrane disruption by SO. Based on these findings it may be hypothesised that the interaction of SO + Clu could potentially modify the mode of internalisation of SO by EOC 13.31 cells, leading to more efficient, and less damaging, internalisation as partly suggested by the confocal studies. At the membrane level, our findings imply a protective role of Clu, which is interesting in the light of the present controversy as to whether Clu is predominantly neuroprotective or exacerbates SO toxicity [215, 223–226]. Importantly, the membrane disruption assay used herein was performed at physiologically relevant concentrations, which is a recurring point of criticism for cellular studies, which may inadequately mimic the *in vivo* events. One major limitation of the use of synthetic membranes, however, is the simplification of complex biological systems. Here, we do not control for potential intracellular effects that may counteract membrane disruption. The impact of SO therefore requires additional investigation in the cellular context to provide further insights.
The colocalisation studies indicated that, in the presence of Clu, SO show greater colocalisation with lysotracker, while SO also appear to colocalise with Cathepsin D when SO + Clu are administered simultaneously. The overall weak colocalisation with LAMP1 may be due to the time point of 30 minutes chosen for our investigation. It is possible that Aβ1-42 SO and Clu form a complex when administered simultaneously, thereby facilitating its uptake and further processing by microglial cells. Here, it is noteworthy that the present study only provides a snapshot of the early events of SO and microglia encounter. In order to thoroughly assess the trafficking of SO, a time-course experiment over a few hours or real-time imaging would provide a more thorough investigation.

Our exploratory study of the presence of Clu on microglial TNFα release suggested a reduced proinflmmatory response, which would ascribe Clu a protective role in AD. However, the measured TNFα release was lower than expected based on a literature review, while we also acknowledge that a direct comparison is difficult due to a wide array of different experimental designs ranging from the chosen cell model, over the concentration of the activating stimulus, to incubation times, and the ELISA kit used. Despite doubling the Aβ1-42 SO concentration and testing different collection times of the cell medium, the TNFα release could not be increased and the attempt to test for other

the ELISA kit used. Despite doubling the Aβ1-42 SO concentration and testing different collection times of the cell medium, the TNFα release could not be increased and the attempt to test for other pro- as well as an anti-inflammatory cytokines remained unsuccessful. A possible explanation for the discrepancy in our results to those of others may be attributable to the significantly longer incubation times used in those experiments (up to 48 h, whereas we exposed cells to SO for only 0.5 h) along with higher Aβconcentration (up to 20 µM). A longer incubation time is likely to provide an environment for continued aggregation of Aβ1-42 SO that could result in different species, such as fibrils, which are not the focus of this study. Further exploration of the stimulation of cytokine release by SO should therefore be continued at the transcription level. The exploratory qPCR experiment showed a measurable effect on EOC 13.31 TNFα mRNA levels, however, these findings need to be confirmed with SO at different concentrations and incubation times.

In recent years, new links between endogenous proteins of the immune system, such as Lys, and Aβ have been made. An unpublished study by Sandin et al. showed that the uptake of TAMRA-labelled Aβ1-42 by SH-SY5Y cells was significantly reduced with the highest degree of reduction measured at a 1:2 Aβ1-42-to-Lys molar ratio [198]. These findings, as well as earlier reports suggesting a protective role of Lys in various AD models provided the foundation for the experimental design outlined in Chapter 5 [196, 197, 256]. Our preliminary studies of the aggregation kinetics of Aβ1-42 in the presence of Lys suggest that Lys can extend the lag phase in a concentration-dependent manner, assuming that the reduction in ThT fluorescence is an indication of the inhibition of the macromolecular Aβ self-assembly process in line with previous findings reported by Luo et al. [171]. However, additional repeats as well as control experiments, such as TEM analysis of resulting Aβ species and the quantification of resulting Aβ monomers need to be performed in order to ensure that fluorescence self-quenching through binding of ThT to the amyloid fibrils do not contribute to the observed effect.

In the presence of Lys, our confocal microscopy analysis suggests that microglial cells may internalise a larger amount of SO, which also appeared to be the case when Clu was present. This effect, however, was only observed when Lys and SO were administered simultaneously, which could point at the necessity of spatial and temporal proximity as determining factors for their interaction and the herein observed effects. Our attempt to investigate the complex formation of Lys and SO in different treatment conditions was hampered by challenges that likely arose from the chosen experimental method, namely an immunoprecipitation assay. The sticky nature of Aβ1-42 may have been the underlying cause of non-specific binding, however, requires further investigation. Based on

our previously optimised protocols, a colocalisation study with fluorescently labelled Lys as well as Aβ1-42 SO could provide additional insights into their interaction patterns. Strikingly, the increased amount of internalised SO elicited contrasting microglial responses: while the presence of Clu appeared to induce microglial activation, Lys seemed to mask the activating effect of SO as indicated by a higher percentage of resting cells. Being highly glycosylated, Clu has been shown to interact with microglial receptors, such as TREM2. This interaction can increase the uptake of Aβ by microglial cells and could provide a route of internalisation of the SO + Clu complex observed in this study [177, 250]. TREM2 therefore presents an interesting inhibition target for further investigation into SO internalisation. Moreover, we are comparing different incubation times here (0.5 h for Clu vs. 1.5 h for Lys). It is possible that the extended incubation with Lys results in a different, less toxic, Aβ1-42 species, which might also contribute to the reduced microglial activation.

Lastly, the flow cytometry studies provide additonal insights into the effect of Lys on SO internalisation at the level of cell membrane interactions between SO and EOC 13.31 microglia. The reduction in SO-microglia association across all treatment conditions induced by Fucoidan, both at longer and shorter incubation times and at reduced temperature, implies that the effect of Lys on SO membrane interaction may, at least in part, be receptor-independent. Fucoidan has been previously shown to alter the properties of cell surfaces in the context of anti-viral studies although the underlying molecular mechanisms are unknown [291]. A similar effect on microglial cell membranes could explain the results observed here. However, further studies are needed to draw meaningful conclusions. It should also be noted that the inhibitory properties of Fucoidan are broad, which means that with our current knowledge, we cannot pinpoint specific underlying mechanisms for the observed results. Additional receptor inhibitors should therefore be tested in order to further explore the effects of Lys on SO.

Taken together, the experimental data within this thesis suggest that Lys may counteract Aβ1-42 aggregation and potentially exerts a protective effect on synthetic Aβ1-42 SO membrane interactions. The simultaneous administration seems to enhance SO uptake, without inducing microglial activation. Lys has shown an overall protective effect on the interactions between SO and microglia, which appear to take place at the membrane level. The search for receptor involvement in this process has not been exhaustive. However, the results in this thesis have demonstrated how different biomolecules can alter Aβ1-42 SO internalisation by EOC 13.31 microglia cells and thereby potentially reduce SO toxicity. Our results further suggest that the underlying molecular mechanisms of these interactions differ between the chaperone Clu and the biomolecule Lys, while additional ex-

periments are needed in order to validate these observations. In the next Section, future steps are discussed that could address limitations, provide additional context to these findings and ultimately, contribute to the broader understanding of the interplay between Aβ1-42 SO, neuroinflammation, and the role of protecitve innate biomolecules.

6.2 Future work

This study offers informative insights into the interplay of Aβ1-42 SO, microglial cells and their pro-inflammatory response, as well as the largely protective effects of chaperones and proteins of the innate immune system. The findings presented herein therefore provide an impetus to further explore the underlying molecular mechanisms of our observations. We already touched upon some of the shorter term experiments that could improve our understanding, such as developing a less subjective scoring method of microglial morphology, investigating the effect of additional receptor inhibitors on Aβ1-42 SO internalisation, optimising the qPCR method for evaluation of microglial cytokine release, and performing a colocalisation study of labelled Aβ1-42 SO and Lys to further investigate their mode of interaction.

More broadly, there are four main areas that would provide valuable insights into the underlying mechanisms of our observations, namely a study of the interaction of Lys and Aβ1-42 SO over longer periods of time, a study of the molecular events of Aβ1-42 SO and microglia at the membrane level, and a comprehensive study of the downstream processes of Aβ1-42 SO and microglia, both, in terms of intracellular trafficking as well as at the transcription level. Here, we provide snapshots of events taking place after 0.5 h and 1.5 h incubation, respectively. It is likely that longer incubation times lead to different Aβ1-42 species. A systematic study of Aβ1-42 morphology in our treatment conditions could provide a possible explanation for the Aβ1-42 membrane interactions described here. Moreover, it would be insightful to explore the interactions between Lys and microglial cells in normal, "non-disease" conditions to compare to the effects of Aβ1-42 SO exposure. Moreover, real-time imaging studies would be well-suited to track the internalised Aβ1-42 SO to determine whether the presence of Clu and Lys influence their intracellular trafficking. While our initial studies did not reveal any visible effects of Clu on Aβ1-42 SO trafficking, different time points along the journey need to be assessed. Finally, the use of Fucoidan has hinted at the effects of Aβ1-42, Clu, and Lys on the downstream processes that result from their microglial interactions. However, at this point we lack the molecular information to draw conclusions from our observations. For instance, Fucoidan has been shown to inhibit NO synthesis in cells by down-regulating the expression of iNOS along with

pro-inflammatory cytokines (TNFα, IL-6, and IL-1b) [292]. Selective assessment of the underlying pathways could provide an explanation for our findings at the transcription level. Taken together with our findings, these approaches would provide a well-rounded assessment of the influence of Clu and Lys on microglial internalisation and trafficking of Aβ1-42 SO.

Bibliography

[1] F. Chiti and C. M. Dobson, "Protein misfolding, functional myloid, and human disease," *Annu. Rev. Biochem*, vol. 75, pp. 333–66, 2006.

[2] C. Soto, "Protein misfolding and disease; protein refolding and therapy," *FEBS Letters*, 2001.

[3] S. P. Bell and A. Dutta, "DNA replication in eukaryotic cells," *Annual Review of Biochemistry*, vol. 71, pp. 333–374, 2002.

[4] C. R. Matthews, "Pathways of protein folding.," *Annual review of biochemistry*, vol. 62, pp. 653–83, 1993.

[5] D. Baker, "A surprising simplicity to protein folding," *Nature*, vol. 405, no. 6782, pp. 39–42, 2000.

[6] M. Heim, L. Römer, and T. Scheibel, "Hierarchical structures made of proteins. The complex architecture of spider webs and their constituent silk proteins," *Chem. Soc. Rev.*, vol. 39, pp. 156–164, 2010.

[7] O. Bieri and T. Kiefhaber, "Elementary steps in protein folding," *Biological chemistry*, vol. 380, no. 7-8, pp. 923–9, 1999.

[8] K. Mace and R. Gillet, "Origins of tmRNA: The missing link in the birth of protein synthesis?," *Nucleic Acids Research*, vol. 44, no. 17, pp. 8041–8051, 2016.

[9] T. K. Chaudhuri and S. Paul, "Protein-misfolding diseases and chaperone-based therapeutic approaches," *FEBS Journal*, vol. 273, no. 7, pp. 1331–1349, 2006.

[10] J. S. Valastyan and S. Lindquist, "Mechanisms of protein-folding diseases at a glance," *Disease models & mechanisms*, vol. 7, no. 1, pp. 9–14, 2014.

[11] E. T. Powers and W. E. Balch, "Diversity in the origins of proteostasis networks - a driver for protein function in evolution.," *Nature reviews. Molecular cell biology*, vol. 14, no. 4, pp. 237–48, 2013.

[12] A. Iram and A. Naeem, "Protein folding, misfolding, aggregation and their implications in human diseases: Discovering therapeutic ways to amyloid-associated diseases," *Cell Biochemistry and Biophysics*, vol. 70, no. 1, pp. 51–61, 2014.

[13] M. Takalo, A. Salminen, H. Soininen, M. Hiltunen, and A. Haapasalo, "Protein aggregation and degradation mechanisms in neurodegenerative diseases," *American journal of neurodegenerative disease*, vol. 2, no. 1, pp. 1–14, 2013.

[14] D. M. Smith, G. Kafri, Y. Cheng, D. Ng, T. Walz, and A. L. Goldberg, "ATP binding to PAN or the 26S ATPases causes association with the 20S proteasome, gate opening, and translocation of unfolded proteins," *Molecular Cell*, 2005.

[15] D. Glick, S. Barth, and K. F. Macleod, "Autophagy : Cellular and molecular mechanisms," *Journal of Pathology The*, vol. 221, no. 1, pp. 3–12, 2010.

[16] G. E. Mortimore and C. M. Schworer, "Induction of autophagy by amino-acid deprivation in perfused rat liver," *Nature*, 1977.

[17] L. Jahreiss, F. M. Menzies, and D. C. Rubinsztein, "The itinerary of autophagosomes: From peripheral formation to kiss-and-run fusion with lysosomes," *Traffic*, 2008.

[18] C. De Duve and R. Wattiaux, "Functions of lysosomes.," 1966.

[19] J. Ahlberg and H. Glaumann, "Uptake-Microautophagy-and degradation of exogenous proteins by isolated rat liver lysosomes. Effects of pH, ATP, and inhibitors of proteolysis," *Experimental and Molecular Pathology*, 1985.

[20] H. L. Chiang, S. R. Terlecky, C. P. Plant, and J. F. Dice, "A role for a 70-kilodaton heat shock protein in lysosomal degradation of intracellular proteins," *Science*, 1989.

[21] A. M. Cuervo, S. R. Terlecky, J. F. Dice, and E. Knecht, "Selective binding and uptake of ribonuclease A and glyceraldehyde-3- phosphate dehydrogenase by isolated rat liver lysosomes," *Journal of Biological Chemistry*, 1994.

[22] A. M. Cuervo and J. F. Dice, "Age-related decline in chaperone-mediated autophagy," *Journal of Biological Chemistry*, 2000.

[23] S. H. Lecker, A. L. Goldberg, and W. E. Mitch, "Protein degradation by the ubiquitin-proteasome pathway in normal and disease states.," *Journal of the American Society of Nephrology : JASN*, vol. 17, no. 7, pp. 1807–1819, 2006.

[24] T. Lamitina, C. G. Huang, and K. Strange, "Genome-wide RNAi screening identifies protein damage as a regulator of osmoprotective gene expression," *Proceedings of the National Academy of Sciences of the United States of America*, 2006.

[25] T. J. Van Ham, K. L. Thijssen, R. Breitling, R. M. Hofstra, R. H. Plasterk, and E. A. Nollen, "C. elegans model identifies genetic modifiers of α-synuclein inclusion formation during aging," *PLoS Genetics*, 2008.

[26] C. Yun, A. Stanhill, Y. Yang, Y. Zhang, C. M. Haynes, C. F. Xu, T. A. Neubert, A. Mor, M. R. Philips, and D. Ron, "Proteasomal adaptation to environmental stress links resistance to proteotoxicity with longevity in Caenorhabditis elegans," *Proceedings of the National Academy of Sciences of the United States of America*, 2008.

[27] S. A. Houck, S. Singh, and D. M. Cyr, "Cellular responses to misfolded proteins and protein aggregates.," *Methods in molecular biology (Clifton, N.J.)*, vol. 832, pp. 455–61, 2012.

[28] F. Chiti, P. Webster, N. Taddei, A. Clark, M. Stefani, G. Ramponi, and C. M. Dobson, "Designing conditions for in vitro formation of amyloid protofilaments and fibrils," *Proceedings of the National Academy of Sciences of the United States of America*, 1999.

[29] E. Herczenik and M. F. B. G. Gebbink, "Molecular and cellular aspects of protein misfolding and disease.," *The FASEB journal*, vol. 22, no. 7, pp. 2115–2133, 2008.

[30] M. A. Rosenfeld, V. B. Leonova, M. L. Konstantinova, and S. D. Razumovskii, "Self-assembly of fibrin monomers and fibrinogen aggregation during ozone oxidation.," *Biochemistry (Moscow)*, vol. 74, no. 1, pp. 41–46, 2009.

[31] L. Zhang, D. Lu, and Z. Liu, "How native proteins aggregate in solution: A dynamic Monte Carlo simulation," *Biophysical Chemistry*, vol. 133, no. 1-3, pp. 71–80, 2008.

[32] M. Stefani, "Protein folding and misfolding on surfaces," *International Journal of Molecular Sciences*, vol. 9, no. 12, pp. 2515–2542, 2008.

[33] C. M. Dobson, "Protein folding and misfolding," *Nature*, vol. 426, no. December, pp. 884–890, 2003.

[34] K. W. Tipping, P. van Oosten-Hawle, E. W. Hewitt, and S. E. Radford, "Amyloid Fibres: Inert end-stage Aggregates or key players in disease?," *Trends in Biochemical Sciences*, vol. 40, no. 12, pp. 719–727, 2015.

[35] E. D. Eanes and G. G. Glenner, "X-ray diffraction studies on amyloid filaments.," *The journal of histochemistry and cytochemistry : official journal of the Histochemistry Society*, 1968.

[36] M. Sunde, L. C. Serpell, and M. Bartlam, "Common core structure of amyloid fibrils by synchrotron X-ray diffraction," *Journal of Molecular Biology*, vol. 273, no. 3, pp. 729–739, 1997.

[37] C. M. Dobson, B. E. Swoboda, M. Joniau, and C. Weissman, "The structural basis of protein folding and its links with human disease," in *Philosophical Transactions of the Royal Society B: Biological Sciences*, 2001.

[38] A. S. Cohen and E. Calkins, "Electron Microscopic Observations on a fibrous component in amyloid of diverse origins," *Nature*, 1959.

[39] J. E. Gillam and C. E. MacPhee, "Modelling amyloid fibril formation kinetics: mechanisms of nucleation and growth," *Journal of Physics: Condensed Matter*, vol. 25, no. 37, p. 373101, 2013.

[40] A. Lomakin, D. B. Teplow, D. A. Kirschner, and G. B. Benedek, "Kinetic theory of fibrillogenesis of amyloid beta-protein.," *Proceedings of the National Academy of Sciences of the United States of America*, vol. 94, no. 15, pp. 7942–7, 1997.

[41] L. A. Munishkina and A. L. Fink, "Fluorescence as a method to reveal structures and membrane-interactions of amyloidogenic proteins," *Biochimica et Biophysica Acta - Biomembranes*, vol. 1768, no. 8, pp. 1862–1885, 2007.

[42] T. P. J. Knowles, M. Vendruscolo, and C. M. Dobson, "The amyloid state and its association with protein misfolding diseases.," *Nature reviews. Molecular cell biology*, vol. 15, no. 6, pp. 384–96, 2014.

[43] P. Arosio, T. P. J. Knowles, and S. Linse, "On the lag phase in amyloid fibril formation," *Physical Chemistry Chemical Physics*, vol. 17, no. 12, pp. 7606–7618, 2015.

[44] S. I. Cohen, S. Linse, L. M. Luheshi, E. Hellstrand, D. A. White, L. Rajah, D. E. Otzen, M. Vendruscolo, C. M. Dobson, and T. P. Knowles, "Proliferation of amyloid-β42 aggregates occurs through a secondary nucleation mechanism," *Proceedings of the National Academy of Sciences of the United States of America*, 2013.

[45] S. C. Hook, K. Roberts, J. R. Kumita, and J. J. Yerbury, "The interplay of protein aggregates, microglia and neuroinflammation in neurodegenerative disease," in *Microglia: Physiology, Regulation and Health Implications*, 2015.

[46] C. M. Dobson, "Protein misfolding, evolution and disease," *Trends in Biochemical Sciences*, 1999.

[47] F. Chiti, M. Stefani, N. Taddei, G. Ramponi, and C. M. Dobson, "Rationalization of the effects of mutations on peptide and protein aggregation rates," *Nature*, 2003.

[48] G. G. Tartaglia, A. P. Pawar, S. Campioni, C. M. Dobson, F. Chiti, and M. Vendruscolo, "Prediction of aggregation-prone regions in structured proteins," *Journal of Molecular Biology*, 2008.

[49] V. L. Feigin, E. Nichols, and T. Alam, "Global, regional, and national burden of neurological disorders, 1990â2016: a systematic analysis for the global burden of disease study 2016," *The Lancet Neurology*, 2019.

[50] J. Xu, Y. Zhang, C. Qiu, and F. Cheng, "Global and regional economic costs of dementia: a systematic review," *The Lancet*, 2017.

[51] K. Maurer, S. Volk, and H. Gerbaldo, "Auguste D and Alzheimer's disease," *Lancet*, 1997.

[52] G. G. Glenner and C. W. Wong, "Alzheimer's disease: Initial report of the purification and characterization of a novel cerebrovascular amyloid protein," *Biochemical and Biophysical Research Communications*, 1984.

[53] C. L. Masters, G. Simms, and N. A. Weinman, "Amyloid plaque core protein in Alzheimer disease and Down syndrome," *Proceedings of the National Academy of Sciences of the United States of America*, 1985.

[54] J. P. Brion, H. Passareiro, J. Nunez, and J. Flament-Durand, "Mise en evidence immunologique de la proteine tau au niveau des lesions de degenerescence neurofibrillaire de la maladie d'Alzheimer," *Archives de Biologie*, 1985.

[55] I. Grundke-Iqbal, K. Iqbal, and Y. C. Tung, "Abnormal phosphorylation of the microtubule-associated protein tau (tau) in Alzheimer cytoskeletal pathology.," *Proceedings of the National Academy of Sciences of the United States of America*, 1986.

[56] Y. Ihara, N. Nukina, R. Miura, and M. Ogawara, "Phosphorylated tau protein is integrated into paired helical filaments in alzheimer's disease," *Journal of Biochemistry*, 1986.

[57] M. Goedert, M. G. Spillantini, and N. J. Cairns, "Tau proteins of Alzheimer paired helical filaments: Abnormal phosphorylation of all six brain isoforms," *Neuron*, 1992.

[58] J. Avila, J. J. Lucas, M. Pérez, and F. Hernández, "Role of tau protein in both physiological and pathological conditions," *Physiological Reviews*, 2004.

[59] J. Miao, R. Shi, L. Li, F. Chen, Y. Zhou, Y. C. Tung, W. Hu, C.-X. Gong, K. Iqbal, and F. Liu, "Pathological tau from Alzheimer's brain induces site-specific hyperphosphorylation and SDS- and reducing agent-resistant aggregation of tau in vivo," *Frontiers in Aging Neuroscience*, 2019.

[60] J. E. Tobin, J. C. Latourelle, M. F. Lew, C. Klein, O. Suchowersky, H. A. Shill, L. I. Golbe, M. H. Mark, J. H. Growdon, G. F. Wooten, B. A. Racette, J. S. Perlmutter, R. Watts, M. Guttman, K. B. Baker, S. Goldwurm, G. Pezzoli, C. Singer, M. H. Saint-Hilaire, A. E. Hendricks, S. Williamson, M. W. Nagle, J. B. Wilk, T. Massood, J. M. Laramie, A. L. Destefano, I. Litvan, G. Nicholson, A. Corbett, S. Isaacson, D. J. Burn, P. F. Chinnery, P. P. Pramstaller, S. Sherman, J. Al-Hinti, E. Drasby, M. Nance, A. T. Moller, K. Ostergaard, R. Roxburgh, B. Snow, J. T. Slevin, F. Cambi, J. F. Gusella, and R. H. Myers, "Haplotypes and gene expression implicate the MAPT region for Parkinson disease: The GenePD Study," *Neurology*, 2008.

[61] J. Simón-Sánchez, C. Schulte, J. M. Bras, M. Sharma, J. R. Gibbs, D. Berg, C. Paisan-Ruiz, P. Lichtner, S. W. Scholz, D. G. Hernandez, R. Krüger, M. Federoff, C. Klein, A. Goate, J. Perlmutter, M. Bonin, M. A. Nalls, T. Illig, C. Gieger, H. Houlden, M. Steffens, M. S. Okun, B. A. Racette, M. R. Cookson, K. D. Foote, H. H. Fernandez, B. J. Traynor, S. Schreiber, S. Arepalli, R. Zonozi, K. Gwinn, M. Van Der Brug, G. Lopez, S. J. Chanock, A. Schatzkin, Y. Park, A. Hollenbeck, J. Gao, X. Huang, N. W. Wood, D. Lorenz, G. Deuschl, H. Chen, O. Riess, J. A. Hardy, A. B. Singleton, and T. Gasser, "Genome-wide association study reveals genetic risk underlying Parkinson's disease," *Nature Genetics*, 2009.

[62] A. M. Pittman, A. J. Myers, P. Abou-Sleiman, H. C. Fung, M. Kaleem, L. Marlowe, J. Duckworth, D. Leung, D. Williams, L. Kilford, N. Thomas, C. M. Morris, D. Dickson, N. W. Wood, J. Hardy, A. J. Lees, and R. De Silva, "Linkage disequilibrium fine mapping and haplotype association analysis of the tau gene in progressive supranuclear palsy and corticobasal degeneration," *Journal of Medical Genetics*, 2005.

[63] M. Hutton, C. L. Lendon, P. Rizzu, M. Baker, S. Froelich, H. H. Houlden, S. Pickering-Brown, S. Chakraverty, A. Isaacs, A. Grover, J. Hackett, J. Adamson, S. Lincoln, D. Dickson, P. Davies, R. C. Petersen, M. Stevena, E. De Graaff, E. Wauters, J. Van Baren, M. Hillebrand, M. Joosse, J. M. Kwon, P. Nowotny, L. K. Che, J. Norton, J. C. Morris, L. A. Reed, J. Trojanowski, H. Basun, L. Lannfelt, M. Neystat, S. Fahn, F. Dark, T. Tannenberg, P. R. Dodd, N. Hayward, J. B. Kwok, P. R. Schofield, A. Andreadis, J. Snowden, D. Craufurd, D. Neary, F. Owen, B. A. Costra,

J. Hardy, A. Goate, J. Van Swieten, D. Mann, T. Lynch, and P. Heutink, "Association of missense and 5'-splice-site mutations in tau with the inherited dementia FTDP-17," *Nature*, 1998.

[64] P. Poorkaj, T. D. Bird, E. Wijsman, E. Nemens, R. M. Garruto, L. Anderson, A. Andreadis, W. C. Wiederholt, M. Raskind, and G. D. Schellenberg, "Tau is a candidate gene for chromosome 17 frontotemporal dementia," *Annals of Neurology*, 1998.

[65] J. Hardy and D. Allsop, "Amyloid deposition as the central event in the aetiology of Alzheimer's disease," *Trends in Pharmacological Sciences*, 1991.

[66] K. Beyreuther and C. L. Masters, "Amyloid Precursor Protein (APP) and ÎZA4 amyloid in the etiology of Alzheimer's disease: Precursorâproduct relationships in the derangement of neuronal function," *Brain Pathology*, 1991.

[67] J. A. Hardy and G. A. Higgins, "Alzheimer's disease: The amyloid cascade hypothesis," *Science*, 1992.

[68] D. J. Selkoe, "The molecular pathology of Alzheimer's disease," *Neuron*, 1991.

[69] S. A. Small and K. Duff, "Linking Aβ and tau in late-onset Alzheimer's disease: A dual pathway hypothesis," *Neuron*, 2008.

[70] L. M. Ittner and J. Götz, "Amyloid-β and tau - A toxic pas de deux in Alzheimer's disease," *Nature Reviews Neuroscience*, 2011.

[71] G. S. Bloom, "Amyloid-β and tau - The trigger and bullet in Alzheimer disease pathogenesis," *JAMA Neurology*, 2014.

[72] T. L. Spires-Jones and B. T. Hyman, "The intersection of amyloid beta and tau at synapses in Alzheimer's disease," *Neuron*, 2014.

[73] E. S. Musiek and D. M. Holtzman, "Three dimensions of the amyloid hypothesis: time, space and 'wingmen'," *Nat Neurosci*, vol. 18, no. 6, pp. 800–806, 2015.

[74] S. D. Yan, X. Chen, J. Fu, M. Chen, H. Zhu, A. Roher, T. Slattery, L. Zhao, M. Nagashima, J. Morser, A. Migheli, P. Nawroth, D. Stern, and A. M. Schmidt, "RAGE and amyloid-β peptide neurotoxicity in Alzheimer's disease," *Nature*, 1996.

[75] A. Cagnin, D. J. Brooks, A. M. Kennedy, R. N. Gunn, R. Myers, F. E. Turkheimer, T. Jones, and R. B. Banati, "In-vivo measurement of activated microglia in dementia," *Lancet*, 2001.

[76] M. Kitazawa, T. R. Yamasaki, and F. M. LaFerla, "Microglia as a potential bridge between the amyloid β-peptide and tau," in *Annals of the New York Academy of Sciences*, 2004.

[77] K. A. Walker, R. C. Hoogeveen, A. R. Folsom, C. M. Ballantyne, D. S. Knopman, B. G. Windham, C. R. Jack, and R. F. Gottesman, "Midlife systemic inflammatory markers are associated with late-life brain volume: The ARIC study," *Neurology*, 2017.

[78] M. A. Pericak-Vance, L. H. Yamaoka, C. S. Haynes, M. C. Speer, J. L. Haines, P. C. Gaskell, W. Y. Hung, C. M. Clark, A. L. Heyman, J. A. Trofatter, J. P. Eisenmenger, J. R. Gilbert, J. E. Lee, M. J. Alberts, D. V. Dawson, R. J. Bartlett, N. L. Earl, T. Siddique, J. M. Vance, P. M. Conneall, and A. D. Roses, "Genetic linkage studies in Alzheimer's disease families," *Experimental Neurology*, 1988.

[79] E. H. Corder, A. M. Saunders, W. J. Strittmatter, D. E. Schmechel, P. C. Gaskell, G. W. Small, A. D. Roses, J. L. Haines, and M. A. Pericak-Vance, "Gene dose of apolipoprotein E type 4 allele and the risk of Alzheimer's disease in late onset families," *Science*, 1993.

[80] W. J. Strittmatter, A. M. Saunders, D. Schmechel, M. Pericak-Vance, J. Enghild, G. S. Salvesen, and A. D. Roses, "Apolipoprotein E: High-avidity binding to β-amyloid and increased frequency of type 4 allele in late-onset familial Alzheimer disease," *Proceedings of the National Academy of Sciences of the United States of America*, 1993.

[81] D. Harold, R. Abraham, P. Hollingworth, and E. Al., "Genome-wide association study identifies variants at CLU and PICALM associated with Alzheimer's disease," *Nature Genetics*, vol. 41, no. 10, pp. 1088–1093, 2009.

[82] M. P. Lambert, A. K. Barlow, B. A. Chromy, C. Edwards, R. Freed, M. Liosatos, T. E. Morgan, I. Rozovsky, B. Trommer, K. L. Viola, P. Wals, C. Zhang, C. E. Finch, G. A. Krafft, and W. L. Klein, "Diffusible, nonfibrillar ligands derived from Aβ1-42 are potent central nervous system neurotoxins," *Proceedings of the National Academy of Sciences of the United States of America*, 1998.

[83] M. Giri, M. Zhang, and Y. Lu, "Genes associated with Alzheimer's disease: An overview and current status," 2016.

[84] S. Yoshikai, H. Sasaki, K. Doh-ura, H. Furuya, and Y. Sakaki, "Genomic organization of the human amyloid beta-protein precursor gene," *Gene*, 1990.

[85] A. Goate, M. C. Chartier-Harlin, and M. Mullan, "Segregation of a missense mutation in the amyloid precursor protein gene with familial Alzheimer's disease," *Nature*, 1991.

[86] E. Levy-Lahad, W. Wasco, and P. Poorkaj, "Candidate gene for the chromosome 1 familial Alzheimer's disease locus," *Science*, 1995.

[87] R. Sherrington, E. I. Rogaev, and Y. Liang, "Cloning of a gene bearing missense mutations in early-onset familial Alzheimer's disease," *Nature*, 1995.

[88] J. T. Jarrett, E. P. Berger, and P. T. Lansbury, "The carboxy terminus of the β amyloid protein Is critical for the seeding of amyloid formation: Implications for the pathogenesis of Alzheimer's disease," *Biochemistry*, 1993.

[89] G. Bitan, M. D. Kirkitadze, and A. Lomakin, "Amyloid-beta protein (Abeta) assembly: Abeta 40 and Abeta 42 oligomerize through distinct pathways," *Proceedings of the National Academy of Sciences of the United States of America*, 2003.

[90] M. P. Murphy and H. Levine, "Alzheimer's disease and the amyloid-β peptide," *Journal of Alzheimer's Disease*, 2010.

[91] P. E. Spies, M. M. Verbeek, T. Van Groen, and J. A. Claassen, "Reviewing reasons for the decreased CSF Abeta42 concentration in Alzheimer disease," *Frontiers in Bioscience*, 2012.

[92] National Institute of Health, "https://www.ninds.nih.gov/Disorders/Patient-Caregiver-Education/Life-and-Death-Neuron," 2019.

[93] L. Bertram, C. M. Lill, and R. E. Tanzi, "The genetics of Alzheimer disease: Back to the future," *Neuron*, 2010.

[94] L. Shen and J. Jia, "An overview of genome-wide association studies in Alzheimer's disease," *Neuroscience Bulletin*, 2016.

[95] L. M. Bekris, C. E. Yu, T. D. Bird, and D. W. Tsuang, "Review article: Genetics of Alzheimer disease," *Journal of Geriatric Psychiatry and Neurology*, 2010.

[96] G. Giaccone, F. Tagliavini, G. Linoli, and E. Al., "Down patients: Extracellular preamyloid deposits precede neuritic degeneration and senile plaques," *Neuroscience Letters*, 1989.

[97] P. B. Verghese, J. M. Castellano, and D. M. Holtzman, "Apolipoprotein E in Alzheimer's disease and other neurological disorders," *The Lancet Neurology*, 2011.

[98] R. W. Mahley and S. C. Rall, "Apolipoprotein E: Far more than a lipid transport protein," *Annual Review of Genomics and Human Genetics*, 2000.

[99] L. Bertram and R. E. Tanzi, "Genome-wide association studies in Alzheimer's disease," *Human Molecular Genetics*, 2009.

[100] J. Ghiso, E. Matsubara, and A. Koudinov, "The cerebrospinal-fluid soluble form of Alzheimer's amyloid beta is complexed to SP-40,40 (apolipoprotein J), an inhibitor of the complement membrane-attack complex.," *The Biochemical journal*, vol. 293 (Pt 1, pp. 27–30, 1993.

[101] I. Benilova, E. Karran, and B. De Strooper, "The toxic Aβ oligomer and Alzheimer's disease: An emperor in need of clothes," *Nature Neuroscience*, 2012.

[102] R. M. Williams, Z. Obradovi, V. Mathura, W. Braun, E. C. Garner, J. Young, S. Takayama, C. J. Brown, and A. K. Dunker, "The protein non-folding problem: amino acid determinants of intrinsic order and disorder.," *Pacific Symposium on Biocomputing*, 2001.

[103] S. J. C. Lee, E. Nam, H. J. Lee, M. G. Savelieff, and M. H. Lim, "Towards an understanding of amyloid-β oligomers: Characterization, toxicity mechanisms, and inhibitors," *Chemical Society Reviews*, 2017.

[104] P. E. Wright and H. J. Dyson, "Intrinsically disordered proteins in cellular signalling and regulation," *Nature Reviews Molecular Cell Biology*, 2015.

[105] H. J. Dyson, "Making sense of intrinsically disordered proteins," *Biophysical Journal*, 2016.

[106] T. Iwatsubo, A. Odaka, N. Suzuki, and H. Mizusawa, "Visualization of AP42 (43) and AP40 in senile plaques with end-specific AP monoclonals : Evidence Thai an Initially D & posited Species Is AP42 (43)," *Neuron*, 1994.

[107] S. A. Gravina, L. Ho, C. B. Eckman, K. E. Long, L. Otvos, L. H. Younkin, N. Suzuki, and S. G. Younkin, "Amyloid β protein (Aβ) in Alzheimer's disease brain. Biochemical and immunocytochemical analysis with antibodies specific for forms ending at Aβ40 or Aβ42(43)," *Journal of Biological Chemistry*, 1995.

[108] M. Iljina, G. A. Garcia, A. J. Dear, J. Flint, P. Narayan, T. C. Michaels, C. M. Dobson, D. Frenkel, T. P. Knowles, and D. Klenerman, "Quantitative analysis of co-oligomer formation by amyloid-beta peptide isoforms," *Scientific Reports*, 2016.

[109] Y. M. Kuo, M. R. Emmerling, C. Vigo-Pelfrey, T. C. Kasunic, J. B. Kirkpatrick, G. H. Murdoch, M. J. Ball, and A. E. Roher, "Water-soluble Aβ (N-40, N-42) oligomers in normal and Alzheimer disease brains," *Journal of Biological Chemistry*, 1996.

[110] L.-F. Lue, Y.-M. Kuo, and A. E. Roher, "Soluble amyloid β peptide concentration as a predictor of synaptic change in Alzheimer's disease," *The American Journal of Pathology*, vol. 155, no. 3, pp. 853–862, 1999.

[111] C. A. McLean, R. A. Cherny, and F. W. Fraser, "Soluble pool of Aβ amyloid as a determinant of severity of neurodegeneration in Alzheimer's disease," *Annals of Neurology*, vol. 46, no. 6, pp. 860–866, 1999.

[112] J. Näslund, V. Haroutunian, R. Mohs, K. L. Davis, P. Davies, P. Greengard, and J. D. Buxbaum, "Correlation between elevated levels of amyloid β-peptide in the brain and cognitive decline," *Journal of the American Medical Association*, 2000.

[113] D. M. Walsh, I. Klyubin, J. V. Fadeeva, W. K. Cullen, R. Anwyl, M. S. Wolfe, M. J. Rowan, and D. J. Selkoe, "Naturally secreted oligomers of amyloid β protein potently inhibit hippocampal long-term potentiation in vivo," *Nature*, 2002.

[114] M. Kolarova, F. García-Sierra, A. Bartos, J. Ricny, and D. Ripova, "Structure and pathology of tau protein in Alzheimer disease," 2012.

[115] D. G. Georganopoulou, L. Chang, and J. M. Nam, "Nanoparticle-based detection in cerebral spinal fluid of a soluble pathogenic biomarker for Alzheimer's disease," *Proceedings of the National Academy of Sciences of the United States of America*, 2005.

[116] T. Yang, T. T. O'Malley, D. Kanmert, J. Jerecic, L. R. Zieske, H. Zetterberg, B. T. Hyman, D. M. Walsh, and D. J. Selkoe, "A highly sensitive novel immunoassay specifically detects low levels of soluble Aβ oligomers in human cerebrospinal fluid," *Alzheimer's Research and Therapy*, 2015.

[117] K. Blennow, N. Mattsson, M. Schöll, O. Hansson, and H. Zetterberg, "Amyloid biomarkers in Alzheimer's disease," *Trends in Pharmacological Sciences*, 2015.

[118] S. Matsumura, K. Shinoda, M. Yamada, S. Yokojima, M. Inoue, T. Ohnishi, T. Shimada, K. Kikuchi, D. Masui, S. Hashimoto, M. Sato, A. Ito, M. Akioka, S. Takagi, Y. Nakamura, K. Nemoto, Y. Hasegawa, H. Takamoto, H. Inoue, S. Nakamura, Y. I. Nabeshima, D. B. Teplow, M. Kinjo, and M. Hoshia, "Two distinct amyloid β-protein (Aβ) assembly pathways leading to oligomers and fibrils identified by combined fluorescence correlation spectroscopy, morphology, and toxicity analyses," *Journal of Biological Chemistry*, 2011.

[119] D. J. Selkoe and J. Hardy, "The amyloid hypothesis of Alzheimer's disease at 25 years," *EMBO Molecular Medicine*, 2016.

[120] E. N. Cline, M. A. Bicca, K. L. Viola, and W. L. Klein, "The Amyloid-β oligomer hypothesis: Beginning of the third decade," *Journal of Alzheimer's Disease*, 2018.

[121] C. G. Glabe, "Conformation-dependent antibodies target diseases of protein misfolding," *Trends in Biochemical Sciences*, 2004.

[122] P. N. Lacor, M. C. Buniel, P. W. Furlow, A. S. Clemente, P. T. Velasco, M. Wood, K. L. Viola, and W. L. Klein, "Aβ oligomer-induced aberrations in synapse composition, shape, and density provide a molecular basis for loss of connectivity in Alzheimer's disease," *Journal of Neuroscience*, 2007.

[123] P. T. Velasco, M. C. Heffern, A. Sebollela, I. A. Popova, P. N. Lacor, K. B. Lee, X. Sun, B. N. Tiano, K. L. Viola, A. L. Eckermann, T. J. Meade, and W. L. Klein, "Synapse-binding subpopulations of Aβ oligomers sensitive to peptide assembly blockers and scFv antibodies," *ACS Chemical Neuroscience*, 2012.

[124] A. Laganowsky, C. Liu, M. R. Sawaya, J. P. Whitelegge, J. Park, M. Zhao, A. Pensalfini, A. B. Soriaga, M. Landau, P. K. Teng, D. Cascio, C. Glabe, and D. Eisenberg, "Atomic view of a toxic amyloid small oligomer," *Science*, 2012.

[125] H. B. Pollard, N. Arispe, and E. Rojas, "Ion channel hypothesis for Alzheimer amyloid peptide neurotoxicity," *Cellular and Molecular Neurobiology*, 1995.

[126] N. Arispe, "Architecture of the Alzheimer's AβP ion channel pore," *Journal of Membrane Biology*, 2004.

[127] P. Walsh, G. Vanderlee, J. Yau, J. Campeau, V. L. Sim, C. M. Yip, and S. Sharpe, "The mechanism of membrane disruption by cytotoxic amyloid oligomers formed by prion protein(106-126) is dependent on bilayer composition," *Journal of Biological Chemistry*, 2014.

[128] M. Meyer-Luehmann, J. Coomaraswamy, T. Bolmont, S. Kaeser, C. Schaefer, E. Kilger, A. Neuenschwander, D. Abramowski, P. Frey, A. L. Jaton, J. M. Vigouret, P. Paganetti, D. M. Walsh, P. M. Mathews, J. Ghiso, M. Staufenbiel, L. C. Walker, and M. Jucker, "Exogenous induction of cerebral β-amyloidogenesis is governed bf agent and host," *Science*, 2006.

[129] M. Cohen, B. Appleby, and J. G. Safar, "Distinct prion-like strains of amyloid beta implicated in phenotypic diversity of Alzheimer's disease," *Prion*, 2016.

[130] L. C. Walker, J. Schelle, and M. Jucker, "The prion-like properties of amyloid-β assemblies: Implications for Alzheimer's disease," *Cold Spring Harbor Perspectives in Medicine*, 2016.

[131] H. Hillen, S. Barghorn, and A. Striebinger, "Generation and therapeutic efficacy of highly oligomer-specific β-amyloid antibodies," *Journal of Neuroscience*, 2010.

[132] R. Kayed, Y. Sokolov, B. Edmonds, T. M. McIntire, S. C. Milton, J. E. Hall, and C. G. Glabe, "Permeabilization of lipid bilayers is a common conformation-dependent activity of soluble amyloid oligomers in protein misfolding diseases," *Journal of Biological Chemistry*, 2004.

[133] R. Kayed, E. Head, F. Sarsoza, T. Saing, C. W. Cotman, M. Necula, L. Margol, J. Wu, L. Breydo, J. L. Thompson, S. Rasool, T. Gurlo, P. Butler, and C. G. Glabe, "Fibril specific, conformation dependent antibodies recognize a generic epitope common to amyloid fibrils and fibrillar oligomers that is absent in prefibrillar oligomers," *Molecular Neurodegeneration*, 2007.

[134] H. W. Wang, J. F. Pasternak, H. Kuo, H. Ristic, M. P. Lambert, B. Chromy, K. L. Viola, W. L. Klein, W. B. Stine, G. A. Krafft, and B. L. Trommer, "Soluble oligomers of β amyloid (1-42) inhibit long-term potentiation but not long-term depression in rat dentate gyrus," *Brain Research*, 2002.

[135] B. A. Chromy, R. J. Nowak, M. P. Lambert, K. L. Viola, L. Chang, P. T. Velasco, B. W. Jones, S. J. Fernandez, P. N. Lacor, P. Horowitz, C. E. Finch, G. A. Krafft, and W. L. Klein, "Self-Assembly of Aβ1-42 into globular neurotoxins," *Biochemistry*, 2003.

[136] P. Aran Terol, J. R. Kumita, S. C. Hook, C. M. Dobson, and E. K. Esbjörner, "Solvent exposure of Tyr10 as a probe of structural differences between monomeric and aggregated forms of the amyloid-β peptide," *Biochemical and Biophysical Research Communications*, vol. 468, no. 4, pp. 696–701, 2015.

[137] Y. Gong, L. Chang, and K. L. Viola, "Alzheimer's disease-affected brain: Presence of oligomeric A ligands (ADDLs) suggests a molecular basis for reversible memory loss," *Proceedings of the National Academy of Sciences*, vol. 100, no. 18, pp. 10417–10422, 2003.

[138] F. Alliot, I. Godin, and B. Pessac, "Microglia derive from progenitors, originating from the yolk sac, and which proliferate in the brain," *Developmental Brain Research*, 1999.

[139] F. Ferrini and Y. De Koninck, "Microglia control neuronal network excitability via BDNF signalling," *Neural Plasticity*, 2013.

[140] K. Sato, "Effects of microglia on neurogenesis," *GLIA*, 2015.

[141] L. J. Lawson, V. H. Perry, P. Dri, and S. Gordon, "Heterogeneity in the distribution and morphology of microglia in the normal adult mouse brain," *Neuroscience*, 1990.

[142] M. Mittelbronn, K. Dietz, H. J. Schluesener, and R. Meyermann, "Local distribution of microglia in the normal adult human central nervous system differs by up to one order of magnitude," *Acta Neuropathologica*, 2001.

[143] S. Bachiller, I. Jiménez-Ferrer, A. Paulus, Y. Yang, M. Swanberg, T. Deierborg, and A. Boza-Serrano, "Microglia in neurological diseases: A road map to brain-disease dependent-inflammatory response," *Frontiers in Cellular Neuroscience*, 2018.

[144] M. T. Heneka, M. K. O'Banion, D. Terwel, and M. P. Kummer, "Neuroinflammatory processes in Alzheimer's disease," *Journal of Neural Transmission*, 2010.

[145] A. Shemer, D. Erny, S. Jung, and M. Prinz, "Microglia plasticity during health and disease: An immunological perspective," *Trends in Immunology*, 2015.

[146] A. Karperien, H. Ahammer, and H. F. Jelinek, "Quantitating the subtleties of microglial morphology with fractal analysis," *Frontiers in Cellular Neuroscience*, 2013.

[147] D. Gomez-Nicola and V. H. Perry, "Microglial dynamics and role in the healthy and diseased brain: A paradigm of functional plasticity," *Neuroscientist*, 2015.

[148] Q. Li and B. A. Barres, "Microglia and macrophages in brain homeostasis and disease," *Nature Reviews Immunology*, 2018.

[149] A. Nimmerjahn, F. Kirchhoff, and F. Helmchen, "Neuroscience: Resting microglial cells are highly dynamic surveillants of brain parenchyma in vivo," *Science*, 2005.

[150] N. A. Charles, E. C. Holland, and R. Gilbertson, "The brain tumor microenvironment," *GLIA*, 2011.

[151] R. N. Dilger and R. W. Johnson, "Aging, microglial cell priming, and the discordant central inflammatory response to signals from the peripheral immune system," *Journal of Leukocyte Biology*, 2008.

[152] M. W. Salter and S. Beggs, "Sublime microglia: Expanding roles for the guardians of the CNS," *Cell*, 2014.

[153] K. Saijo, A. Crotti, and C. K. Glass, "Regulation of microglia activation and deactivation by nuclear receptors," *GLIA*, 2013.

[154] C. Cunningham, "Central and systemic endotoxin challenges exacerbate the local inflammatory response and increase neuronal death during chronic neurodegeneration," *Journal of Neuroscience*, vol. 25, no. 40, pp. 9275–9284, 2005.

[155] C. Holmes, C. Cunningham, E. Zotova, and E. Al., "Systemic inflammation and disease progression in Alzheimer disease.," *Neurology*, vol. 73, no. 10, pp. 768–74, 2009.

[156] N. Stence, M. Waite, and M. E. Dailey, "Dynamics of microglial activation: A confocal time-lapse analysis in hippocampal slices," *GLIA*, vol. 33, no. 3, pp. 256–266, 2001.

[157] K. Tahara, H.-D. Kim, and J.-J. Jin, "Role of toll-like receptor signalling in Aβ uptake and clearance," *Brain*, vol. 129, no. 11, pp. 3006–3019, 2006.

[158] G. Bu and S. Rennke, "Receptor-associated protein is a folding chaperone for low density lipoprotein receptor-related protein," *Journal of Biological Chemistry*, 1996.

[159] M. E. Harris-White, Z. Balverde, G. P. Lim, P. Kim, S. A. Miller, H. Hammer, D. Galasko, and S. A. Frautschy, "Role of LRP in TGFβ2-mediated neuronal uptake of Aβ and effects on memory," *Journal of Neuroscience Research*, 2004.

[160] S. Mayor and R. E. Pagano, "Pathways of clathrin-independent endocytosis," 2007.

[161] J. P. Lim and P. A. Gleeson, "Macropinocytosis: An endocytic pathway for internalising large gulps," *Immunology and Cell Biology*, 2011.

[162] S. Mukherjee, R. N. Ghosh, and F. R. Maxfield, "Endocytosis (Review)," *Physiological Reviews*, 1997.

[163] S. Solé-Domènech, D. L. Cruz, E. Capetillo-Zarate, and F. R. Maxfield, "The endocytic pathway in microglia during health, aging and Alzheimer's disease," *Ageing Research Reviews*, 2016.

[164] S. Koizumi, Y. Shigemoto-Mogami, K. Nasu-Tada, Y. Shinozaki, K. Ohsawa, M. Tsuda, B. V. Joshi, K. A. Jacobson, S. Kohsaka, and K. Inoue, "UDP acting at P2Y6 receptors is a mediator of microglial phagocytosis," *Nature*, 2007.

[165] K. Ohsawa, Y. Irino, Y. Nakamura, C. Akazawa, K. Inoue, and S. Kohsaka, "Involvement of P2X4 and P2Y12 receptors in ATP-induced microglial chemotaxis," *GLIA*, 2007.

[166] T. Jiang, L. Tan, and X. C. Zhu, "Upregulation of TREM2 ameliorates neuropathology and rescues spatial cognitive impairment in a transgenic mouse model of Alzheimer's disease,"

Neuropsychopharmacology : official publication of the American College of Neuropsychopharmacology, vol. 39, no. 13, pp. 2949–2962, 2014.

[167] S. Walter and J. Buchner, "Molecular chaperones–cellular machines for protein folding," *Angewandte Chemie (International ed. in English)*, vol. 41, no. 7, pp. 1098–113, 2002.

[168] J. J. Yerbury, S. Poon, S. Meehan, B. Thompson, J. R. Kumita, C. M. Dobson, and M. R. Wilson, "The extracellular chaperone clusterin influences amyloid formation and toxicity by interacting with prefibrillar structures," *The FASEB Journal*, 2007.

[169] M. Beeg, M. Stravalaci, M. Romeo, A. D. Carrá, A. Cagnotto, A. Rossi, L. Diomede, M. Salmona, and X. M. Gobbi, "Clusterin binds to Aβ1-42 oligomers with high affinity and interferes with peptide aggregation by inhibiting primary and secondary nucleation," *Journal of Biological Chemistry*, 2016.

[170] A. Fleming, "On a remarkable bacteriolytic element found," *Proceedings of the Royal Society B*, 1922.

[171] J. Luo, S. K. Wärmländer, A. Gräslund, and J. P. Abrahams, "Human lysozyme inhibits the in vitro aggregation of Aβ peptides, which in vivo are associated with Alzheimer's disease," *Chemical Communications*, 2013.

[172] P. Cunin, C. Beauvillain, C. Miot, J. F. Augusto, L. Preisser, S. Blanchard, P. Pignon, M. Scotet, E. Garo, I. Fremaux, A. Chevailler, J. F. Subra, P. Blanco, M. R. Wilson, P. Jeannin, and Y. Delneste, "Clusterin facilitates apoptotic cell clearance and prevents apoptotic cell-induced autoimmune responses," *Cell Death and Disease*, 2016.

[173] J. Tschopp, A. Chonn, S. Hertig, and L. E. French, "Clusterin, the human apolipoprotein and complement inhibitor, binds to complement C7, C8 beta, and the b domain of C9.," *Journal of immunology*, 1993.

[174] S. Poon, S. B. Easterbrook-Smith, M. S. Rybchyn, J. A. Carver, and M. R. Wilson, "Clusterin is an ATP - Independent chaperone with very broad substrate specificity that stabilizes stressed proteins in a folding-competent state," *Biochemistry*, 2000.

[175] M. E. Rosenberg and J. Silkensen, "Clusterin: Physiologic and pathophysiologic considerations," *The International Journal of Biochemistry & Cell Biology*, vol. 27, no. 7, pp. 633–645, 1995.

[176] M. R. Wilson and S. B. Easterbrook-Smith, "Clusterin is a secreted mammalian chaperone," *Trends in Biochemical Sciences*, 2000.

[177] J. T. Kapron, G. M. Hilliard, J. N. Lakins, M. P. R. Tenniswood, K. A. West, S. A. Carr, and J. W. Crabb, "Identification and characterization of glycosylation sites in human serum clusterin," *Protein Science*, 2008.

[178] E. M. Stewart, J. A. Aquilina, S. B. Easterbrook-Smith, D. Murphy-Durland, C. Jacobsen, S. Moestrup, and M. R. Wilson, "Effects of glycosylation on the structure and function of the extracellular chaperone clusterin," *Biochemistry*, 2007.

[179] M. Polihronis, K. Paizis, G. Carter, L. Sedal, and B. Murphy, "Elevation of human cerebrospinal fluid clusterin concentration is associated with acute neuropathology," *Journal of the Neurological Sciences*, 1993.

[180] B. F. Murphy, L. Kirszbaum, I. D. Walker, and E. Al., "Sp-40,40, a newly identified normal human serum protein found in the SC5b-9 complex of complement and in the immune deposits in glomerulonephritis," *Journal of Clinical Investigation*, 1988.

[181] N. H. Choi, T. Tobe, K. Hara, H. Yoshida, and M. Tomita, "Sandwich ELISA assay for quantitative measurement of SP-40, 40 in seminal plasma and serum," *Journal of Immunological Methods*, 1990.

[182] B. J. Aronow, S. D. Lund, T. L. Brown, J. A. Harmony, and D. P. Witte, "Apolipoprotein J expression at fluid-tissue interfaces: Potential role in barrier cytoprotection," *Proceedings of the National Academy of Sciences of the United States of America*, 1993.

[183] M. J. Ladu, C. Reardon, L. Van Eldik, A. M. Fagan, G. Bu, D. Holtzman, and G. S. Getz, "Lipoproteins in the central nervous system," in *Annals of the New York Academy of Sciences*, 2000.

[184] D. E. Jenne and J. Tschopp, "Clusterin: the intriguing guises of a widely expressed glycoprotein," *Trends in Biochemical Sciences*, 1992.

[185] S. Poon, T. M. Treweek, M. R. Wilson, S. B. Easterbrook-Smith, and J. A. Carver, "Clusterin is an extracellular chaperone that specifically interacts with slowly aggregating proteins on their off-folding pathway," *FEBS Letters*, 2002.

[186] E. Matsubara, B. Frangione, and J. Ghiso, "Characterization of apolipoprotein J-Alzheimer's Aβ interaction," *Journal of Biological Chemistry*, 1995.

[187] E. Matsubara, C. Soto, S. Governale, B. Frangione, and J. Ghiso, "Apolipoprotein J and Alzheimer's amyloid β solubility," *Biochemical Journal*, 1996.

[188] P. Narayan, A. Orte, R. W. Clarke, B. Bolognesi, S. Hook, K. A. Ganzinger, S. Meehan, M. R. Wilson, C. M. Dobson, and D. Klenerman, "The extracellular chaperone clusterin sequesters oligomeric forms of the amyloid-β 1-40 peptide," *Nature Structural and Molecular Biology*, 2012.

[189] M. Thambisetty, A. Simmons, L. Velayudhan, A. Hye, J. Campbell, Y. Zhang, L. O. Wahlund, E. Westman, A. Kinsey, A. Güntert, P. Proitsi, J. Powell, M. Causevic, R. Killick, K. Lunnon, S. Lynham, M. Broadstock, F. Choudhry, D. R. Howlett, R. J. Williams, S. I. Sharp, C. Mitchelmore, C. Tunnard, R. Leung, C. Foy, D. O'Brien, G. Breen, S. J. Furney, M. Ward, I. Kloszewska, P. Mecocci, H. Soininen, M. Tsolaki, B. Vellas, A. Hodges, D. G. Murphy, S. Parkins, J. C. Richardson, S. M. Resnick, L. Ferrucci, D. F. Wong, Y. Zhou, S. Muehlboeck, A. Evans, P. T. Francis, C. Spenger, and S. Lovestone, "Association of plasma clusterin concentration with severity, pathology, and progression in Alzheimer disease," *Archives of General Psychiatry*, 2010.

[190] M. Martínez-Bujidos, A. Rull, B. González-Cura, M. Pérez-Cuéllar, L. Montoliu-Gaya, S. Villegas, J. Ordoñez-Llaños, and J. L. Sánchez-Quesada, "Clusterin/apolipoprotein J binds to aggregated LDL in human plasma and plays a protective role against LDL aggregation," *FASEB Journal*, 2015.

[191] L. N. Boggs, K. S. Fuson, M. Baez, L. Churgay, D. McClure, G. Becker, and P. C. May, "Clusterin (Apo J) protects against in vitro amyloid-β (1-40) neurotoxicity," *Journal of neurochemistry*, vol. 67, no. 3, pp. 1324–1327, 1996.

[192] M. O. Ogundele, "A novel anti-inflammatory activity of lysozyme: Modulation of serum complement activation," *Mediators of Inflammation*, 1998.

[193] T. Ganz, "Antimicrobial polypeptides," *Journal of Leukocyte Biology*, 2004.

[194] M. Lee, J. Kovacs-Nolan, C. Yang, T. Archbold, M. Z. Fan, and Y. Mine, "Hen egg lysozyme attenuates inflammation and modulates local gene expression in a porcine model of dextran sodium sulfate (DSS)-induced colitis," *Journal of Agricultural and Food Chemistry*, 2009.

[195] J. Luo, S. K. Wärmländer, A. Gräslund, and J. P. Abrahams, "Non-chaperone proteins can inhibit aggregation and cytotoxicity of Alzheimer amyloid ß peptide," *Journal of Biological Chemistry*, 2014.

[196] L. Sandin, L. Bergkvist, S. Nath, C. Kielkopf, C. Janefjord, L. Helmfors, H. Zetterberg, K. Blennow, H. Li, C. Nilsberth, B. Garner, A. C. Brorsson, and K. Kågedal, "Beneficial effects of increased lysozyme levels in Alzheimer's disease modelled in Drosophila melanogaster," *FEBS Journal*, 2016.

[197] L. Helmfors, A. Boman, L. Civitelli, S. Nath, L. Sandin, C. Janefjord, H. McCann, H. Zetterberg, K. Blennow, G. Halliday, A. C. Brorsson, and K. Kågedal, "Protective properties of lysozyme on β-amyloid pathology: Implications for Alzheimer disease," *Neurobiology of Disease*, 2015.

[198] L. Sandin, C. Kielkopf, H. Appelqvist, and N. D. Kloss, "Lysozyme attenuates the cellular uptake of amyloid-β and decreases cytotoxicity," *Unpublished*.

[199] D. M. Walsh, E. Thulin, and A. M. Minogue, "A facile method for expression and purification of the Alzheimer's disease-associated amyloid β-peptide," *FEBS Journal*, vol. 276, no. 5, pp. 1266–1281, 2009.

[200] E. Hellstrand, B. Boland, D. M. Walsh, and S. Linse, "Amyloid β-protein aggregation produces highly reproducible kinetic data and occurs by a two-phase process," *ACS Chemical Neuroscience*, 2010.

[201] M. R. Wilson and S. B. Easterbrook-Smith, "Clusterin binds by a multivalent mechanism to the Fc and Fab regions of IgG," *Biochimica et Biophysica Acta (BBA)/Protein Structure and Molecular*, 1992.

[202] R. J. Johnson, J. Christodoulou, M. Dumoulin, G. L. Caddy, M. J. Alcocer, G. J. Murtagh, J. R. Kumita, G. Larsson, C. V. Robinson, D. B. Archer, B. Luisi, and C. M. Dobson, "Rationalising lysozyme amyloidosis: Insights from the structure and solution dynamics of T70N lysozyme," *Journal of Molecular Biology*, 2005.

[203] Y. C. Lee and D. Yang, "Determination of lysozyme activities in a microplate format," *Analytical Biochemistry*, 2002.

[204] T. L. Riss, R. A. Moravec, and A. L. Niles, "Cell viability assays (Promega)," *Assay Guidance Manual*, 2016.

[205] R. A. McCloy, S. Rogers, and C. E. Caldon, "Partial inhibition of Cdk1 in G2 phase overrides the SAC and decouples mitotic events," *Cell Cycle*, vol. 13, no. 9, pp. 1400–1412, 2014.

[206] E. M. Manders, J. Stap, G. J. Brakenhoff, R. Van Driel, and J. A. Aten, "Dynamics of three-dimensional replication patterns during the S-phase, analysed by double labelling of DNA and confocal microscopy," *Journal of Cell Science*, 1992.

[207] M. Dumoulin, A. M. Last, A. Desmyter, K. Decanniere, D. Canet, G. Larsson, A. Spencer, D. B. Archer, J. Sasse, S. Muyldermans, L. Wyns, C. Redfield, A. Matagne, C. V. Robinson, and C. M.

Dobson, "A camelid antibody fragment inhibits the formation of amyloid fibrils by human lysozyme," *Nature*, 2003.

[208] P. Flagmeier, S. De, D. C. Wirthensohn, and E. Al., "Ultrasensitive measurement of Ca2+ influx into lipid vesicles induced by protein aggregates," *Angewandte Chemie - International Edition*, 2017.

[209] AnaSpec Inc., "https://www.anaspec.com/products/product," 2020.

[210] L. M. Jungbauer, C. Yu, K. J. Laxton, and M. J. LaDu, "Preparation of fluorescently-labeled amyloid-beta peptide assemblies: The effect of fluorophore conjugation on structure and function," in *Journal of Molecular Recognition*, 2009.

[211] I. Kheterpal, A. Williams, C. Murphy, B. Bledsoe, and R. Wetzel, "Structural features of the Aβ amyloid fibril elucidated by limited proteolysis," *Biochemistry*, 2001.

[212] J. Wägele, S. De Sio, B. Voigt, J. Balbach, and M. Ott, "How Fluorescent Tags Modify Oligomer Size Distributions of the Alzheimer Peptide," *Biophysical Journal*, 2019.

[213] S. M. Chafekar, F. Baas, and W. Scheper, "Oligomer-specific Aβ toxicity in cell models is mediated by selective uptake," *Biochimica et Biophysica Acta - Molecular Basis of Disease*, vol. 1782, no. 9, pp. 523–531, 2008.

[214] A. Familian, P. Eikelenboom, and R. Veerhuis, "Minocycline does not affect amyloid β phagocytosis by human microglial cells," *Neuroscience Letters*, 2007.

[215] H. M. Nielsen, S. D. Mulder, J. A. Beliën, and E. Al., "Astrocytic Aβ1-42 uptake is determined by Aβ-aggregation state and the presence of amyloid-associated proteins," *GLIA*, vol. 58, no. 10, pp. 1235–1246, 2010.

[216] Merck Millipore, "https://www.merckmillipore.com/GB/en/product/Anti-Amyloid-Antibody-clone-W0-2,MM_NF-MABN10," 2020.

[217] F. Huang, J. Wang, A. Qu, L. Shen, J. Liu, J. Liu, Z. Zhang, Y. An, and L. Shi, "Maintenance of amyloid β peptide homeostasis by artificial chaperones based on mixed-shell polymeric micelles," *Angewandte Chemie - International Edition*, 2014.

[218] M. I. Maqsood, M. M. Matin, A. R. Bahrami, and M. M. Ghasroldasht, "Immortality of cell lines: Challenges and advantages of establishment," 2013.

[219] W. S. Walker, J. Gatewood, E. Olivas, D. Askew, and C. E. Havenith, "Mouse microglial cell lines differing in constitutive and interferon-γ-inducible antigen-presenting activities for naive and memory CD4+ and CD8+ T cells," *Journal of Neuroimmunology*, 1995.

[220] B. Stansley, J. Post, and K. Hensley, "A comparative review of cell culture systems for the study of microglial biology in Alzheimer's disease," *Journal of Neuroinflammation*, 2012.

[221] J. Cheng-Chung Wei, H. C. Huang, W. J. Chen, and E. al., "Epigallocatechin gallate attenuates amyloid β-induced inflammation and neurotoxicity in EOC 13.31 microglia," *European Journal of Pharmacology*, 2016.

[222] S. C. Hook, "Investigation into the role of the extracellular chaperone, clusterin, in Aß42 oligomer interactions with mammalian cells," in *Thesis*, University of Cambridge, 2013.

[223] R. B. DeMattos, J. R. Cirrito, M. Parsadanian, P. C. May, M. A. O'Dell, J. W. Taylor, J. A. Harmony, B. J. Aronow, K. R. Bales, S. M. Paul, and D. M. Holtzman, "ApoE and clusterin cooperatively suppress Aβ levels and deposition: evidence that ApoE regulates extracellular Aβ metabolism in vivo," *Neuron*, 2004.

[224] R. D. Bell, A. P. Sagare, A. E. Friedman, and E. Al., "Transport pathways for clearance of human Alzheimer's amyloid β-peptide and apolipoproteins E and J in the mouse central nervous system," *Journal of Cerebral Blood Flow & Metabolism*, vol. 27, no. 5, pp. 909–18, 2006.

[225] T. Nuutinen, J. Huuskonen, T. Suuronen, J. Ojala, R. Miettinen, and A. Salminen, "Amyloid-β 1-42 induced endocytosis and clusterin/apoJ protein accumulation in cultured human astrocytes," *Neurochemistry International*, 2007.

[226] S. D. Mulder, H. M. Nielsen, M. A. Blankenstein, P. Eikelenboom, and R. Veerhuis, "Apolipoproteins E and J interfere with amyloid-beta uptake by primary human astrocytes and microglia in vitro," *GLIA*, 2014.

[227] T. Bolmont, F. Haiss, D. Eicke, R. Radde, C. A. Mathis, W. E. Klunk, S. Kohsaka, M. Jucker, and M. E. Calhoun, "Dynamics of the microglial/amyloid interaction indicate a role in plaque maintenance," *Journal of Neuroscience*, 2008.

[228] S. A. Grathwohl, R. E. Kälin, and T. Bolmont, "Formation and maintenance of Alzheimer's disease β-amyloid plaques in the absence of microglia," *Nature Neuroscience*, 2009.

[229] M. Yamamoto, T. Kiyota, and M. Horiba, "Interferon-γ and tumor necrosis factor-α regulate amyloid-β plaque deposition and β-secretase expression in Swedish mutant APP transgenic mice," *American Journal of Pathology*, 2007.

[230] P. Benes, V. Vetvicka, and M. Fusek, "Cathepsin D - Many functions of one aspartic protease," *Critical Reviews in Oncology/Hematology*, 2008.

[231] J. Suh, Y. An, B. C. Tang, C. Dempsey, F. Huang, and J. Hanes, "Real-time gene delivery vector tracking in the endo-lysosomal pathway of live cells," *Microscopy Research and Technique*, 2012.

[232] A. Pierzynska-Mach, P. A. Janowski, and J. W. Dobrucki, "Evaluation of acridine orange, LysoTracker Red, and quinacrine as fluorescent probes for long-term tracking of acidic vesicles," *Cytometry Part A*, 2014.

[233] N. Andrejewski, E. L. Punnonen, and G. Guhde, "Normal lysosomal morphology and function in LAMP-1-deficient mice," *Journal of Biological Chemistry*, 1999.

[234] G. Misinzo, P. L. Delputte, and H. J. Nauwynck, "Inhibition of endosome-lysosome system acidification enhances porcine circovirus 2 infection of porcine epithelial cells," *Journal of Virology*, 2008.

[235] E. J. Davis, T. D. Foster, and W. E. Thomas, "Cellular forms and functions of brain microglia," *Brain Research Bulletin*, 1994.

[236] B. M. Davis, M. Salinas-Navarro, M. F. Cordeiro, and E. Al., "Characterizing microglia activation: A spatial statistics approach to maximize information extraction," *Scientific Reports*, 2017.

[237] L. F. Lue, R. Rydel, E. F. Brigham, L. B. Yang, H. Hampel, G. M. Murphy, L. Brachova, S. D. Yan, D. G. Walker, Y. Shen, and J. Rogers, "Inflammatory repertoire of Alzheimer's disease and nondemented elderly microglia in vitro," *GLIA*, 2001.

[238] J. Rogers and L. F. Lue, "Microglial chemotaxis, activation, and phagocytosis of amyloid β-peptide as linked phenomena in Alzheimer's disease," *Neurochemistry International*, 2001.

[239] Y. Yao, J. Li, Y. Niu, J. Q. Yu, L. Yan, Z. H. Miao, X. X. Zhao, Y. J. Li, W. X. Yao, P. Zheng, and W. Q. Li, "Resveratrol inhibits oligomeric Aβ-induced microglial activation via NADPH oxidase," *Molecular Medicine Reports*, 2015.

[240] M. Jian, J. S. C. Kwan, M. Bunting, R. C. L. Ng, and K. H. Chan, "Adiponectin suppresses amyloid-β oligomer (AβO)-induced inflammatory response of microglia via AdipoR1-AMPK-NF-κB signaling pathway," *Journal of Neuroinflammation*, 2019.

[241] A. M. Floden and C. K. Combs, "β-Amyloid stimulates murine postnatal and adult microglia cultures in a unique manner," *Journal of Neuroscience*, 2006.

[242] K. V. Korneev, A. N. Kondakova, E. N. Sviriaeva, N. A. Mitkin, A. Palmigiano, A. A. Kruglov, G. B. Telegin, M. S. Drutskaya, L. Sturiale, D. Garozzo, S. A. Nedospasov, Y. A. Knirel, and D. V. Kuprash, "Hypoacylated LPS from foodborne pathogen Campylobacter jejuni induces moderate TLR4-mediated inflammatory response in murine macrophages," *Frontiers in Cellular and Infection Microbiology*, 2018.

[243] A. M. Mayer, M. Hall, M. J. Fay, P. Lamar, C. Pearson, W. C. Prozialeck, V. K. Lehmann, P. B. Jacobson, A. M. Romanic, T. Uz, and H. Manev, "Effect of a short-term in vitro exposure to the marine toxin domoic acid on valiability, tumor necrosis factor-alpha, matrix metalloproteinase-9 and superoxide anion release by rat neonatal microglia," *BMC Pharmacology*, 2001.

[244] B. V. Zlokovic, C. L. Martel, E. Matsubara, and E. Al., "Glycoprotein 330/megalin: probable role in receptor-mediated transport of apolipoprotein J alone and in a complex with Alzheimer disease amyloid beta at the blood-brain and blood-cerebrospinal fluid barriers.," *Proceedings of the National Academy of Sciences*, vol. 93, no. 9, pp. 4229–4234, 1996.

[245] S. M. Hammad, S. Ranganathan, E. Loukinova, W. O. Twal, and W. S. Argraves, "Interaction of apolipoprotein J-amyloid β-peptide complex with low density lipoprotein receptor-related protein-2/megalin. A mechanism to prevent pathological accumulation of amyloid β-peptide," *Journal of Biological Chemistry*, vol. 272, no. 30, pp. 18644–18649, 1997.

[246] R. Guerreiro, A. Wojtas, J. Bras, M. Carrasquillo, E. Rogaeva, E. Majounie, C. Cruchaga, C. Sassi, J. S. Kauwe, S. Younkin, L. Hazrati, J. Collinge, J. Pocock, T. Lashley, J. Williams, J. C. Lambert, P. Amouyel, A. Goate, R. Rademakers, K. Morgan, J. Powell, P. S. George-Hyslop, A. Singleton, and J. Hardy, "TREM2 variants in Alzheimer's disease," *New England Journal of Medicine*, 2013.

[247] T. Jonsson, H. Stefansson, S. Steinberg, I. Jonsdottir, P. V. Jonsson, J. Snaedal, S. Bjornsson, J. Huttenlocher, A. I. Levey, J. J. Lah, D. Rujescu, H. Hampel, I. Giegling, O. A. Andreassen, K. Engedal, I. Ulstein, S. Djurovic, C. Ibrahim-Verbaas, A. Hofman, M. A. Ikram, C. M. Van

Duijn, U. Thorsteinsdottir, A. Kong, and K. Stefansson, "Variant of TREM2 associated with the risk of Alzheimer's disease," *New England Journal of Medicine*, 2013.

[248] S. Frank, G. J. Burbach, and M. Bonin, "TREM2 is upregulated in amyloid plaque-associated microglia in aged APP23 transgenic mice," *GLIA*, vol. 56, no. 13, pp. 1438–1447, 2008.

[249] Y. Zhao, X. Wu, X. Li, and E. Al., "TREM2 is a receptor for β-amyloid that mediates microglial function," *Neuron*, 2018.

[250] F. L. Yeh, Y. Wang, I. Tom, L. C. Gonzalez, and M. Sheng, "TREM2 binds to apolipoproteins, including APOE and CLU/APOJ, and thereby facilitates uptake of amyloid-beta by microglia," *Neuron*, vol. 91, no. 2, pp. 328–340, 2016.

[251] X. D. Pan, Y. G. Zhu, N. Lin, J. Zhang, Q. Y. Ye, H. P. Huang, and X. C. Chen, "Microglial phagocytosis induced by fibrillar β-amyloid is attenuated by oligomeric β-amyloid: Implications for Alzheimer's disease," *Molecular Neurodegeneration*, 2011.

[252] J. A. Smith, A. Das, S. K. Ray, and N. L. Banik, "Role of pro-inflammatory cytokines released from microglia in neurodegenerative diseases," *Brain Research Bulletin*, vol. 87, no. 1, pp. 10–20, 2012.

[253] K. Kierdorf and M. Prinz, "Factors regulating microglia activation.," *Frontiers in cellular neuroscience*, vol. 7, no. April, p. 44, 2013.

[254] S. G. Torres-Platas, S. Comeau, and A. Rachalski, "Morphometric characterization of microglial phenotypes in human cerebral cortex," *Journal of Neuroinflammation*, vol. 11, 2014.

[255] S. Mandrekar, Q. Jiang, C. Y. D. Lee, J. Koenigsknecht-Talboo, D. M. Holtzman, and G. E. Landreth, "Microglia mediate the clearance of soluble Aß through fluid phase macropinocytosis," *Journal of Neuroscience*, 2009.

[256] M. Matarin, D. A. Salih, and M. Yasvoina, "A Genome-wide gene-expression analysis and database in transgenic mice during development of amyloid or tau pathology," *Cell Reports*, 2015.

[257] U. Mamat, K. Wilke, D. Bramhill, A. B. Schromm, B. Lindner, T. A. Kohl, J. L. Corchero, A. Villaverde, L. Schaffer, S. R. Head, C. Souvignier, T. C. Meredith, and R. W. Woodard, "Detoxifying Escherichia coli for endotoxin-free production of recombinant proteins," *Microbial Cell Factories*, 2015.

[258] H. Bausinger, D. Lipsker, U. Ziylan, S. Manié, J. P. Briand, J. P. Cazenave, S. Muller, J. F. Haeuw, C. Ravanat, H. de la Salle, and D. Hanau, "Endotoxin-free heat-shock protein 70 fails to induce APC activation," *European Journal of Immunology*, 2002.

[259] B. Gao and M. F. Tsan, "Endotoxin contamination in recombinant human heat shock protein 70 (Hsp70) preparation is responsible for the induction of tumor necrosis factor α release by murine macrophages," *Journal of Biological Chemistry*, 2003.

[260] S. J. Wakelin, I. Sabroe, C. D. Gregory, I. R. Poxton, J. L. Forsythe, O. J. Garden, and S. E. Howie, ""Dirty little secrets"-Endotoxin contamination of recombinant proteins," 2006.

[261] P. Arosio, R. Cukalevski, B. Frohm, T. P. Knowles, and S. Linse, "Quantification of the concentration of Aβ42 propagons during the lag phase by an amyloid chain reaction assay," *Journal of the American Chemical Society*, 2014.

[262] J. Domert, S. B. Rao, L. Agholme, A. C. Brorsson, J. Marcusson, M. Hallbeck, and S. Nath, "Spreading of amyloid-β peptides via neuritic cell-to-cell transfer is dependent on insufficient cellular clearance," *Neurobiology of Disease*, 2014.

[263] P. S. Vassar and C. F. Culling, "Fluorescent stains, with special reference to amyloid and connective tissues.," *Archives of pathology*, vol. 68, pp. 487–498, 1959.

[264] H. Naiki, K. Higuchi, M. Hosokawa, and T. Takeda, "Fluorometric determination of amyloid fibrils in vitro using the fluorescent dye, thioflavine T," *Analytical Biochemistry*, 1989.

[265] M. Biancalana and S. Koide, "Molecular mechanism of Thioflavin-T binding to amyloid fibrils," 2010.

[266] H. Levine, "Thioflavine T interaction with synthetic Alzheimer's disease βâamyloid peptides: Detection of amyloid aggregation in solution," *Protein Science*, 1993.

[267] R. Khurana, C. Coleman, C. Ionescu-Zanetti, S. A. Carter, V. Krishna, R. K. Grover, R. Roy, and S. Singh, "Mechanism of thioflavin T binding to amyloid fibrils," *Journal of Structural Biology*, 2005.

[268] M. R. Krebs, E. H. Bromley, and A. M. Donald, "The binding of thioflavin-T to amyloid fibrils: Localisation and implications," *Journal of Structural Biology*, 2005.

[269] T. Scheidt, U. Łapińska, J. R. Kumita, D. R. Whiten, D. Klenerman, M. R. Wilson, S. I. Cohen, S. Linse, M. Vendruscolo, C. M. Dobson, T. P. Knowles, and P. Arosio, "Secondary nucleation

and elongation occur at different sites on Alzheimer's amyloid-b aggregates," *Science Advances*, 2019.

[270] D. J. Lindberg, A. Wenger, E. Sundin, E. Wesén, F. Westerlund, and E. K. Esbjörner, "Binding of Thioflavin-T to Amyloid Fibrils Leads to Fluorescence Self-Quenching and Fibril Compaction," *Biochemistry*, 2017.

[271] J. R. Kumita, L. Helmfors, J. Williams, L. M. Luheshi, L. Menzer, M. Dumoulin, D. A. Lomas, D. C. Crowther, C. M. Dobson, and A.-C. Brorsson, "Disease-related amyloidogenic variants of human lysozyme trigger the unfolded protein response and disturb eye development in Drosophila melanogaster," *The FASEB Journal*, 2012.

[272] J. Herz, J. L. Goldstein, D. K. Strickland, Y. K. Ho, and M. S. Brown, "39-kDa protein modulates binding of ligands to low density lipoprotein receptor-related protein/α2-macroglobulin receptor," *Journal of Biological Chemistry*, 1991.

[273] J. M. Prasad, M. Migliorini, R. Galisteo, and D. K. Strickland, "Generation of a potent low density lipoprotein receptor-related protein 1 (LRP1) antagonist by engineering a stable form of the receptor-associated protein (RAP) D3 domain," *Journal of Biological Chemistry*, 2015.

[274] T. Kanekiyo and G. Bu, "The low-density lipoprotein receptor-related protein 1 and amyloid-β clearance in Alzheimer's disease," *Frontiers in Aging Neuroscience*, 2014.

[275] M. Shibata, S. Yamada, S. Ram Kumar, M. Calero, J. Bading, B. Frangione, D. M. Holtzman, C. A. Miller, D. K. Strickland, J. Ghiso, and B. V. Zlokovic, "Clearance of Alzheimer's amyloid-β1-40 peptide from brain by LDL receptor-related protein-1 at the blood-brain barrier," *Journal of Clinical Investigation*, 2000.

[276] M. B. Mansour, R. Balti, L. Yacoubi, V. Ollivier, F. Chaubet, and R. M. Maaroufi, "Primary structure and anticoagulant activity of fucoidan from the sea cucumber Holothuria polii," *International Journal of Biological Macromolecules*, 2019.

[277] J. B. Lee, K. Hayashi, M. Hashimoto, T. Nakano, and T. Hayashi, "Novel antiviral fucoidan from sporophyll of Undaria pinnatifida (Mekabu)," *Chemical and Pharmaceutical Bulletin*, 2004.

[278] Y. Wang, M. Xing, Q. Cao, A. Ji, H. Liang, and S. Song, "Biological activities of fucoidan and the factors mediating its therapeutic effects: A review of recent studies," *Marine Drugs*, 2019.

[279] M. Baba, R. Snoeck, R. Pauwels, and E. De Clercq, "Sulfated polysaccharides are potent and selective inhibitors of various enveloped viruses, including herpes simplex virus, cy-

tomegalovirus, vesicular stomatitis virus, and human immunodeficiency virus," *Antimicrobial Agents and Chemotherapy*, 1988.

[280] T. V. Alekseyenko, S. Y. Zhanayeva, A. A. Venediktova, T. N. Zvyagintseva, T. A. Kuznetsova, N. N. Besednova, and T. A. Korolenko, "Antitumor and antimetastatic activity of fucoidan, a sulfated polysaccharide isolated from the Okhotsk sea Fucus evanescens brown alga," *Bulletin of Experimental Biology and Medicine*, 2007.

[281] N. P. Chandía and B. Matsuhiro, "Characterization of a fucoidan from Lessonia vadosa (Phaeophyta) and its anticoagulant and elicitor properties," *International Journal of Biological Macromolecules*, 2008.

[282] H. Y. Park, M. H. Han, C. Park, C. Y. Jin, G. Y. Kim, I. W. Choi, N. D. Kim, T. J. Nam, T. K. Kwon, and Y. H. Choi, "Anti-inflammatory effects of fucoidan through inhibition of NF-κB, MAPK and Akt activation in lipopolysaccharide-induced BV2 microglia cells," *Food and Chemical Toxicology*, 2011.

[283] J. H. Jhamandas, M. B. Wie, K. Harris, D. MacTavish, and S. Kar, "Fucoidan inhibits cellular and neurotoxic effects of β-amyloid (Aβ) in rat cholinergic basal forebrain neurons," *European Journal of Neuroscience*, 2005.

[284] E. K. Esbjörner, F. Chan, and E. Rees, "Direct observations of amyloid β Self-assembly in live cells provide insights into differences in the kinetics of Aβ(1-40) and Aβ(1-42) aggregation," *Chemistry and Biology*, 2014.

[285] C. Yu, E. Nwabuisi-Heath, K. Laxton, and M. J. Ladu, "Endocytic pathways mediating oligomeric Aβ42 neurotoxicity," *Molecular Neurodegeneration*, 2010.

[286] E. J. Fernandez-Perez, C. Peters, and L. G. Aguayo, "Membrane Damage Induced by Amyloid Beta and a Potential Link with Neuroinflammation," *Current Pharmaceutical Design*, 2016.

[287] M. P. Mattson, S. W. Barger, B. Cheng, I. Lieberburg, V. L. Smith-Swintosky, and R. E. Rydel, "β-Amyloid precursor protein metabolites and loss of neuronal Ca2+ homeostasis in Alzheimer's disease," 1993.

[288] M. Kawahara, I. Ohtsuka, S. Yokoyama, M. Kato-Negishi, and Y. Sadakane, "Membrane incorporation, channel formation, and disruption of calcium homeostasis by Alzheimer's -amyloid protein," 2011.

[289] A. Drews, J. Flint, N. Shivji, P. Jönsson, D. Wirthensohn, E. De Genst, C. Vincke, S. Muyldermans, C. Dobson, and D. Klenerman, "Individual aggregates of amyloid beta induce temporary calcium influx through the cell membrane of neuronal cells," *Scientific Reports*, 2016.

[290] J. R. Kumita, S. Poon, G. L. Caddy, C. L. Hagan, M. Dumoulin, J. J. Yerbury, E. M. Stewart, C. V. Robinson, M. R. Wilson, and C. M. Dobson, "The Extracellular Chaperone Clusterin Potently Inhibits Human Lysozyme Amyloid Formation by Interacting with Prefibrillar Species," *Journal of Molecular Biology*, 2007.

[291] A. I. Usov and M. I. Bilan, "Fucoidans â sulfated polysaccharides of brown algae," *Russian Chemical Reviews*, 2009.

[292] H. Do, S. Pyo, and E. H. Sohn, "Suppression of iNOS expression by fucoidan is mediated by regulation of p38 MAPK, JAK/STAT, AP-1 and IRF-1, and depends on up-regulation of scavenger receptor B1 expression in TNF-α- and IFN-γ-stimulated C6 glioma cells," *Journal of Nutritional Biochemistry*, 2010.

[293] C. M. Vander Zanden, L. Wampler, I. Bowers, E. B. Watkins, J. Majewski, and E. Y. Chi, "Fibrillar and nonfibrillar amyloid beta structures drive two modes of membrane-mediated toxicity," *Langmuir*, 2019.